

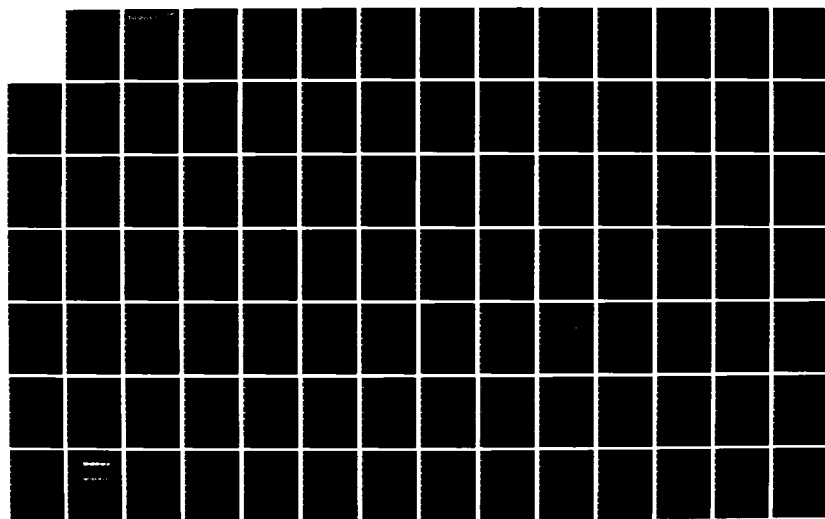
AD-A136 996

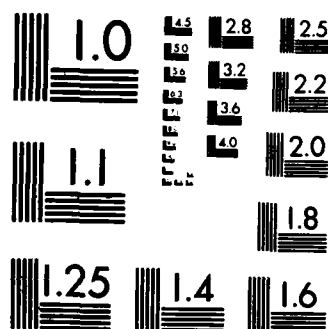
INTERFACIAL TENSION BETWEEN WATER AND SELECTED  
SUPERHEATED LIQUIDS BY GUA. (U) YALE UNIV NEW HAVEN CT  
DEPT OF MECHANICAL ENGINEERING C J HSU DEC 83 TM-4  
N00014-76-C-0527 F/G 7/4

1/2

UNCLASSIFIED

NL





MICROCOPY RESOLUTION TEST CHART  
NATIONAL BUREAU OF STANDARDS-1963-A

# YALE UNIVERSITY

MECHANICAL ENGINEERING

12

AD A 136996

OFFICE OF NAVAL RESEARCH  
CONTRACT NO. N00014-76-C-0527

TECHNICAL MEMORANDUM  
No. 4

INTERFACIAL TENSION BETWEEN WATER AND SELECTED SUPERHEATED  
LIQUIDS BY QUADRUPOLE OSCILLATIONS OF DROPS

by

Chaur-Jian Hsu

December 1983

DTIC  
ELECTE  
JAN 17 1984

D

DTIC FILE COPY

Approved for public release; distribution unlimited.  
Reproduction in whole or in part is permitted for any purpose  
of the United States Government.

84 01 16 C02

Unclassified

SECURITY CLASSIFICATION OF THIS PAGE (When Data Entered)

REPORT DOCUMENTATION PAGE		READ INSTRUCTIONS BEFORE COMPLETING FORM
1. REPORT NUMBER 4	2. GOVT ACCESSION NO. AD-A136996	3. RECIPIENT'S CATALOG NUMBER
4. TITLE (and Subtitle) INTERFACIAL TENSION BETWEEN WATER AND SELECTED SUPERHEATED LIQUIDS BY QUADRUPOLE OSCILLATIONS OF DROPS		5. TYPE OF REPORT & PERIOD COVERED Technical 1981-1983
		6. PERFORMING ORG. REPORT NUMBER
7. AUTHOR(s) Chaur-Jian Hsu		8. CONTRACT OR GRANT NUMBER(s) N00014-76-C-0527
9. PERFORMING ORGANIZATION NAME AND ADDRESS Dept. of Mechanical Engineering Yale University, P.O. Box 2159 Yale Station 9 Hillhouse Ave., New Haven, CT 06520		10. PROGRAM ELEMENT, PROJECT, TASK AREA & WORK UNIT NUMBERS
11. CONTROLLING OFFICE NAME AND ADDRESS Office of Naval Research Physics Division Office Arlington, VA 22217		12. REPORT DATE December 1983
		13. NUMBER OF PAGES 145
14. MONITORING AGENCY NAME & ADDRESS (if different from Controlling Office)		15. SECURITY CLASS. (of this report) Unclassified
		15a. DECLASSIFICATION/DOWNGRADING SCHEDULE
16. DISTRIBUTION STATEMENT (of this Report) Approved for public release; distribution unlimited.		
17. DISTRIBUTION STATEMENT (of the abstract entered in Block 20, if different from Report)		
18. SUPPLEMENTARY NOTES Ph.D. dissertation of Chaur-Jian Hsu at Yale University, December 1983		
19. KEY WORDS (Continue on reverse side if necessary and identify by block number) Interfacial tension, Superheated liquids, Butane, Isobutane, Propane, Acoustic levitation, Drop deformation due to acoustic radiation, Shape (quadrupole) oscillations of drops, Adiabatic compressibility, Fowkes' theory. Simplified model.		
20. ABSTRACT (Continue on reverse side if necessary and identify by block number) A technique is presented for measuring the interfacial tension between two liq- uids, one of which may be in a metastable state. A drop of one liquid is acoustically levitated in the other liquid (host) and also acoustically driven into quadrupole shape oscillations. The frequencies associated with several phase angles near the quadrupole resonance of the drop and the diameter of the drop are measured, which allows the interfacial tension to be calculated given the densities of both the drop and the host liquids. Because the host liquid		

DD FORM 1473

1 JAN 73

EDITION OF 1 NOV 65 IS OBSOLETE  
S/N 0102-LF-014-6601

Unclassified

SECURITY CLASSIFICATION OF THIS PAGE (When Data Entered)

Conx  
Unclassified

SECURITY CLASSIFICATION OF THIS PAGE (When Data Entered)

provides a very smooth and clean container for the levitated drop, and because the shape oscillation is excited acoustically, without contact with a solid surface, the drop may survive in the superheated state for a long enough time for the experiments to be conducted.

A simplified model was developed for describing the free oscillation and forced oscillation of a drop freely suspended in a host. The results of the simplified model agree well with that of previous theories.

The accuracy of this technique was tested by measuring the interfacial tension between water and each of two common liquids. Experiments were conducted for measuring the interfacial tension between water and each of the three superheated liquids; butane, isobutane, and propane, at room temperature and atmospheric pressure. Data for the compressibility of these superheated liquids were also obtained using an established acoustic levitation technique. Some other possible applications of the drop deformation technique are mentioned.

Accession For	
NTIS GRA&I	<input checked="checked" type="checkbox"/>
DTIC TAB	<input type="checkbox"/>
Unannounced	<input type="checkbox"/>
Justification	
By	
Distribution/	
Availability Codes	
Dist	Avail and/or Special
Al	

copy  
inspected

Unclassified

SECURITY CLASSIFICATION OF THIS PAGE (When Data Entered)

## TABLE OF CONTENTS

LIST OF FIGURES . . . . .	iii
LIST OF TABLES . . . . .	v

### Chapter

### page

1. INTRODUCTION . . . . .	1
Interfacial Tension . . . . .	2
Traditional Methods for Interfacial Tension Measurements . . . . .	3
Superheated Liquids . . . . .	4
Acoustic Levitation . . . . .	6
Oscillations of a Spherical Drop . . . . .	8
Fowkes' Equation for Interfacial Tension . . . . .	10
Purpose and Scope . . . . .	11
2. THEORY . . . . .	13
Problem and Basic Assumptions . . . . .	13
Previous Theories for Shape Oscillations of a Drop . . . . .	14
Drop and Host Liquid of Negligible Viscosity . . . . .	14
Resonance Frequency . . . . .	14
Damping . . . . .	16
Drop and Host of Viscous Liquids . . . . .	16
A Simplified Model for Shape Oscillation of a Drop . . . . .	18
Analogy with the Basic Mass and Spring System . . . . .	19
Resonance Frequency of a Mass and Spring System . . . . .	19
The Shape Oscillation of a Drop in Another Liquid . . . . .	22
Velocity Profile for an Inviscid Drop in an Inviscid Host . . . . .	23
A Modified Velocity Distribution with Small Viscosity . . . . .	27
Tangential Component of the Interfacial Velocity . . . . .	27
Damping of Free Oscillation . . . . .	29
Dissipation in the Inner Irrotational Flow . . . . .	30
Dissipation in the Outer Irrotational Flow . . . . .	31
Dissipation in the Inner Boundary Layer . . . . .	31
Dissipation in the Outer Boundary Layer . . . . .	32
The Total Energy of the Oscillation . . . . .	33
Damping Constant . . . . .	33
Examples and Comparison with the Previous Theories . . . . .	35
Phase-Frequency Relation in Forced Oscillation . . . . .	39
Driving Force . . . . .	39
Impedance Due to Stiffness . . . . .	40

	Impedance Due to Inertia . . . . .	43
	Impedance Due to Viscosity . . . . .	44
	Total Impedance . . . . .	47
	Comparison with the Theory by Marston . . . . .	50
	Compressadensity Measurement . . . . .	53
3.	APPARATUS . . . . .	55
	Levitation and Shape Oscillation . . . . .	57
	Detection of Shape Oscillation . . . . .	60
	Frequency and Phase Measurements . . . . .	61
	Size Measurement . . . . .	64
	Measurement of Sound Speed and Density . . . . .	65
4.	PROCEDURE . . . . .	67
	Drop Levitation . . . . .	68
	Drop Making and Transportation . . . . .	70
	Procedure for the Size Measurements . . . . .	73
	Procedure for the Phase-Frequency Measurement . . . . .	73
	Tuning of the Carrier Frequency . . . . .	74
	Phase-Frequency Measurement . . . . .	77
	Procedure for the Compressadensity Measurement . . . . .	78
5.	RESULTS AND DISCUSSION . . . . .	79
	Non-superheated Sample Liquids . . . . .	79
	Approximation by Newton's Iteration . . . . .	82
	Approximation Method . . . . .	82
	Examples . . . . .	84
	Gel Effect . . . . .	88
	Data Reduction by the Method of Least-squares . . . . .	92
	Model and Procedure . . . . .	92
	Examples . . . . .	93
	Measurements for Non-superheated Liquids . . . . .	99
	Interfacial Tension . . . . .	99
	Damping and Viscosity . . . . .	101
	Measurements for Superheated Liquids . . . . .	105
	Test Liquid . . . . .	105
	Measurements for Butane and Isobutane . . . . .	108
	Measurements for Propane . . . . .	111
	Comparison with Fowkes Theory . . . . .	119
	Measurements for Compressadensity . . . . .	121
	Control Experiment . . . . .	121
	Compressadensity of Superheated Liquids . . . . .	122
6.	SUMMARY AND CONCLUSIONS . . . . .	125
	APPENDIX A: METHODS FOR DATA REDUCTION . . . . .	129
	APPENDIX B: AN EXAMPLE FOR THE LEAST-SQUARES FITTING . . . . .	133
	REFERENCES . . . . .	137

## LIST OF FIGURES

<u>Figure</u>	<u>page</u>
2.1 (a) Geometrical representation of Eq. (14). (b) Impedance diagram for the system described by Eq. (14). (c) Phase vs. frequency for the system described by Eq. (14); $\omega(90^\circ)$ is given by Eq. (15). (d) Schematic impedance diagram for the shape oscillation of a drop in another liquid.....	21
2.2 Schematic stream line pattern resulting from quadrupole oscillation of a drop in an host; inviscid flow was assumed.....	26
2.3 The ratio of the experimental to the predicted damping as a function of drop radius. The experimental data were taken from the work by Trinh et al. The predictions are given by the simplified model and Marston's theory respectively....	38
2.4 Schematic impedance diagram for the quadrupole oscillation of a drop-host system.....	49
2.5 Phase vs. frequency curves given by the simplified model and Marston's theory respectively: Example for host, water; drop, hexane; drop radius, 0.0825 cm.....	52
3.1 Diagram of apparatus.....	56
4.1 Procedure for introducing superheated liquid drops into the host water in the levitation cell.....	72
4.2 Schematic drawing showing the time variations of (a) the carrier signal ( $\sim 500$ kHz), (b) the modulation signal ( $\sim 50$ Hz), (c) the modulated input ( $v_c \times v_m$ ) responsible for the drop's shape oscillation, (d) acoustic radiation pressure, and (e) the displacement of the drop with a phase assumed to be $90^\circ$ .....	76
5.1 Phase vs. frequency for one experiment which involved no gel in the preparation of the drop.....	87
5.2 Phase vs. frequency for one experiment in which gel was used in the preparation of the drop. ....	91
5.3 Some statistics for the least-squares fitting for $\gamma$ : Example for host, water; drop, hexane; drop radius, 0.0825 cm (referred to figure 5.1 and Table 3).....	97
5.4 Some statistics for the least-squares fitting for $\gamma$ : Example for host, water; drop, hexane; drop radius, 0.0766 cm (referred to figure 5.2 and Table 4).....	98



5.5	Surface tension of propane at various temperatures; curve extrapolated from literature data taken at equilibrium state.....	107
5.6	Variation of frequency with time for three selected phase angles, experiment 0409.....	113
5.7	Variation of drop radius with time for experiment 0409...	114
5.8	Variation of the interfacial tension between water and propane with time for experiment 0409.....	114
5.9	Variation of frequency with time for three selected phase angles, experiment 0411.....	115
5.10	Variation of drop radius with time for experiment 0411...	116
5.11	Variation of the interfacial tension between water and propane with time for experiment 0411.....	116
5.12	Variation of frequency with time for three selected phase angles, experiment 0408.....	117
5.13	Variation of drop radius with time for experiment 0408...	118
5.14	Variation of the interfacial tension between water and propane with time for experiment 0408.....	118
5.15	Comparison between data and Fowkes theory.....	120

## LIST OF TABLES

<u>Table</u>	<u>page</u>
1. Some physical properties of two sample liquids and the host. . .	81
2. Data for one quadrupole oscillation experiment. . . . .	86
3. Fitting for one water-hexane experiment (droplet radius 0.825 mm) . . . . .	97
4. Fitting for one water-hexane experiment (droplet radius 0.766 mm) . . . . .	98
5. Measurements for non-superheated liquids. . . . .	103
6. Variation of damping with viscosity (I). . . . .	104
7. Variation of damping with viscosity (II). . . . .	104
8. Some physical properties of three superheated liquids . . . .	106
9. Measurements for butane and isobutane. . . . .	110
10. Results of levitation technique for compressadensity measurement. . . . .	124

## Chapter 1

### INTRODUCTION

In various fields like physical chemistry, chemical engineering, and fluid mechanics, surface and interfacial tension have long been interesting subjects. They have proven to be of fundamental importance in studies of the properties of solutions, intermolecular forces, molecular orientation on liquid surfaces, colloid phenomena, capillarity, phase transitions, and numerous aspects of theoretical and industrial chemistry. Various methods of measurement have been developed and numerous results of the surface and interfacial tensions of different liquids have been reported in the literature. On the other hand, for the situations where one liquid is in metastable state, say superheated, the traditional methods for measuring interfacial tension are unsuitable and data are unavailable. Also, none of the existing theories has been proved universally applicable in predicting interfacial tensions in various circumstances. In this work we study an experimental technique for measuring interfacial tension and apply it to determine the interfacial tensions between water and each of three superheated liquids. Another bulk property, the compressibility, of the three superheated liquids is also studied using a similar technique.

### 1.1 Interfacial Tension

When a liquid touches another fluid, a boundary forms and a transitional region is established. Generally, we call the contact region an interface if the other fluid is a liquid, or a surface if the other component is a gas. Interfacial and surface tension are natural consequences of the differential attraction force across the transitional region. For example, let us first consider the simpler one, surface tension. In each bulk phase, the molecules are, on the average, subject to a spherically symmetric attractive force field. The force is much stronger in the liquid phase than it is in the vapor or gas phase. Because of the difference in forces, the molecules in the interfacial region are subject to an asymmetric intermolecular attraction. Therefore, work must be done against the attractive forces within the interior of the liquid to bring molecules to the surface region. This work is called the free surface energy and can be defined as the work required to increase a unit surface area at constant temperature. The commonly used dimension of free surface energy or surface tension is ergs per square centimeter or, in SI units, newtons per meter. The potential energy decreases and the stability increases as the surface area decreases. This implies the tendency for the surface to attain a minimum area; this is essentially where the term surface "tension" came from. The transitional region is estimated to be about two molecules thick [1]. Compared with most interesting dimensions in fluid mechanics and certainly in this work, this thickness is so small that the transitional region can be treated as a discontinuity.

The origin of interfacial tension is the same as that of surface tension, except that it is concerned with both cohesive forces between similar molecular species, and adhesive forces between two different species. The magnitude of the cohesion and adhesion could be comparable. It is reasonable to expect that the interfacial tension  $\sigma_{AB}$  between liquids A and B will be no more than  $\sigma_A + \sigma_B$ , where  $\sigma_A$  and  $\sigma_B$  are the surface tensions against their vapors of liquids A and B.  $\sigma_{AB}$  will equal  $\sigma_A + \sigma_B$  if adhesion is negligible. Therefore, in general, the increase of similarity in structure between two liquid species is reflected in a smaller value of interfacial tension and a greater tendency for mutual molecular dispersion, that is, miscibility. The interfacial tension must be positive for the stable existence of an interface.

## 1.2 Traditional Methods for Interfacial Tension Measurements

The methods of measuring surface and interfacial tension may be generally divided into two classes, dynamic and static. In the dynamic methods, the interface periodically expands and contracts, and the interfacial tension operates to restore the interface to a minimum area. By measuring the parameters of the periodic motion, such as the frequency, the interfacial tension can be calculated. The ones mentioned in the literature involve the method of oscillating jets, oscillating drops, and ripples [1]. In the static methods, quiescent interfaces are involved, and the interfacial tension plays the role of balancing other forces on the interface due to either the gravitational

field or the pressure differential across the interface. The capillary-height method, the ring detachment method, and the drop-weight method are three examples [1].

In general, dynamic methods do not give results as reproducible and consistent as static methods. Also, the results obtained by dynamic methods do not generally agree with those obtained by static methods. This discrepancy is especially significant when either of the two liquids is a solution of surface active solutes. When a solution is in equilibrium, the composition in the interfacial region is different from that in the bulk phase. The true interfacial tension can be obtained only when all involved liquids are in equilibrium. Therefore, if the time required by the diffusion of the solute molecules to establish the state of equilibrium is significant compared to the time scale of measurement, dynamic methods can not give the true interfacial tension [2] [1].

### 1.3 Superheated Liquids

At atmospheric pressure, 100°C is referred to as the normal boiling point of water. It is also known that, under the same pressure, there are circumstances in which water can be heated beyond 100°C without boiling; we call water in this state "superheated". A superheated liquid is one particular instance of a metastable state of matter. In thermodynamics, the stable states of matter are separated by equilibrium lines in pressure-temperature coordinates. Matter that starts from a

stable state and transgresses an equilibrium line without phase conversion enters a metastable state. How far the state deviates from equilibrium is characterized by the depth of penetration--the corresponding temperature or pressure difference. A metastable state can survive for a very long time even under large variations in the thermodynamic parameters. On the other hand, the metastable state may revert to a stable phase if that phase (like vapor bubbles in the above example of superheated water) is introduced in some way into the metastable state.

Generally, phase transitions can be either of two types. The first type is homogeneous nucleation. This happens if the nucleus of the new phase arises spontaneously due to thermal fluctuations and intermolecular interactions. But usually the phase transition starts at the walls of the container or on foreign inclusions. This type of process, called heterogeneous nucleation, requires a much lower degree of superheat [3]. Therefore, one expects that a difficulty in experimental studies of superheated liquids is the prevention of heterogeneous nucleation. Metastable liquids are of interest in fields like molecular physics and in problems such as the study of the initial stage of phase transition, where the interfacial or surface tension is a very important parameter. The vaporization of superheated liquids may be explosive in character. One of the motivations for this work is that the unintentional contact of a cold liquid, like liquified natural gas (LNG), with a much warmer stable liquid, like water, may cause dramatic vapor explosions [4]. The interfacial tension may be needed in modeling

this phenomenon if the superheat mechanism is assumed to be the initiator of the physical explosion.

#### 1.4 Acoustic Levitation

To measure the interfacial tension between water and a superheated liquid, most of the commonly used techniques have to be ruled out because of the involvement of solid surfaces which would trigger the vaporization of the superheated liquid. The idea of oscillating drops seems to be the natural choice. If we can put a drop of a superheated liquid (say a hydrocarbon) into an immiscible "host" liquid (say water), then the host will act as a very smooth and clean container for the drop, thereby reducing the probability of the presence of solid heterogeneous nucleation sites. If a hydrocarbon drop oscillates in water, then the interfacial tension which provides the restoring force in the interfacial disturbances could be inferred from some measurements of the oscillation.

The method which we use to introduce a superheated hydrocarbon drop into water will be described in chapter 4. But, how do we excite the drop into oscillation and take measurement of the oscillation? Acoustic levitation is a very appropriate technique for this situation [5]. A strong acoustic standing wave can be established in a host liquid, water in this work, and produce an acoustic force on an immersed drop. By adjusting this force to balance the gravitational force on the drop, acoustic levitation is achieved. Several features of acoustic



levitation are particularly useful in this experiment. First of all, the host water is a very good container for the superheated drop as mentioned above. Secondly, the drop can be held in water very steadily in a certain position. In the traditional method of oscillating drops, measurements have to be made while the drops are rising or falling. So acoustic levitation allows accurate measurements of the drop's size and oscillation frequency with comparative ease. Furthermore, another acoustic wave can be coupled into the system, providing a means to excite the drop into oscillations without touching the drop with any solid object.

The acoustic force exerted on a levitated drop is a known function of the densities and compressibilities of the drop and host liquids. By a simple technique of comparing the voltages needed to levitate two drops of different liquids, one as a reference and the other one as an unknown, at the same position, the parameter "compressadensity" of the unknown liquid can be obtained providing that the properties (density and compressibility) of both the reference and host liquids are known [5]. Compressadensity is a known function of density and adiabatic compressibility as expressed in Eq. (60), therefore, if we know the density, then the compressibility can be calculated. This compressadensity of a superheated liquid can also be obtained when the interfacial tension is measured. It, too, is difficult to measure by other methods and provides additional thermodynamic data in temperature regimes where little data exist (e.g. [6]).

### 1.5 Oscillations of a Spherical Drop

To evaluate the interfacial tension between a levitated drop and its host liquid, we need a model relating the interfacial tension with other parameters, such as the oscillation frequency, the size of the drop and the densities and viscosities of the drop and host liquids. The equilibrium shape of the drop should be approximately spherical, since the gravitational and acoustical forces in this experiment are insignificant compared to the interfacial forces. For the frequencies and the drop deformations in this work, the drops behave incompressibly. Therefore, the disturbance of the interface is accompanied by the drop's shape oscillation about a spherical shape without volume change. The quadrupole mode (alternatively prolate and oblate), which is the simplest mode of shape oscillation, is studied in this experiment.

The small oscillations of a liquid mass about its spherical equilibrium shape was derived by Rayleigh [7]. Lamb generalized the problem by supposing that the liquid drop was surrounded by an infinite mass of another liquid [8]. The liquids were assumed inviscid by both authors so that viscosity did not enter their expressions for the oscillation frequency. Lamb also discussed the effect of small viscosity on the small oscillations of a mass of liquid about the spherical form; no host liquid was included in this calculation [8]. Miller and Scriven [9] did an analysis of small oscillations of a viscous fluid droplet immersed in another viscous fluid. The frequency and rate of damping of free oscillations were derived for arbitrary values of the physical properties of the fluids as well as interfacial

viscosity and elasticity coefficients. Marston [10] independently derived the same general results for free oscillations, and found a new term to correct the decay time. The phase-frequency relation for forced oscillation was also established for the first time in this work of Marston.

On the experimental side, Marston and Apfel have measured the interfacial tension between water and p-xylene [11]. The p-xylene drops were levitated in water and excited into quadrupole shape oscillations by acoustic forces. The oscillations were detected by a rainbow photometry technique which utilized light scattered by a drop at the scattering angle normally associated with the rainbow. The interfacial tension obtained was 4% lower than static measurements with an uncertainty of about 10%. Trinh, Zwern, and Wang [12] have done experimental studies of drop oscillations with emphasis on the frequencies of the first few modes and the damping constant for the fundamental (quadrupole) mode. They used a slit and the shadow of the uniformly illuminated drop to detect the oscillation.

Viscosity, which causes energy dissipation, should relate to the damping of the drop oscillation. In his theory, Marston gave a relation between a measured damping constant and the viscosities of the two liquids, though the experiment data for p-xylene drops in water did not show very good agreement with it [11].

### 1.6 Fowkes' Equation for Interfacial Tension

There is a need for a theory that predicts the interfacial tension between two liquids based on some other properties such as the surface tensions of each liquid against its vapor. Unfortunately, there has not been a theory that can be satisfactorily applied to all different cases. Here, we briefly introduce a semi-empirical model developed by Fowkes [13] for water-hydrocarbon interfaces. Fowkes' model has been widely used, though it is also criticized by some people (e.g. [14]).

The interfacial tension  $\sigma_{AB}$  between liquid A and B is the work needed to expand one unit area of the interface by bringing molecules A and B from the interior to the interface. It may be regarded as the sum of the work for overcoming the cohesion between similar molecules of each liquid minus the work done by adhesion between the two different species across the interfacial region. So

$$\sigma_{AB} = \sigma_A + \sigma_B - W_{AB},$$

where  $W_{AB}$  is the work done per unit area by the adhesion or, equivalently, the increase in free surface energy upon separating the interface AB. There are different kinds of intermolecular forces such as the London dispersion force, dipole-dipole force, and hydrogen bonding. For the water-hydrocarbon system, Fowkes assumed that the interaction between water and hydrocarbon molecules is only due to the dispersion force, since the hydrocarbon molecules are non-polar. The geometric mean was applied to give  $W_{AB}$ , so that

$$\sigma_{WH} = \sigma_W + \sigma_H - 2(\sigma_W^d \cdot \sigma_H)^{\frac{1}{2}} \quad (1)$$

where the subscripts W and H represent water and hydrocarbon respectively, and the superscript d stands for dispersion part of the intermolecular force, For hydrocarbons  $\sigma_H^d = \sigma_H$ . For water  $\sigma_W = \sigma_W^h + \sigma_W^d$  where the superscript h denotes the intermolecular force due to hydrogen bond. The value of  $\sigma_W^d$  was given as  $21.8 \pm 0.7$  dyne/cm according to Fowkes' calculation based on the literature data of the interfacial tensions between water and each of eight kinds of hydrocarbons.

The data obtained in the experiments described in this manuscript will provide additional tests of the applicability of different theories of interfacial tension, such as Fowkes'. It should supplement the existing interfacial tension data in a region never before investigated, and could in the future be useful in the development of more accurate models of liquid-liquid interfaces.

### 1.7 Purpose and Scope

The purpose of this study is to obtain experimentally the interfacial tension between water and each of three superheated liquids, butane, isobutane, and propane, at room temperature and atmospheric pressure. The data and method of this work may have applications in different areas. For example, as discussed before, they may be important in modeling the early stage of the phase transition (vapor explosion) of these superheated liquids in contact with water. Also the data may be useful in testing or developing models on interfacial tension. In addition to interfacial tension, measurements of the compressibilities

of the superheated liquids will be reported, thereby providing data on this thermodynamic property previously unavailable in the literature.

The technique developed for this experiment is based on the shape oscillations of one liquid drop in another liquid--the host. The method developed by Marston and Apfel [11] has been modified to fit this special circumstance and to improve the accuracy. The detection of the drop's oscillation is adapted from the work of Trinh, Zwern, and Wang [12].

A simplified model for the quadrupole oscillation of a drop in another liquid will be presented in chapter 2. The purpose is to reveal the physical nature of the problem more explicitly while appealing to less sophisticated mathematics. The simplified model will also be compared with the previous theories.

In the next chapter, we begin with a review of the previous theories on the shape oscillation of a drop. A simplified model is then developed. This chapter ends with the equations needed for the compressadensity measurement employing the established acoustic levitation technique. In chapter 3 and 4 we describe the experimental equipment and procedures respectively. Then we present and discuss the experimental results in chapter 5. Finally, chapter 6 will include a summary and conclusions of this work.

## Chapter 2

### THEORY

In this chapter we discuss the theoretical model which we use, in conjunction with experimental measurements, to determine interfacial tension. We first describe the problem and basic assumptions. We then review several previous theories for the oscillation of a drop in another fluid. Most of this chapter is devoted to the derivation of a simplified model which we developed for computing the damping of a freely oscillating drop and the phase-frequency relation of the forced oscillation of a drop in its quadrupole mode (section 2.3). The chapter ends with a brief review of equations used in the acoustic levitation technique for measuring compressadensity..

#### 2.1 Problem and Basic Assumptions

The physical phenomena of the method of oscillating drops for measuring interfacial tension can be simplified and described as a drop, which is immersed in another fluid and has a spherical equilibrium shape, undergoes shape oscillation with small amplitude, under the following assumptions:

- 1) The gravitational force and the levitational acoustic force on the drop balance each other, and their effects on the equilibrium shape of the drop are negligible compared with the interfacial tension.

Therefore, the drop has no steady motion relative to the host fluid, and the drop is spherical at equilibrium.

2) The drop behaves incompressibly; thus there is no volume change but only shape change accompanies the oscillation.

3) The interface is free from surface active contaminants, and the interfacial tension is a constant, uniform value.

4) The amplitude of the shape oscillation is so small that the response of the drop-host system is linear with the driving force.

5) The liquids of the drop and the host are immiscible, so that there is negligible mass transport across the interface. The interface is so thin (see section 1.1) that it may be considered as a two-dimensional discontinuity; the physical properties of the fluids on each side of the interface are uniform.

## 2.2 Previous Theories for Shape Oscillations of a Drop

For analyzing the above problem of an oscillating drop in a host, several previous theories are relevant and are briefly reviewed in this section. We first review some theories in which both the drop and host liquids were assumed inviscid. We then review some theories in which small viscosity of both the liquids were assumed.

### 2.2.1 Drop and Host Liquid of Negligible Viscosity

#### 2.2.1.1 Resonance Frequency



Rayleigh [7] investigated small oscillations of a liquid mass about its spherical shape of equilibrium, and obtained the resonance frequency

$$\omega = \left[ \frac{n(n-1)(n+2)\sigma}{\rho R^3} \right]^{\frac{1}{2}}, \quad (2)$$

where  $\omega$  is the angular frequency,  $n$  is the mode,  $\sigma$  is the surface tension,  $\rho$  is the density of the liquid, and  $R$  is the radius of the drop at equilibrium. The host medium and viscosity were not considered, which may be an acceptable approximation in studying, say, a water drop in air.

Lamb [8] later discussed the small oscillations of a liquid drop about its spherical form, and generalized the question by supposing that the drop is surrounded by an infinite mass of another liquid. He obtained the following resonance frequency:

$$\omega^* = \left[ \frac{n(n+1)(n-1)(n+2)\sigma}{\{(n+1)\rho_i + n\rho_o\}R^3} \right]^{\frac{1}{2}}, \quad (3)$$

where  $\omega^*$  is the angular frequency,  $n$  is the mode,  $\sigma$  is the interfacial tension,  $\rho_i$  and  $\rho_o$  are the densities of the inner (drop) and outer (host) liquid respectively, and  $R$  is the mean radius of the drop. When  $\rho_o$  is negligible compared with  $\rho_i$ , Eq. (3) is equivalent to Eq. (2). The viscosities of the two liquids were ignored in the derivation of Eq. (3). The calculated values of  $\omega^*$  are higher than the measured resonance frequency, for example, by about 10% for a p-xylene drop of mm size in water [11], where both liquids are similar in density and in viscosity.

### 2.2.1.2 Damping

Lamb [8] also discussed the effect of small viscosity on the small oscillation of a liquid drop. Assuming that the motion is irrotational and the velocity potential of inviscid flow is applicable, he calculated the energy dissipation and gave the damping constant:

$$\frac{1}{s} = \frac{R^2}{(n-1)(2n+1)\nu} \quad (4)$$

where  $s$  is the damping constant and  $\nu$  is the kinematic viscosity of the liquid of the drop. The damping constant is defined in such a way that if  $A$  is the amplitude of a damped oscillation,  $t$  is the time, then  $A \propto e^{-ts}$ . Eq. (4) ignores the host medium, which is reasonable if the host is a gas of negligible density and viscosity.

Lamb also derived the damping for a spherical bubble in a liquid with viscosity  $\nu$  by a similar method:

$$\frac{1}{s} = \frac{R^2}{(n+2)(2n+1)\nu} \quad (5)$$

For a quadropole mode,  $n=2$ , this equation gives an  $s$  that is four times the  $s$  of Eq.(4).

### 2.2.2 Drop and Host of Viscous Liquids

Miller and Scriven [9] gave a rather comprehensive analysis of a viscous drop immersed in another viscous fluid, by which the frequency and rate of damping of free oscillations can be calculated for arbitrary values

of drop size, physical properties of the fluids, and interfacial viscosity and elasticity coefficients.

Marston [10] independently derived similar results for free oscillation of a drop for a situation in which both drop and host liquids have small viscosity so that the "viscous wavelength" at each side of the interface is much smaller than the radius of the drop. He found a new term to correct the decay time for free oscillation. Also, for the first time, Marston derived the phase-frequency relation for forced oscillation of a drop immersed in another fluid. In his theory, the damping constant for free oscillation is given as

$$s = (41)\omega^{* \frac{1}{2}} + \frac{1}{2}\gamma - \frac{1}{2}\alpha^2 \quad (6)$$

For forced oscillation, the phase-frequency is given as

$$\tan \xi = (\alpha \omega^{3/2} + \gamma \omega) / (\omega^{*2} - \alpha \omega^{3/2} - \omega^2) \quad (7)$$

Here,

$$\alpha = \frac{(2n+1)^2 (\mu_i \mu_o \rho_i \rho_o)^{\frac{1}{2}}}{2^{\frac{1}{2}} R \Gamma [(\mu_i \rho_i)^{\frac{1}{2}} + (\mu_o \rho_o)^{\frac{1}{2}}]} \quad (8)$$

$$\gamma = \frac{(2n+1) \{ 2(n^2-1) \mu_i^2 \rho_i + 2n(n+2) \mu_o^2 \rho_o + \mu_i \mu_o [(n+2) \rho_i - (n-1) \rho_o] \}}{R^2 \Gamma [(\mu_i \rho_i)^{\frac{1}{2}} + (\mu_o \rho_o)^{\frac{1}{2}}]^2} \quad (9)$$

and

$$\Gamma = (n+1) \rho_i + n \rho_o \quad (10)$$

In the above equations,

$s$  = damping constant of the free oscillation (see Eq.(4)),

$\omega^*$  = Lamb's natural frequency, as given in Eq. (3),

$\xi$  = the phase of the displacement relative to the driving force in the forced oscillation,

$\omega$  = the frequency associated with phase  $\xi$ ,

$n$  = the mode,

$\rho_i$  = the density of the inner (drop) fluid,

$\rho_o$  = the density of the outer (host) fluid,

$\mu_i$  = the dynamic viscosity of the inner (drop) fluid,

$\mu_o$  = the dynamic viscosity of the outer (host) fluid, and

$R$  = the radius of the drop in spherical form.

Marston further approximated Eq. (7) by applying Newton's method of iteration and obtained the following expressions:

$$\begin{aligned}\omega(90^\circ) &\approx \omega^* - (\alpha/2)\omega^{*1/2} + \alpha^2/4 \\ &\approx \omega^* - s\end{aligned}\quad (11)$$

$$\begin{aligned}\omega(\xi) &\approx \omega(90^\circ) - s/\tan\xi + \alpha^2/(2\tan\xi)^2 \\ &\approx \omega(90^\circ) - s/\tan\xi\end{aligned}\quad (12)$$

Eqs. (11) and (12) were used directly in calculating the interfacial tension in the experimental work done by Marston and Apfel [11] in the following way (also see section 5.2). The damping constant  $s$  was given by Eq. (12) with measured  $\omega(\xi)$  and  $\omega(90^\circ)$ , and  $\omega^*$  was then obtained via Eq. (11). With this  $\omega^*$  substituted in Eq. (3), the interfacial tension  $\sigma$  was obtained.

### 2.3 A Simplified Model for Shape Oscillation of a Drop

Eqs. (2) and (3), though straightforward in derivation, can not accurately describe the oscillation of a liquid drop in another host liquid due to the neglect of viscosity. On the other hand, Eqs. (6) and (7) show much better agreement with experiments, but the derivation is rather lengthy and complicated. With the purpose of revealing the

physical nature of this problem more explicitly and appealing to less sophisticated mathematics, we developed a simplified model. The basic idea and the derivation are described in this section.

### 2.3.1 Analogy with the Basic Mass and Spring System

Although the motion of the small oscillation of a drop in a host fluid in a certain mode is three-dimensional, there is only one degree of freedom. Let us compare this drop-host system with a basic mass-spring system.

#### 2.3.1.1 Resonance Frequency of a Mass and Spring System

For an object of mass  $m$  acted on by a spring of spring constant  $k$ , without driving force, the equation of motion is

$$m \frac{d^2x}{dt^2} + kx = 0 ,$$

where the  $x$  is the displacement of the mass relative to its equilibrium position. The natural frequency is then

$$\omega = (k/m)^{1/2}. \quad (13)$$

When this mass-spring system is subject to a resistive force, proportional to velocity, and is driven by a force  $F_0 \cos(\omega t)$ , the equation of motion becomes:

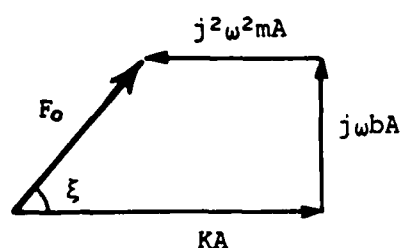
$$m \frac{d^2x}{dt^2} + b \frac{dx}{dt} + kx = F_0 \cos \omega t. \quad (14)$$

The resonance frequency, if we define it as the frequency with  $90^\circ$  phase angle, has the same form as that given in Eq. (13):

$$\omega(90^\circ) = (k/m)^{1/2} . \quad (15)$$

Notice that the damping term  $b$  does not appear in Eq. (15), therefore, the spring constant  $k$  can be obtained by knowing only  $\omega(90^\circ)$  and  $m$ . The phase-frequency relation may be illustrated more explicitly by an schematic impedance diagram shown in Fig. 2.1(b), accompanied by a vector representation of Eq. (14) in Fig. 2.1(a), and with a typical phase-frequency diagram in Fig. 2.1(c) [15]. In Fig. 2.1(b), the component due to damping,  $j\omega b$ , has a phase angle of  $90^\circ$ ; this fact is responsible for the resonance frequency,  $\omega(90^\circ)$ , being independent of the damping coefficient  $b$ .

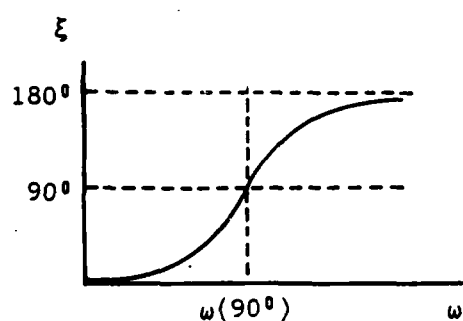
assume  $x = A \cdot \cos(\omega t + \xi)$



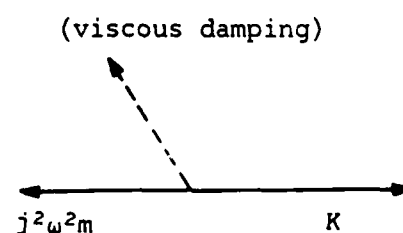
(a)



(b)



(c)



(d)

Figure 2.1: (a) Geometrical representation of Eq. (14).

(b) Impedance diagram for the system described by Eq. (14).

(c) Phase vs. frequency for the system described by Eq. (14);  $\omega(90^\circ)$  is given by Eq. (15).

(d) Schematic impedance diagram for the shape oscillation of a drop in another liquid.

### 2.3.1.2 The Shape Oscillation of a Drop in Another Liquid

Let us consider the analogy between a mass-spring system and a drop-host system. The interfacial tension, which we want to measure in the experiment, is equivalent to the spring, providing the restoring force. The equivalent mass of the drop-host system should be a function of the densities of the two fluids and the size of the drop. The damping is due to the viscous dissipation in the drop and host fluid.

For the free oscillation of a drop-host system without damping, the natural frequency is given by Eq. (3). For the quadrupole mode,  $n=2$ , we have

$$\omega^* = \left[ \frac{24\sigma}{R^3(3\rho_i + 2\rho_o)} \right]^{1/2}. \quad (16)$$

Eqs. (16) and (13) show clearly the analogy between the drop-host system and the mass-spring system. However, when the viscosity of the two fluids is non-negligible, due to the nature of the viscous damping in liquid, the resonance frequency  $\omega(90^\circ)$  is no longer the same as the  $\omega^*$  in Eq. (16). The  $\omega(90^\circ)$  is not only a function of stiffness  $k$  and mass  $m$ , but also a function of viscosity,

$$\omega(90^\circ) = \text{function}(k, m, \text{viscosity}).$$

The above function has to be derived, which is the essential goal of our simplified model. The impedance diagram for a drop-host system may be something like the one shown in Fig. 2.1(d).



### 2.3.2 Velocity Profile for an Inviscid Drop in an Inviscid Host

For simplicity, all the following expressions are for oscillations in the quadrupole mode only. Nevertheless, the method can be applied similarly to other modes. Spherical coordinates with polar angle  $\theta$  and radius  $r$  are used to describe the motion. Due to the symmetry with respect to the vertical axis through the center of the spherical drop, expressions are independent of the azimuthal angle.

For small quadrupole oscillation about a spherical form, the radial position of the interface,  $r$ , at any instant may be given as [8] [7]:

$$r = R_0 + \epsilon Y_2(\theta) \sin(\omega t). \quad (17)$$

where

$r$  = the radial position of the interface relative to the center of the equilibrium sphere,

$R$  = the equilibrium radius,

$R_0$  = a value close to but not equal to the equilibrium radius  $R$

$$= R \left[ 1 + \frac{4\epsilon^2}{5R^2} \right]^{-1}, \quad (18)$$

$\epsilon$  = the amplitude of the oscillation,

$\omega$  = the angular frequency,

$Y_2(\theta)$  = spherical harmonic function of order 2

$$= 3\cos^2\theta - 1.$$

The spherical harmonic function of order  $n$  satisfies the Laplace equation in the following way:

$$\nabla^2(r^n Y_n) = 0, \quad \nabla^2(r^{-n-1} Y_n) = 0.$$

Assuming the flow is inviscid, we have the velocity potential which is determined by the boundary condition in Eq. (17), at the internal points [8],

$$\phi_i = - \frac{\omega R}{2} \frac{r^2}{R^2} \varepsilon Y_2(\theta) \cos(\omega t) , \quad (19)$$

and, at the external points,

$$\phi_o = - \frac{\omega R}{3} \frac{R^3}{r^3} \varepsilon Y_2(\theta) \cos(\omega t) , \quad (20)$$

We use subscripts i and o to denote the terms related to the inner (drop) and the outer (host) flow, respectively.

The corresponding velocity distribution is readily obtained from the velocity potential,

$$\vec{u} = u_r \vec{e}_r + u_\theta \vec{e}_\theta = -\nabla \phi , \quad (21)$$

where the subscripts r and  $\theta$  denote the components in the direction of r and  $\theta$  respectively. From Eqs. (19), (20), and (21), the radial and tangential component of the flow velocity in the inner and outer region are:

$$u_{ri} = (1/R) \varepsilon \omega r (3 \cos^2 \theta - 1) \cos(\omega t) , \quad (22)$$

$$u_{\theta i} = (-3/2R) \varepsilon \omega r \sin(2\theta) \cos(\omega t) , \quad (23)$$

$$u_{ro} = (R/r)^4 \varepsilon \omega (3 \cos^2 \theta - 1) \cos(\omega t) , \text{ and} \quad (24)$$

$$u_{\theta o} = (R/r)^4 \varepsilon \omega \sin(2\theta) \cos(\omega t) . \quad (25)$$

Fig. 2.2 shows a schematic diagram of the streamlines at a certain instant when the drop is moving from a spherical shape toward a prolate shape.

For very small amplitude  $s$ , the velocity at the interface may be considered as the value of the above functions evaluated at  $r=R$ . Notice that the radial velocity is continuous across the interface as expected,

$$\left. \frac{\partial r}{\partial t} \right|_{r=R} = U_{ri} = U_{ro} = \varepsilon \omega (3 \cos^2 \theta - 1) \cos(\omega t) , \quad (26)$$

where  $U_{ri}$  and  $U_{ro}$  are the values of  $u_{ri}$  and  $u_{ro}$  evaluated at  $r=R$  respectively. But the tangential velocities at the two sides of the interface are opposite in direction and have their magnitudes related as:

$$\begin{aligned} U_{\theta i} &= - (3/2) U_{\theta o} \\ &= - (3/2) \varepsilon \omega \sin(2\theta) \cos(\omega t) , \end{aligned} \quad (27)$$

where  $U_{\theta i}$  and  $U_{\theta o}$  are the values of  $u_{\theta i}$  and  $u_{\theta o}$  evaluated at  $r=R$  respectively.

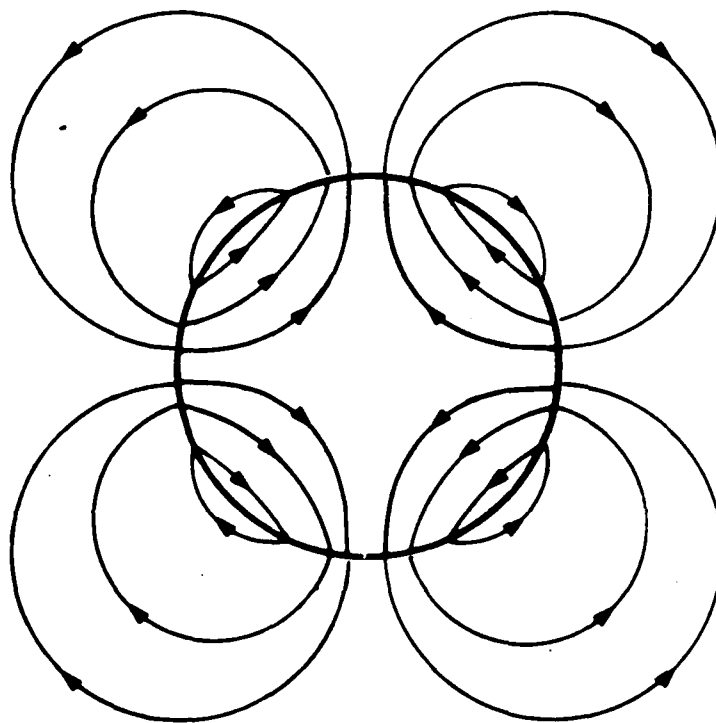


Figure 2.2: Schematic stream line pattern resulting from quadrupole oscillation of a drop in an host; inviscid flow was assumed.

### 2.3.3 A Modified Velocity Distribution with Small Viscosity

The velocity distribution predicted by the velocity potential of inviscid flow, as shown in Fig. 2.2, is found to agree with the outcome of a qualitative photographic study done by Trinh, Zwern, and Wang [12]. On the other hand, the discontinuity of the tangential velocity across the interface can not be true physically. This velocity "jump" has to be smoothed out by viscosity.

We assume the viscosities of both inner and outer fluid are small, so that the boundary layer thickness (or viscous wavelength) at each side of the interface is smaller than, say,  $1/10$  of the radius of the drop. Then we may model the flow distribution in an ad hoc way by combining a thin boundary layer at each side of the interface with the potential flow, derived on the inviscid assumption, at all points other than the boundary layer. Based on this approximate flow distribution, we compute the damping rate and the phase-frequency relation.

To consider the flow in the boundary layer around the interface, we take a rather simple approach. We first estimate the tangential velocity of the interface,  $u_s$ , and then consider the boundary layer at each side of the interface separately as a consequence of an enforced oscillation of a solid boundary.

#### 2.3.3.1 Tangential Component of the Interfacial Velocity

If we assume that there is no pure rotation associated with this oscillation, then the interface should oscillate in phase with the potential flow, as does  $u_s$ --the tangential component of the velocity of the interface. Physically, we know that the amplitude of  $U_s$  must be in between  $U_{\theta i}$  and  $U_{\theta o}$ . The ratio  $U_s/U_{\theta i}$  or  $U_s/U_{\theta o}$  should be determined by the following two factors: 1) The momentum carried by the "external stream", which is a function of the density and velocity. 2) The diffusivity of momentum, that is, the viscosity.

Assume that for the tangential velocity in the boundary layer the gradient in radial direction is much greater than the gradient in tangential direction. In other words, the boundary layer thickness is much smaller than, say, a quarter of the circumference of the space. Then, locally, we may approximate the flow in the boundary layer as a stream of viscous, incompressible fluid over a parallel stream of different density and viscosity. Also, to a first approximation, we may use  $U_{\theta i}$  and  $U_{\theta o}$  as the "external stream velocities". Under these approximation, the results of the work "The Velocity Distribution in the Laminar Boundary Layer between Parallel Stream" done by Lock [16] can be applied to compute the  $U_s$  as follows:

$$c \equiv \frac{U_s}{U_{\theta i}} = \frac{\lambda + (\delta/\mu)}{1 + (\delta/\mu)}, \quad (28)$$

$$\frac{\delta}{\mu} = \left[ \frac{1.425\lambda + 0.858}{2.283\lambda\rho\mu} \right]^{1/2}, \quad (29)$$

$$\text{where } \lambda = \frac{U_{\theta o}}{U_{\theta i}} = -\frac{2}{3} \text{ (see Eq. (27))}, \quad \delta = \frac{\delta_o}{\delta_i}, \quad \rho = \frac{\rho_o}{\rho_i}, \quad \mu = \frac{\mu_o}{\mu_i},$$

$\delta$  denotes boundary layer thickness,  $\rho$  denotes density, and  $\mu$  denotes dynamic viscosity. The value  $c$  given in Eq. (28) depends upon the velocity, density, and viscosity of the two parallel streams, as expected\*. With a given  $U_s$ , the boundary layer at each side of the interface can be modeled as the flow over an oscillating boundary, as described in the next subsection.

#### 2.3.4 Damping of Free Oscillation

In this subsection we discuss the damping rate of the free oscillation of a drop immersed in another fluid, making use of the flow distribution described in section 2.3.3. The resultant damping rate is expressed in terms of known parameters including the inner and outer density,  $\rho_i$  and  $\rho_o$ ; the inner and outer viscosity,  $\mu_i$  and  $\mu_o$ ; the radius of the drop  $R$ ; and the oscillation frequency  $\omega$ . The result will be used in the derivation of phase-frequency relation.

---

\* We give two extreme cases as examples for Eq. (28)

a) For a water drop in air,  $\lambda = -(2/3)$ ,  $\rho\mu = (\rho_o\mu_o)/(\rho_i\mu_i) \approx 2 \times 10^{-5}$ ,

$(\delta/\mu) \gg 1$ , then  $c \approx 1.0$ , which means that  $U_s$  is very close to  $U_{\theta i}$ , the tangential velocity of the water surface.

b) For an opposite case of an air bubble in water,  $\lambda = -(2/3)$ ,  $\rho\mu \approx 6 \times 10^4$ ,

$(\delta/\mu) \ll 1$ ,  $c \approx \lambda = -(2/3)$ , which means that  $U_s$  is very close to  $U_{\theta o}$ , the tangential velocity of the surface of the water host.

The damping rate is a function of the instantaneous total energy of the system and the rate of dissipation at that instant, as governed by the following expression:

$$\frac{d}{dt} (\text{total energy}) = (\text{rate of dissipation}) .$$

In the problem of an oscillatory drop in a host, the total energy T.E. is the sum of the instantaneous potential energy P.E. and kinetic energy K.E. The potential energy is a function of the interfacial tension, and the change of the interfacial area. The kinetic energy is a function of the density and the flow distribution. The energy dissipation is due to the viscous dissipation in the boundary layer near the interface and in the potential flow at the other points.

The viscous dissipation may be considered as the sum of the following four parts:

- 1) the dissipation in the inner irrotational flow,
- 2) the dissipation in the outer irrotational flow,
- 3) the dissipation in the inner boundary layer, and
- 4) the dissipation in the outer boundary layer.

#### 2.3.4.1 Dissipation in the Inner Irrotational Flow

The dissipation in a spherical mass of fluid with radius  $r$ , calculated on the assumption that the motion is irrotational, is, by art. 355 of [8],

$$\mu \iint \frac{\partial u^2}{\partial r} r^2 d\Omega = \mu r^2 \frac{\partial}{\partial r} \iint u^2 d\Omega , \quad (30)$$



where  $u^2 = u_r^2 + u_\theta^2$ ,  $\Omega$  denotes the solid angle, and  $d\Omega = 2\pi \sin\theta d\theta$ . Velocity  $u$  can be expressed in terms of velocity potential  $\phi$ , and the following relation is applied,

$$\iint u^2 d\Omega = \frac{1}{r^2} \frac{\partial}{\partial r} \iint \phi \frac{\partial \phi}{\partial r} r^2 d\Omega. \quad (31)$$

We substitute Eqs. (19) and (31) in Eq. (30), take the time average over one period  $2\pi/\omega$ , which yields for the  $\cos^2(\omega t)$  term a result of  $\frac{1}{2}$ , then evaluate Eq. (30) at  $r = R$ . The result is

$$\frac{\omega}{2\pi} \int_{t=0}^{2\pi/\omega} dt \mu \iint \frac{\partial u^2}{\partial r} r^2 d\Omega = 8\pi\mu_i \varepsilon^2 R \omega^2. \quad (32)$$

The above expression gives the dissipation in the irrotational flow in the drop, on the assumption that the amplitude of oscillation and the boundary layer thickness are much smaller than the radius of the drop.

#### 2.3.4.2 Dissipation in the Outer Irrotational Flow

The same method can be applied to the irrotational flow outside the drop and gives the rate of dissipation, averaged over one period  $2\pi/\omega$  as:

$$(64/3)\pi\mu_o \varepsilon^2 R \omega^2. \quad (33)$$

#### 2.3.4.3 Dissipation in the Inner Boundary Layer

In an oscillatory boundary layer, the time average, over one cycle, of the rate of dissipation in the boundary layer per unit area of the surface (boundary) is, as given in [17],

$$\frac{\mu U^2}{2\delta}, \quad (34)$$

where  $U$  is the amplitude of the oscillatory velocity of the irrotational flow outside the boundary layer (external stream velocity), and  $\delta$  is the boundary layer thickness. The boundary layer thickness goes up with the viscosity (diffusivity of momentum) and with the time that the diffusion of momentum takes place. We approximate the boundary layer thickness

as:  $\delta = (2\nu/\omega)^{1/2}$  [17]. Suppose the boundary layer thickness is much smaller than the radius of the drop, so Eq. (34) is applicable and the amplitude of the "external stream velocity" may be approximated by

$U_{\theta i} - U_s$ .  $U_s$  is the tangential velocity of the interface and  $U_s = cU_{\theta i}$  (see Eq. (28)). On making use of Eqs. (23), (28), and (34), integrating over the interface  $r=R$ , we have the rate of dissipation in the inner boundary layer as:

$$\iint \frac{\mu(1-c)^2[(3/2)\epsilon\omega\sin(2\theta)]^2}{2(2\nu_i/\omega)^{1/2}} dA = \frac{12\pi(1-c)^2\mu_i\epsilon^2R^2\omega^{5/2}}{5(2\nu_i)^{1/2}}. \quad (35)$$

#### 2.3.4.4 Dissipation in the Outer Boundary Layer

Again, assuming that the outer boundary layer is much thinner than the radius of the drop and the amplitude of the external stream velocity may be approximated by  $U_{\theta o} - U_s$ , making use of Eqs. (25), (27), (28), and (34), we apply the same method as that in the above paragraph and obtain the time averaged rate of dissipation in the outer boundary layer

$$\iint \frac{\mu_o(1+1.5c)^2\epsilon^2\omega^2(\sin 2\theta)^2}{2(2\nu_i/\omega)^{1/2}} dA = \frac{16\pi(1+1.5c)^2\mu_o\epsilon^2R^2\omega^{5/2}}{15(2\nu_o)^{1/2}}. \quad (36)$$

#### 2.3.4.5 The Total Energy of the Oscillation

The total energy at any instant is the sum of the instantaneous potential and kinetic energy. The kinetic energy reaches its maximum value, while the potential energy is (set) zero (see section 2.3.5.2), at, say,  $t=0$  in Eq. (17). We take this maximum kinetic energy as the total energy of the drop-host system in oscillation. Kinetic energy is a function of velocity and, therefore, is a function of velocity potential [17],

$$\begin{aligned} \text{K.E.} &= \frac{1}{2}\rho \iint \phi \vec{u} \cdot \vec{n} dA \\ &= \frac{1}{2}\rho \iint \phi u_r dA . \end{aligned}$$

The velocity potential with an assumed amplitude is given in Eqs. (19) and (20). Based on the same velocity potential, we calculated the rate of dissipation in the previous section. Assuming that the interface is approximated by  $r=R$ , and substituting Eqs. (19) and (20) in the above equation, we have

$$\text{K.E.})_{\text{inner,max}} = (4/5)\pi\epsilon^2 R^3 \rho_i \omega^2 . \quad (37)$$

Similarly, we have

$$\text{K.E.})_{\text{outer,max}} = (8/15)\pi\epsilon^2 R^3 \rho_o \omega^2 . \quad (38)$$

Therefore, the total energy is

$$\text{T.E.}) = (4/15)\pi\epsilon^2 R^3 (3\rho_i + 2\rho_o) \omega^2 . \quad (39)$$

#### 2.3.4.6 Damping Constant

If the total energy  $\text{T.E.} = p\epsilon^2$ , and the rate of dissipation is  $q\epsilon^2$ , then

$$\frac{d}{dt}(p\epsilon^2) = - q\epsilon^2 .$$

This reduces to

$$\varepsilon = \varepsilon_0 e^{(-\frac{1}{2})(q/p)t},$$

where  $\varepsilon_0$  represents the amplitude at the time  $t=0$ , and  $\varepsilon$  represents the amplitude at the time  $t$ . If we define damping constant  $S$  in such a way

that  $\varepsilon = \varepsilon_0 e^{-1}$  when  $t=1/S$ , then

$$S = (\frac{1}{2})(q/p) . \quad (40)$$

By using the total energy and the rate of dissipation obtained above, together with the Eq. (40), we have the damping constant  $S$  as:

$$S = S_b + S_i + S_o , \quad (41)$$

where

$$S_b = \frac{(2\omega)^{\frac{1}{2}}}{R\Gamma} [2.25(1-c)^2(\mu_i \rho_i)^{\frac{1}{2}} + (1+1.5c)^2(\mu_o \rho_o)^{\frac{1}{2}}],$$

$$S_i = \frac{15\mu_i}{R^2\Gamma} ,$$

$$S_o = \frac{40\mu_o}{R^2\Gamma} ;$$

$$\Gamma = 3\rho_i + 2\rho_o ,$$

where the subscripts  $b$  denotes the contribution of dissipation from the boundary layer,  $i$  denotes the contribution from the inner irrotational flow, and  $o$  denotes the contribution from the outer irrotational flow.

Comparing this expression with Lamb's formula, we see that the  $S_i$  is

equivalent to the  $s$  in Eq. (4), and the  $S_o$  is equivalent to the  $s$  in Eq.

(5).

### 2.3.4.7 Examples and Comparison with the Previous Theories

We take three examples to illustrate the calculation and to compare the results with that obtained by previous theories and with one set of experimental data from previous work.

1) For an air bubble of radius 0.1 cm in water,  $\rho_i = 0.0012 \text{ g/cm}^3$ ,  $\mu_i = 0.018 \text{ cp}$ ,  $\rho_o = 0.997 \text{ g/cm}^3$ ,  $\mu_o = 0.894 \text{ cp}$ ,  $\sigma = 72 \text{ dyne/cm}$ .

(a) By Marston's theory, (see table 1 and 2 of [10])

$$\omega^*/2\pi = 148.03 \text{ Hz (by Eq. (3)) ,}$$

$$\omega / 2\pi = 147.9 \text{ Hz (by Eq. (11)) ,}$$

$$\begin{aligned} s &= \frac{1}{2}\alpha\omega^{*2} + \frac{1}{2}\gamma - \frac{1}{2}\alpha^2 \\ &= 0.6 + 17.75 - 0.0008 \\ &= 18.35 \text{ Hz .} \end{aligned}$$

(b) By Lamb's formula (Eq. (5)),

$$\nu = \mu_o / \rho_o = 0.897 \text{ cSt ,}$$

$$s = 17.94 \text{ Hz .}$$

(c) By this simplified model:

$$\omega / 2\pi = 147.9 \text{ Hz (a given value)}$$

$$(\rho_o \mu_o) / (\rho_i \mu_i) = 4.1 \times 10^4$$

$$c = -0.6667 \quad (U_s \approx U_{\theta o})$$

$$\begin{aligned} S &= S_b + S_i + S_o \\ &= 0.627 + 0.135 + 17.898 \\ &= 18.66 \text{ Hz.} \end{aligned}$$

The damping constants obtained by both models are very close, and the

simplified model gives a little higher value. The dominant term is due to the dissipation in the outer irrotational flow, as should be expected.

2) For a water drop of radius 0.1 cm in air,

(a) By Marston's theory,

$$\omega^*/2\pi = 120.87 \text{ Hz (by Eq. (3))}$$

$$\omega / 2\pi = 120.81 \text{ Hz (by Eq. (11))}$$

$$\begin{aligned} s &= \frac{1}{2}\alpha\omega^{*\frac{1}{2}} + \frac{1}{2}\gamma - \frac{1}{2}\alpha^2 \\ &= 0.376 + 4.498 - 0.00035 \\ &= 4.87 \text{ Hz} \end{aligned}$$

(b) By Lamb's formula (Eq. (4))

$$\nu = \mu_i / \rho_i = 0.897 \text{ cSt}$$

$$s = 4.49 \text{ Hz}$$

(c) By this simplified model,

$$\omega/2\pi = 120.81 \text{ Hz (a given value)}$$

$$(\rho_o \mu_o) / (\rho_i \mu_i) = 2.4 \times 10^{-5}$$

$$c = 1.0 \quad (u_s \approx u_{\theta i})$$

$$\begin{aligned} S &= S_b + S_i + S_o \\ &= 0.378 + 4.480 + 0.241 \\ &= 5.10 \text{ Hz} . \end{aligned}$$

Again, the calculated damping constant obtained by this simplified model is close to and a little higher than the calculated value by Marston's theory. The dominant term is due to the dissipation in the inner

irrotational flow, as one expects.

3) Trinh, Zwern, and Wang did some experimental work on the free oscillation of a drop in another liquid [12]. One set of their data for phenetole drops in a mixture of water and methanol was compared with the theoretical predictions given by Marston's theory and the simplified model, the result is shown in Fig. 2.3. It shows good agreement between the data and the calculated values based on both models. This set of data is chosen because of the small viscosity of the inner liquid, for which  $R/\delta_i \sim 10$ . Good agreement is also found between other sets of data and the simplified model even when  $R/\delta_i \sim 5$ , although the discrepancy grows as the ratio  $R/\delta_i$  decreases, as we expect. For example, in the experiments with drops of mixture consisting of silicon oil and  $\text{CCl}_4$  in water host, done by Trinh et al,  $\rho_i = 0.999 \text{ g/cm}^3$ ,  $\rho_o = 0.997 \text{ g/cm}^3$ ,  $\mu_i = 16.5 \text{ cp}$ ,  $\mu_o = 0.89 \text{ cp}$ ,  $R \sim 0.5 \text{ cm}$ , the calculation using our simplified model gives  $R/\delta_i \sim 3$ , and the predicted damping constant is about 40% higher than their measured value.

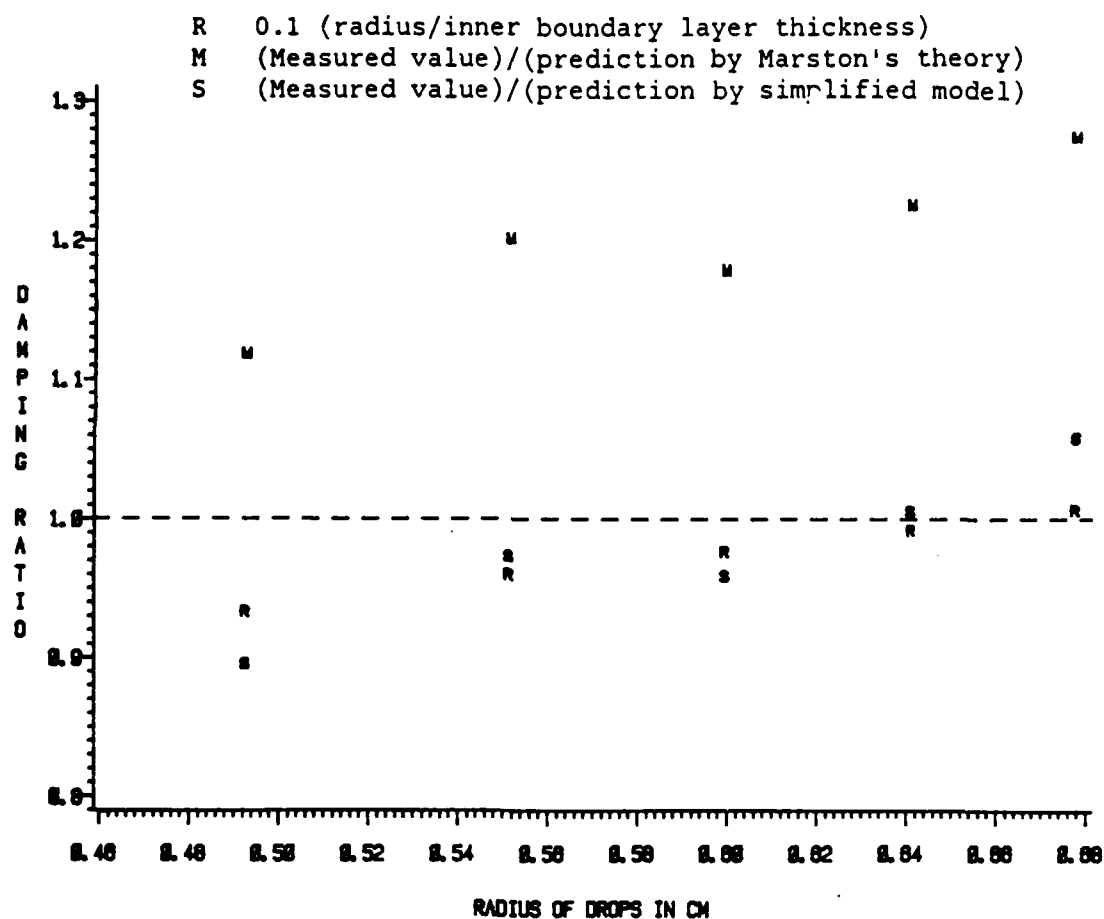


Figure 2.3: The ratio of the experimental to the predicted damping as a function of drop radius. The experimental data were taken from the work by Trinh et al. The predictions are given by the simplified model and Marston's theory respectively.



### 2.3.5 Phase-Frequency Relation in Forced Oscillation

As mentioned in section 2.2.1, the phase-frequency relation for forced oscillation is readily obtained if we know each component (both magnitude and phase) of the impedance corresponding to stiffness, inertia, and damping, respectively. Here, the impedance is defined as:

$$\text{impedance} \equiv \frac{p}{\Delta} \equiv \frac{\text{driving pressure (associated with quadrupole mode)}}{\text{displacement (of quadrupole mode)}} \quad (42)$$

Thus, the phase of the displacement is relative to the driving pressure.

We compute each component of the impedance separately by the following approach. First, the phase angle is determined by physical reasoning. We then compute, by energy balance or force balance, the driving pressure associated with the quadrupole displacement described by  $r = R + \epsilon Y_2(\theta) \sin(\omega t)$  (see Eq. (17)).

#### 2.3.5.1 Driving Force

In experiments described in this manuscript, the drop is driven into oscillation by a modulated acoustic wave (see section 3.1). Detailed analysis of the acoustic radiation force, which is a time averaged second order effect [18], exerted on the interface would require the first order pressure distribution of the incident wave in the specific configuration of this experiment, and the scattered wave incorporated with the boundary condition at the interface of the drop and the host. The normal and tangential component of the resultant radiation stress may be obtained by radial and tangential projection; further expansion

of the radiation stress in terms of spherical harmonic functions will give the normal and tangential component of the radiation stress responsible for the quadrupole oscillation [10] [19].

Yosioka and Kawasima [20] derived the acoustical radiation force on a compressible sphere, the tangential radiation stress is vanished in their derivation due to the inviscid assumption. Some experiments for measuring "compressadensity" using acoustical levitation technique is based on their theory, and the results of measurement show very good agreement with the theory [5]. Herrey [21] has shown that the tangential radiation stress is much smaller than the normal stress at a highly reflecting metallic surface in water induced by a sound beam. For a liquid-liquid interface, the boundary is relatively "free" to move compared with the boundary of liquid-solid interface; hence the velocity gradient and the stress at the liquid-liquid boundary would be expected even smaller. Also, the viscosities of both inner and outer liquids in our experiments are small. In the following calculation, we assume that the tangential component of the radiation stress is much smaller than the normal component, and the power input due to the tangential radiation stress is negligible compared with the contribution of normal radiation stress.

#### 2.3.5.2 Impedance Due to Stiffness

The displacement of a component of pure stiffness subject to a driving force is in phase with this driving force, that is,  $\xi = 0$ . In the problem of an oscillating drop, stiffness is due to the interfacial

tension, as assumed in section 2.1. We derive the impedance due to stiffness, denoted by  $K$ , in two different ways which employ force balance and energy balance, respectively, as follows:

1) The fluid pressure is discontinuous at a curved surface of separation; the pressure differential is

$$p_i - p_o = \sigma(R_1^{-1} + R_2^{-1}) . \quad (43)$$

This is Laplace's formula, where  $R_1$  and  $R_2$  are the principal radii. Since we are only interested in the pressure variation accompanying the quadrupole oscillation, let us set  $p_o = 0$  at equilibrium (the ambient pressure). Then,  $p_i = \sigma(2/R)$  at equilibrium. The inner pressure  $p_i$  will not vary with the shape oscillation, since there is no volume change and there is no mass involved in this discussion. The interface is described as (see Eq. (17))

$$r = R + \epsilon Y_2(\theta) \sin(\omega t) ,$$

which gives [8]

$$1/R_1 + 1/R_2 = 2/R + (4/R^2)\epsilon Y_2(\theta) \sin(\omega t) . \quad (44)$$

Therefore, the variation of  $p_o$  accompanying the shape oscillation due to the interfacial tension is, from Eqs. (43) and (44),

$$p_o = - (4/R^2)\sigma\epsilon Y_2(\theta) \sin(\omega t) , \quad (45)$$

where the minus sign indicates that the outer pressure at the two poles reaches a maximum when the drop is in an oblate shape with maximum displacement. For this reason, we define the displacement  $\Delta$  in the following way, so that the displacement is in phase with the driving pressure for a pure stiffness,

$$\Delta = R - r = - \epsilon Y_2(\theta) \sin(\omega t) . \quad (46)$$

Since  $p_i$  is constant,  $p_o$  equals the driving pressure  $p$ . Thus the component of the impedance due to stiffness is

$$K = \frac{p}{\Delta} = \frac{4\sigma}{R^2} . \quad (47)$$

2) The potential energy, set zero when the drop is in a spherical shape at equilibrium, equals the product of the interfacial tension and the change of the interfacial area. For a small quadrupole displacement with an amplitude  $\varepsilon$ , as in Eq. 17 with  $t=\pi/(2\omega)$ , the potential energy is  $(32\pi/5)\sigma\varepsilon^2$  [7]. The driving pressure on the interface responsible for the quadrupole displacement can be assumed to be  $p = -PY_2(\theta)\sin(\omega t)$ , where  $P$  is the amplitude, and the minus sign is assigned to give the correct phase angle as discussed previously (see Eq. (45)). The instantaneous power input per unit area is therefore

$$p \frac{d\Delta}{dt} = PY_2^2(\theta)\varepsilon\omega\sin(\omega t)\cos(\omega t) . \quad (48)$$

The integration of the above expression over the interface  $r=R$ , and over the period from  $t=0$  to  $t=\pi/(2\omega)$  is found to be  $(8\pi/5)P\varepsilon R^2$ , which should equal the potential energy,  $(32\pi/5)\sigma\varepsilon^2$ , corresponding to the displacement  $\Delta = -\varepsilon Y_2(\theta)$  at  $t=\pi/(2\omega)$ . Hence  $P = 4\sigma\varepsilon/R^2$ . We therefore have

$$K = \frac{p}{\Delta} = \frac{4\sigma}{R^2} ,$$

which is identical with that obtained via force balance, in Eq. (47).

### 2.3.5.3 Impedance Due to Inertia

The acceleration of a mass is in phase with its driving force, so the displacement lags by  $180^\circ$  the driving force;  $\xi = 180^\circ$ . Here we compute the pressure on the interface required to drive a spherical liquid mass into the oscillation described as  $r = R + \varepsilon Y_2(\theta) \sin(\omega t)$ . The calculation is first carried via force balance and then via energy balance.

1) With the inviscid assumption, the velocity potential is determined by the boundary condition, as given in Eqs. (19) and (20). Then the pressure variation at both sides of the interface accompany this potential flow is

$$p_i = \rho_i \frac{\partial \phi_i}{\partial t} \bigg|_{r=R} = (1/2) \rho_i R \omega^2 \varepsilon Y_2(\theta) \sin(\omega t) ,$$

$$p_o = \rho_o \frac{\partial \phi_o}{\partial t} \bigg|_{r=R} = -(1/3) \rho_o R \omega^2 \varepsilon Y_2(\theta) \sin(\omega t) .$$

The required driving pressure is  $p = p_i - p_o$ , and

$$p = p_i - p_o = (1/6) R \omega^2 (3\rho_i + 2\rho_o) \varepsilon Y_2(\theta) \sin(\omega t) . \quad (49)$$

Thus the component of the impedance due to inertia, denoted by  $M$ , is, from Eqs. (42), (46), and (49),

$$M = \frac{p}{\Delta} = j^2 (1/6) \omega^2 R (3\rho_i + 2\rho_o) , \quad (50)$$

where  $j$  is  $(-1)^{1/2}$ .

It is worth noticing that  $K + M = 0$  when the driving force has a frequency  $\omega$  that

$$\omega^2 = \frac{24\sigma}{R^3(3\rho_i + 2\rho_o)} \quad (51)$$

which is the quadrupole resonance frequency for the inviscid situation, as in Eq. (3).

2) The kinetic energy reaches its maximum value

$(4\pi/15)\omega^2 R^3(3\rho_i + 2\rho_o)\varepsilon^2$  (see Eq. (39)), when  $t = 0$ , and it is zero when  $t = \pi/(2\omega)$ . The driving pressure may be written as:  $p = PY_2(\theta)\sin(\omega t)$ , so that the acceleration,  $d^2\Delta/dt^2 = \varepsilon\omega^2 Y_2(\theta)\sin(\omega t)$ , is in phase with the driving pressure. For instance, when  $t = \pi/(2\omega)$ , the driving pressure is positive and maximum at the two poles, while the acceleration at the two poles are inward and maximum. Then, during this period, from  $t = 0$  to  $t = \pi/(2\omega)$ , the power "input" is  $-(8\pi/5)P\varepsilon R^2$  (see Eqs. (46) and (48)). This power input should equal the maximum kinetic energy, thus  $-(8\pi/5)P\varepsilon R^2 = -(4\pi/15)\omega^2 \varepsilon^2 R^3(3\rho_i + 2\rho_o)$ . We obtain an expression for  $P$  and therefore

$$M = \frac{p}{\Delta} = j^2 \frac{\omega^2 R}{6} (3\rho_i + 2\rho_o) \quad ,$$

which is identical with that obtained via force balance as in Eq. (50).

#### 2.3.5.4 Impedance Due to Viscosity

The question of what is the impedance due to viscosity is equivalent to the question of what is the driving pressure on the interface needed to supply the energy dissipation in the motion  $r = R + \varepsilon Y_2(\theta)\sin(\omega t)$ .

1) Let us first look at the irrotational flow. In the irrotational flow associated with the oscillatory drop, the velocity at every point is oscillating in phase, since the fluids behave incompressibly. The viscous stress, which is proportional to the spatial gradient of velocity distribution, is therefore in phase with the potential velocity. Hence, the driving pressure on the interface is in phase with the potential velocity and has a phase lead of  $90^\circ$  over the displacement

$$\Delta = -\epsilon Y_2(\theta) \sin(\omega t) .$$

The radial velocity of the interface is

$$\frac{d\Delta}{dt} = -\epsilon \omega Y_2(\theta) \cos(\omega t) .$$

The driving pressure, which is in phase with the velocity, is assumed in the form

$$p = -P Y_2(\theta) \cos(\omega t) .$$

Then the instantaneous power input by the driving pressure acting on the interface is

$$\iint p \frac{d\Delta}{dt} dA = (16\pi/5) \epsilon \omega R^2 P \cos^2(\omega t) , \quad (52)$$

which should equal the rate of energy dissipation. (a) In the inner irrotational flow, the rate of dissipation has been obtained (see Eq. (32)) as:

$$16\pi \mu_1 \epsilon^2 R \omega^2 \cos^2(\omega t) .$$

By equating this rate of dissipation with the power input (Eq. (52)), we get an expression for  $P$ ,  $P = 5\mu_1 \epsilon / R$ , which leads to  $B_{pi}$ , the component of impedance due to viscous dissipation in the inner irrotational flow,

$$B_{pi} = \frac{P}{\Delta} = j \frac{5\mu_1 \omega}{R} . \quad (53)$$

(b) In the outer irrotational flow, the instantaneous rate of dissipation is (see Eq. (33))

$$(128/3)\pi\mu_0\varepsilon^2R\omega^2\cos^2(\omega t) .$$

By equating the power input (Eq. (52)) and this rate of dissipation, we have  $B_{po}$ , the component of the impedance due to the viscous dissipation in the outer irrotational flow,

$$B_{po} = j(40/3R)\mu_0\omega . \quad (54)$$

2) Now we consider the energy dissipation only in the boundary layer, and compute the associated impedance. The velocity distribution in the boundary layer may be described as [17]:

$$v(y,t) = Ue^{i\omega t}(1-\exp[-(1+j)y/\delta]) ,$$

where  $Ue^{i\omega t}$  is the external stream velocity,  $y$  is the coordinate normal and relative to the boundary. The frictional stress at the boundary is the real part of the following expression [17]:

$$\mu \frac{\partial u}{\partial y} \Big|_{y=0} = \mu(1+j) \frac{U}{\delta} e^{i\omega t} ,$$

so this skin friction has a phase lead of  $\pi/4$  over the external stream velocity  $Ue^{i\omega t}$ . In this problem of an oscillating drop, the external stream velocity is in phase with the potential velocity, as discussed in section 2.3.3.1. The tangential component of the acoustic radiation stress, which is the driving force, though small, has to be in phase with the skin friction, in considering the balance of tangential stress on the interface. Therefore the phase of the radiation stress is  $\pi/4$  ahead of the potential velocity and is  $3\pi/4$  ahead of the interfacial displacement, that is,  $\xi=135^\circ$ . For the motion  $r=R+\varepsilon Y_2(\theta)\sin(\omega t)$ , we



have (see Eq. (46))

$$\frac{d\Delta}{dt} = -\varepsilon\omega Y_2(\theta)\cos(\omega t) .$$

Writing

$$p = -PY_2(\theta)\cos(\omega t + \pi/4) ,$$

the power input averaged over one cycle along the whole interface is then

$$(\omega/2\pi) \int_{t=0}^{2\pi/\omega} dt \iint p \frac{d\Delta}{dt} dA = (4\pi 2^{1/2}/5) \varepsilon R^2 \omega P , \quad (55)$$

where the contribution of the power input due to the tangential radiation stress has been neglected.

In considering the rate of dissipation, we assume the tangential radiation stress is much smaller than the normal component, so that the model of the flow distribution developed in section 2.3.3 is still a good approximation for the flow in the forced oscillation. We then have the time averaged rate of dissipation in the boundary layer as given in Eqs. (35) and (36). By equating this time averaged rate of dissipation with the above time averaged power input in Eq. (55), we have an expression for  $P$  and thus obtain the component of impedance (see Eq. (42)) due to viscous dissipation in boundary layer,  $B_b$ , as:

$$B_b = [(j-1)/\sqrt{2}](2/3)\omega^{3/2} [2.25(1-c)^2(\mu_i \rho_i)^{1/2} + (1+1.5c)^2(\mu_o \rho_o)^{1/2}] . \quad (56)$$

#### 2.3.5.5 Total Impedance

The total impedance is the vector sum of these components given in Eqs. (47), (50), (53), (54), and (56).

$$\text{impedance} = K + M + B_p + B_b, \quad (57)$$

$$\text{where } B_p = B_{pi} + B_{po},$$

$$= j(\omega/R)[5\mu_i + (40/3)\mu_o],$$

$$K = 4\sigma/R^2,$$

$$M = (j^2/6)\omega^2 R(3\rho_i + 2\rho_o),$$

$$B_b = [(j-1)/\sqrt{2}](2/3)\omega^{3/2}[2.25(1-c)^2(\mu_i\rho_i)^{1/2} + (1+1.5c)^2(\mu_o\rho_o)^{1/2}].$$

A schematic vector diagram of the four components is shown in Fig. 2.4.

We obtain, finally, the phase-frequency relation as the following

$$\tan\xi = (B_p + B_b/\sqrt{2})/(K-M-B_b/\sqrt{2}). \quad (58)$$

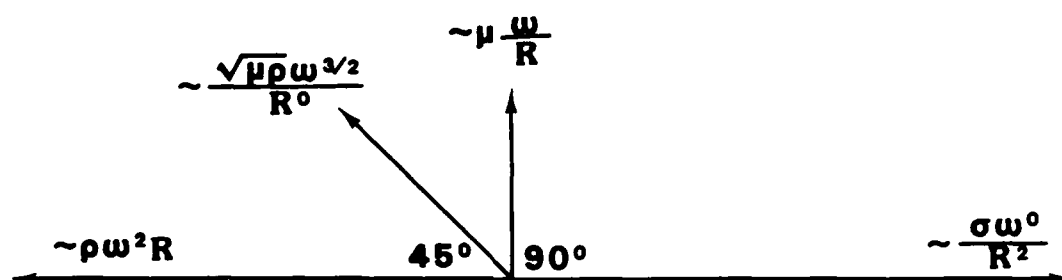


Figure 2.4: Schematic impedance diagram for the quadrupole oscillation of a drop-host system.

### 2.3.5.6 Comparison with the Theory by Marston

Eq. (7) is the phase-frequency relation derived in the work done by Marston. We change the form of Eq. (7) by multiplying each term with  $(3\rho_i + 2\rho_o)R/6$  to get the "equivalent components of the impedance" as follows:

$$K' = 4\sigma/R^2 ,$$

$$M' = j^2(1/6)\omega^2 R(3\rho_i + 2\rho_o) , \quad (59)$$

$$B_p' = \frac{j5\omega[\mu_i^2\rho_i + (8/3)\mu_o^2\rho_o + (1/6)\mu_i\mu_o(4\rho_i - \rho_o)]}{R[(\mu_i\rho_i)^{\frac{1}{2}} + (\mu_o\rho_o)^{\frac{1}{2}}]^2} ,$$

$$B_b' = \frac{(j-1)25\omega^{3/2}(\mu_i\mu_o\rho_i\rho_o)^{\frac{1}{2}}}{2^{\frac{1}{2}}6[(\mu_i\rho_i)^{\frac{1}{2}} + (\mu_o\rho_o)^{\frac{1}{2}}]} .$$

Compared with the impedance obtained in the simplified model, they have components of similar dependence upon parameters like density, viscosity, and frequency at the same phase angles. The components due to stiffness and inertia are identical. For both inner and outer liquids of small viscosity, the value of  $B_b$  is close to the value of  $B_b'$ , whereas the value of  $B_p$  is much greater than that of  $B_p'$ . Two examples in the following show the typical numerical values of impedance due to damping:

a) For a hexane drop in water,  $\rho_i = 0.655 \text{ g/cm}^3$ ,  $\mu_i = 0.29 \text{ cp}$ ,  $\rho_o = 0.997$

$\text{g/cm}^3$ ,  $\mu_o = 0.89 \text{ cp}$ . On making use of Eqs. (28) and (29), we have

$\delta/\mu = 0.114$ ,  $c = -0.5$ , therefore,  $B_b = 0.15\omega^{3/2}$ ,  $B_b' = 0.13\omega^{3/2}$ , whereas

$B_p = 0.13\omega/R$ ,  $B_p' = 0.07\omega/R$ .

b) For a p-xylene drop in water,  $\rho_i = 0.857 \text{ g/cm}^3$ ,  $\mu_i = 0.614 \text{ cp}$ . Eqs. (28)

and (29) give  $\delta/\mu = 0.19$ , and  $c = -0.4$ . Therefore,  $B_b = 0.22\omega^{3/2}$ ,

$B_b' = 0.17\omega^{3/2}$ ;  $B_p = 0.15\omega/R$ , and  $B_p' = 0.05\omega/R$ .

Fig. 2.5 illustrates the phase-frequency relation for a hexane drop in water predicted by Marston's theory and the simplified model respectively with given drop size and properties of the liquids (interfacial tension, density, and viscosity) as listed in Table 1. This figure is meant to be representative, and good agreement between the simplified model and Marston's theory is shown.

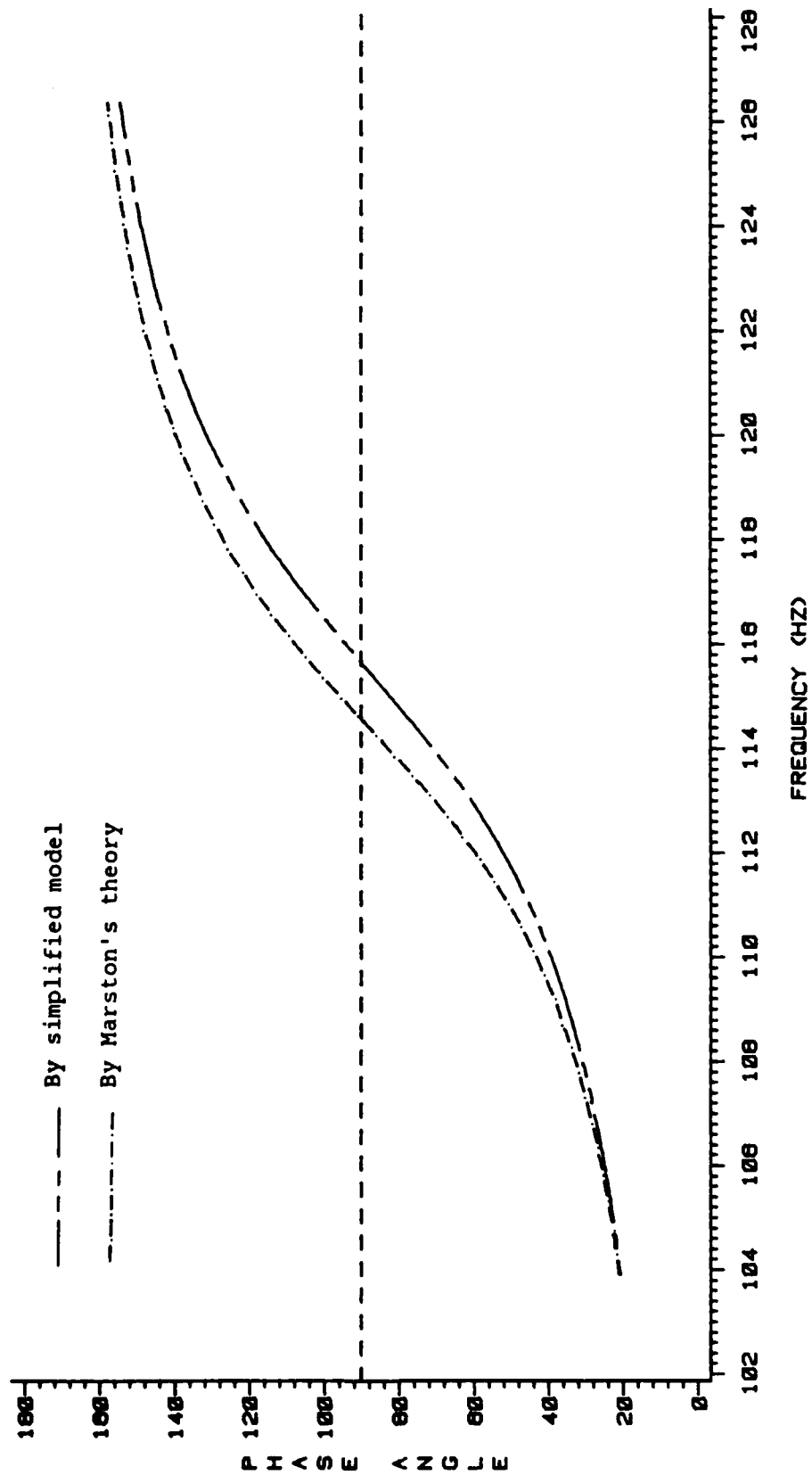


Figure 2.5: Phase vs. frequency curves given by the simplified model and Marston's theory respectively: Example for host, water; drop, hexane; drop radius, 0.0825 cm.

## 2.4 Compressadensity Measurement

The droplet-levitation formula is given by [5]

$$\frac{dP}{dZ} = - \frac{2\rho g}{\beta_s} G\left(\frac{\beta_s^*}{\beta_s}, \frac{\rho^*}{\rho}\right),$$

$$G \equiv \frac{|1 - \rho^*/\rho|}{\beta_s^*/\beta_s - (5\rho^* - 2\rho)/(2\rho^* + \rho)}, \quad (60)$$

where  $P(Z)$  is the acoustic pressure amplitude of the standing wave along the vertical axis ( $Z$ ),  $g$  is the gravitational constant,  $\beta_s^*$  and  $\beta_s$  are the adiabatic compressibility of droplet and host, respectively, and  $\rho^*$  and  $\rho$  are the densities of droplet and host liquid, respectively. The nondimensional function  $G$  is called the "compressadensity" function. The above expression is independent of the size of the drop, based on the assumption that the acoustic wavelength is much greater than the drop's diameter. On the other hand, adiabatic compressibility is used when the thermal wavelength is much smaller than the diameter of the droplet. These assumptions hold in our experiment where the levitation frequency is about 52 kHz and the radii of drops are smaller than 1 mm.

We may extract information about a liquid by using a method of comparison and without measuring the acoustic field [5]. A drop of a "reference" liquid with known compressibility and density is first levitated at a position  $Z=Z_0$  with a levitation voltage  $V'$ , and then a drop of an "unknown" liquid is levitated at the same position with a voltage  $V^*$ . The pressure amplitude  $P(Z_0)$  and pressure gradient  $(dP/dZ)_{Z_0}$

are assumed each proportional to the levitation voltage, so we have the result:

$$\frac{P'(dP/dZ)'}{P^*(dP/dZ)^*} = \frac{V'^2}{V^{*2}} = \frac{G(\beta_s'/\beta_s, \rho'/\rho)}{G(\beta_s^*/\beta_s, \rho^*/\rho)}, \quad (61)$$

where the superscript ' denotes the reference liquid, and the superscript \* denotes the unknown liquid. Eqs. (61) and (60) give us a the compressadensity function of the unknown liquid providing that  $\rho$ ,  $\beta_s$ ,  $\rho'$ ,  $\beta_s'$  are known, and that  $V'$  as well as  $V^*$  are measured. If we know  $\rho^*$ , then  $\beta^*$  can be calculated from Eq. (60), (and vice versa).



## Chapter 3

### APPARATUS

In this chapter, we focus on the equipment used for size and phase-frequency measurements. A schematic diagram of the equipment is shown in Fig. 3.1. We briefly mention some standard instruments used for measuring sound speed and density in the last section.

The equipment in Fig. 3.1 may be described in four parts. The first part is the apparatus used to levitate a drop in water and to drive the drop into shape oscillations. The second optically detects the drop's shape oscillations and converts the oscillations into electric signals. These signals are processed by the third part, and the frequencies corresponding to several phase angles are measured. The fourth part takes pictures of the drop and some calibrated reference objects. These pictures are used to measure the size of the drop. One section of the following will be devoted to describing each of the four parts of the apparatus.

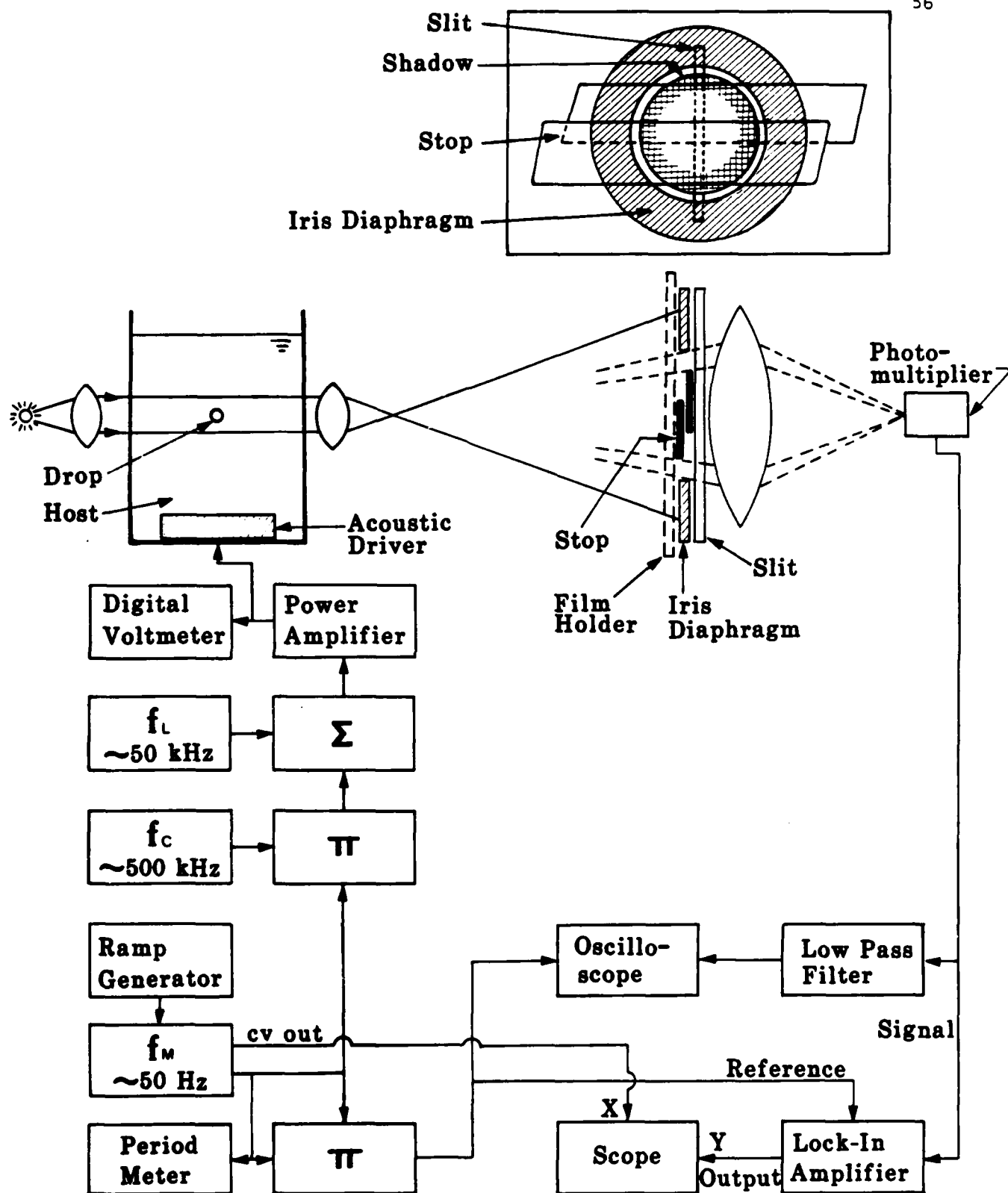


**Figure 3.1: Diagram of apparatus.**

### 3.1 Levitation and Shape Oscillation

The levitation cell, which holds the host liquid and transducer, is a box with a cross section of 5.4 cm square and a height of 11 cm. The box is made of Lucite plates, 3.18 mm in thickness for the walls and 6.35 mm for the bottom, and it is open at the top. This cell sits on a lab jack which adjusts the vertical position. The transducer, which converts electric energy into mechanical motion and generates waves in the host water, is a Channel Industries (Santa Barbara, CA) 5400, Lead Zirconate Titanate piezoelectric ceramic disk with a diameter of 3.9 cm and a thickness of 1.3 cm. The transducer is immersed in water and sits on the bottom plate of the cell.

At a selected height of the water in the cell, and with an input to the transducer at certain frequencies (e.g., two frequencies used in our work are about 52 kHz and 510 kHz), the transducer-water-cell system resonates and generates standing waves in the water column (see section 4.1). A drop of a liquid other than water in this standing wave field is subject to an acoustic radiation force, which is a time averaged (dc) second order effect of the wave. This force tends to drive the immersed drop toward a position of maximum pressure if the drop is more compressible than the water "host", while gravity tends to push the drop up or to pull it down depending on the densities of the drop and the host. If the drop can find a position where the acoustic radiation force counterbalances the gravitational force, it is acoustically levitated at that position. The radial pressure distribution (maximum at the center) forces the drop to the center of the water column if the

drop is more compressible than the host. Also, the local pressure distribution affects the shape of the drop, while the interfacial tension tends to keep it spherical.

An input voltage at about 52 kHz is used to levitate drops. At this frequency and a proper water level, drops can be levitated at an input of only a few volts for all the test liquids in this work. At this frequency, the wavelength is much longer than the diameter of a test drop (less than 2 mm mostly), so that Eqs. (60) and (61) are applicable for calculating compressadensity, and the equilibrium shape of the drop does not deviate from sphericity much.

At about 510 kHz, the wavelength is comparable with the diameter of the drop, the radiation force is stronger [10], and the deformation of the drop is greater. We can further enhance the deformation by turning this signal on and off at a frequency matching a resonance frequency of the drop; this can be done by modulating this high frequency signal (see Fig. 4.2).

Therefore, three sinusoidal electric signals are combined in such a way to give  $v_t$  driving the transducer, that is

$$v_t = v_l + v_c \cdot v_m .$$

According to their functions, we call these signals the levitation signal (~52 kHz), the carrier signal (~510 kHz), and the modulation signal (~50 Hz), associated with subscripts l, c, and m respectively. The circuits for multiplication, using a MC 1595L linear four-quadrant

multiplier, and for summation, using a ML 318S integrated circuit, was built by Marston in previous work [11] (see Fig. 3.1).

The levitation signal is generated by a versatile circuit built by Baxter, Apfel, and Marston [22]. This circuit has features that are very useful in tuning the acoustic levitation system. We can manually scan the resonances of the acoustic levitation system and view the resonances on a storage oscilloscope (Tektronix Model 5103N). The ordinate is a dc manifestation of the current through the transducer, and the abscissa is linear in the frequency. A Tektronix P6016 current probe senses the current through the transducer and produces a voltage signal, which is then converted by the versatile circuit to the dc manifestation.

The carrier signal is generated by a Krohn-Hite Model 4300 generator. A Krohn-Hite Model 1000 generator and a Kepco Model FG100A ramp generator are used for the modulation signal. The Model 1000 generator operates in an external frequency control mode and is driven by the ramp generator, thereby providing easy manipulation of sweeping rate and direction.

The combined signals  $v_t$  are fed into a Krohn-Hite Model 7500 amplifier before going into the transducer. After amplification, the rms value of  $v_1$  is about 4 V or less. The rms value of  $v_t$  is about 5 V or less. A Data Precision Model 5740 frequency counter (also period meter) and a Data Precision Model 3500 digital voltmeter are used in monitoring the system.

### 3.2 Detection of Shape Oscillation

In this work, we study small amplitude (in the order of 10  $\mu\text{m}$ ) shape oscillations of a drop (radius in the order of 1 mm) which can not be touched with any solid object. These two features suggest the use of light to detect the shape oscillation. We use a technique adapted from an experimental work done by Trinh, Zwern, and Wang [12].

We use a microscope illuminator as a light source, which has a Sylvania 1493, 6V, 20 W bulb with a short filament and a lens with a short focal length to give an approximately parallel beam. A dc power supply is used for the lamp. The light beam passes horizontally through the levitation cell, then is enlarged by a lens and is projected onto a plate with a slit on it. The slit is vertical with a width about 1 mm and a height about 5 cm. The light through the slit is focused onto the sensing surface of a photomultiplier (ENI type 9798B). The shadow of a levitated drop centers across the slit and blocks part of the light going through the slit. When the drop oscillates in its quadrupole mode, the amount of light going through the slit changes accordingly, therefore, an ac voltage signal coherent with the drop's oscillation is obtained. The sensitivity of the photomultiplier is a function of the power supply. We use a Pacific Photometric Instruments Model 227 high voltage power supply at 1000 to 1200 V for the photomultiplier.

The shadow of the drop usually is not a uniformly dark circle, but has a bright area in the center part. If the refraction index of the drop liquid is very close to that of water, as the index of refraction of butane is, the shadow looks like a ring of a very thin band. Therefore, we use an adjustable stop to block the light inside the circle of the shadow. Also, we use an iris diaphragm, which is concentric with the shadow and opened a little bigger than the shadow, yielding a "halo" outside the shadow. The stop and the iris diaphragm reduce the light going through the slit and result in two advantages. First, the photomultiplier can operate at a higher sensitivity to give a stronger ac signal for a given amplitude of a drop's oscillations. Secondly, the noise due to light scattering by particles in the path of the light beam is reduced.

### 3.3 Frequency and Phase Measurements

We need to measure the frequencies corresponding to  $90^\circ$  and some other phase angles (of the drop's oscillation relative to its driving force) around the quadrupole resonance of the drop. This is accomplished mainly by the aid of a lock-in amplifier, which is a Princeton Applied Research Model 5101 lock-in amplifier with a common mode rejection typically 85 dB at 1 kHz.

Lock-in amplifiers have an output channel and two input channels, one channel for reference and the other channel for signals to be measured. The signal is compared with the reference, and only those

signal components which are synchronous with the reference yield a net dc output. Noise and other non-synchronous signals do not contribute a net dc output, but only ac fluctuations which can be reduced to very small value by time averaging (filtering). There is a phase control on a lock-in amplifier which allows the phase of the reference drive to the internal circuit of phase sensitive detector to be set at any angle relative to the input reference signal. For example, a sinusoidal signal, say  $v_r \cos(2\pi f_r t)$  is used as reference, signals to be measured have a synchronous component  $v_i \cos(2\pi f_r t + \xi)$ , and the phase control is set at  $\Lambda$ . Then the output of the lock-in amplifier is a dc voltage proportional to the time average of the following product:

$$v_r \cos(2\pi f_r t + \Lambda) \cdot v_i \cos(2\pi f_r t + \xi) .$$

This dc output reaches maximum when  $\Lambda = \xi$  ; it is zero when  $\Lambda = \xi + 90^\circ$ . It is easier to take measurement at zero-output than to take measurement at maximum-output. In this experiment, by setting the phase dial  $\Lambda = \xi + 90^\circ$ , and sweeping the modulation frequency, we get the frequency  $f(\xi)$  which nulls the output of the lock-in amplifier. This process of sweeping is viewed on the storage oscilloscope with the output of the lock-in amplifier as the ordinate and the sweeping frequency as the abscissa. We use the Data Precision Model 5740 counter to measure the period of the modulation signal, then take the reciprocal of the period to get the frequency, because it is easier to measure period than frequency in the low frequency region (on the order of 100 Hz).

When the Model 5101 lock-in amplifier operates in the region of about 100 Hz, the true phase shift  $\Lambda$  is different from the set value on



the dial. So we calibrate this Model 5101 lock-in amplifier. The calibration is carried out by applying two in-phase signals into the reference and signal channel, followed by adjusting the phase control for zero output. Comparing this phase reading with the true value ( $90^\circ$ ), we obtain the error in the phase reading at this frequency. The calibration covers the frequency range from 40 Hz to 140 Hz, the signal level from 0.01 to 0.3 V, and concludes that:

the phase reading from the dial  $+ 40^\circ =$  the true phase, with error less than  $0.2^\circ$  in phase angle. Hereafter, the phase set on the lock-in amplifier mentioned in this manuscript is the corrected phase.

For better phase accuracy, the amplitude of the reference signal is set to 1 V rms as suggested in the manual, in both the actual measurements and the calibration.

When the reference signal sweeps, the internal reference circuit of the lock-in amplifier automatically tracks but with some delay. A relation between the slewing rate  $df/dt$  and the phase error  $\theta$  stated in the manual is  $df/dt = 3 \cdot 10^{-3} \cdot f \cdot \theta$ . In this experiment,  $f \sim 100$  Hz,  $df/dt \leq 1/30$  Hz/sec, so the error in phase angle introduced by sweeping is less than  $0.1^\circ$ .

### 3.4 Size Measurement

As shown in Eq. (3), the interfacial tension goes with the cube of the drop's radius. For a drop with 1 mm radius, an acceptable error of 1% in radius will cause an unacceptable error of 3% in interfacial tension. The size measurement was the most significant factor of the experimental uncertainty in the work of Marston and Apfel [11].

In this experiment, we take pictures of a levitated drop and some reference objects, then enlarge the pictures and obtain the size of the drop. We use a Polaroid #545 film holder loaded with a Polaroid Type 55/Positive-Negative 4x5 land film positioned right in front of the slit and facing the light beam. By turning the toggle switch of the power supply for the lamp on and off for a duration about half second, we get an exposure of the shadow of the drop. The shadow is about ten times larger than the drop. The negative is then further enlarged yielding a positive print which is about 75 times the size of the drop. A truss is built to support the film holder firmly, and two tracks on the truss enable the film holder to slide in and out the optical path.

We take pictures of a drop before and after the frequency-phase measurement. Then we take pictures of the following reference objects: three precision plug gauges of diameters 1.395, 1.614, and 2.018 mm (from Zero-Check Inc.). When we take the picture, the gauge is located through the position where the drop was levitated. Care is exercised to enlarge these negatives by the same factor. The average of the enlargement ratios (between the shadow on the final positive print and

the gauge itself) of the three gauges is used to evaluate the drop's diameter. The consistency of the three ratios indicates the accuracy of the size measurement. Generally, they are good to within 0.15%.

When we take a picture of each gauge, it is important to have the gauge located through the position where the drop was levitated. A filar telescope with magnification of 20 and a ruler horizontally affixed to the plate with the slit on it serve to mark the position of the levitated drop in three dimensions.

### 3.5 Measurement of Sound Speed and Density

We use standard laboratory equipment to measure some properties, sound speed and density, of the non-superheated liquid samples. Since these techniques are well known, we will not discuss these methods in detail. The values obtained are incorporated into the calculation for interfacial tension or compressibility.

We measure the sound speed in hexane, pentane, and heptane by using a Nusonics sonic solution monitor Model 6105 (manufactured by Mapco Inc., Tulsa Oklahoma) (referred to Table 10). The container for the ultrasonic probe and the sample liquid is placed in a water bath which maintains a constant temperature with variations less than  $0.1^{\circ}\text{C}$ . The sound speeds obtained using this technique are good to within 0.1%.

For measuring density, a Mettler/Parr DMA-40 densitometer is used. The chamber for the test liquid is also in a water bath to maintain a constant temperature. The uncertainty of this measurement is less than 0.1%.

## Chapter 4

### PROCEDURE

The procedure for measuring interfacial tension in this experiment is as follows: We first set and tune the levitation system to get a strong acoustic standing wave in the water "host". Then we put a drop of the liquid to be measured into the water. While the drop rises up due to buoyancy, the acoustic field traps the drop and levitates it at a certain position. We take pictures of the enlarged shadow of the drop for measuring the drop's size. Then we drive the drop into quadrupole shape oscillation. Around the resonance, several frequencies corresponding to different phase angles of the oscillation relative to its driving force are measured. Details of the above procedure are described in the following sections.

Some other parameters, such as density and viscosity, are either measured by other techniques (see section 3.5) or obtained from the literature. The procedure for measuring compressadensity by the acoustic levitation technique is described in the last section.

#### 4.1 Drop Levitation

The host liquid in the levitation cell is water for all experiments in this study. Surface active contaminants, even in trace amount, may change the surface or interfacial tension significantly. Therefore, we are very careful in keeping the host water and the apparatus components in contact with the host water clean. Distilled water is fed into a Barnstead Nanopure-A 4-holder system, and circulates through the system to reach a resistivity, which indicates the purity, of 17.7 - 17.9 megohm/cm. The levitation cell, the transducer, and others like syringes and needles are kept away from dirt and are flushed a few times with the clean water before an experiment is conducted. The clean water is degassed and then slowly poured into the levitation cell. Then we place the transducer at the center of the bottom of the cell. There are no bubbles visible in the cell when an experiment is performed.

We tune the levitation system as follows: To find a configuration at which the transducer-water-cell system resonates, we adjust the water level and sweep the levitation frequency, while monitoring the current going through the transducer. The carrier and modulation voltage are zero at this stage. The level of the water is changed by taking out or injecting in small quantities of water with a syringe. The frequency is swept manually. At the same time, we view the resonances of the levitation system on the storage oscilloscope with the display of current versus frequency (see section 3.1). There are several configurations of water level and frequency which give sharp peaks on the current-frequency display. Each configuration requires a different

minimum voltage to trap a drop of a certain kind of liquid, and levitates the drop at a different position with this minimum trapping voltage. The water level (about 8.3 cm from the top of the bottom plate) and the levitation frequency (about 52 kHz) that we chose provide stable levitation at low voltage (about 4 V for hexane drops). The volume of water in the cell is about 220 cm<sup>3</sup>. The levitation position is about at the middle of the height of the water column.

To levitate a drop, we put it into the bottom part of the cell (details described in section 4.2) and trap it as it rises (all the liquids to be measured in this study are less dense than water) by turning on the levitation voltage. After tuning the levitation system, we levitate a hexane drop which serves for checking the tuning and for aligning the optical system. A stable levitation condition at about 4 V for a hexane drop indicates good tuning of this levitation system. The positions of the cell and the enlarger lens are adjusted to project a sharp shadow onto the film plane and to center across the slit. Then we use the filar telescope and the ruler to mark the position of the drop in three dimensions (see section 3.4).

After finishing these procedure for preparation , we release the hexane drop for alignment and levitate a drop of the liquid to be measured at the same position as that of the hexane drop for alignment. The size and frequency-phase measurements are then conducted.

#### 4.2 Drop Making and Transportation

For non-superheated liquids like hexane and pentane, we use a threaded plunger syringe and a needle (from Hamilton company) to transport the liquid. A drop that adheres to the tip of the needle can be detached by a little disturbance; then the drop rises up and is trapped by the acoustic field.

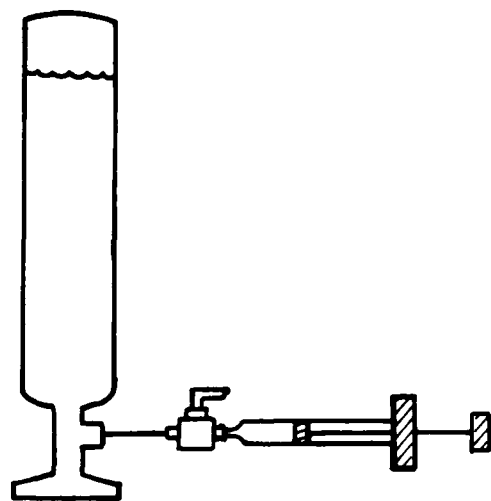
Introducing superheated drops is somewhat complicated compared to non-superheated drops. The process is shown in Fig. 4.1. The test liquid is contained in a lecture bottle and is in equilibrium with its vapor at room temperature. Some of the liquid is drawn into a threaded plunger syringe with a miniature inert valve (from Hamilton Company) fitted on the tip of the syringe. The threaded plunger and the valve can take pressure so as to keep the liquid in equilibrium (not superheated) (referred to Fig. 4.1(a)). The syringe is precooled for working with propane. A glass tube of 5 mm i.d. has been filled with gel and cooled in a freezer. The gel is composed of (by weight) 1 part of water, 1 parts of glycerine, and 1.25 parts of water soluble Aquasonic 100 ultrasound transmission gel (from Packer Laboratories, Inc., NJ), mixed uniformly and centrifuged to remove gas bubbles. We put this glass tube into a pressure vessel, pressurize it with nitrogen gas at a pressure a little over the vapor pressure of this liquid at room temperature. Then we push the needle of the syringe containing the liquid through a septum, open the miniature valve, and inject the liquid into the gel forming liquid drops (referred Fig. 4.1(b)). After releasing the pressure, we get "superheated" drops in the gel. The



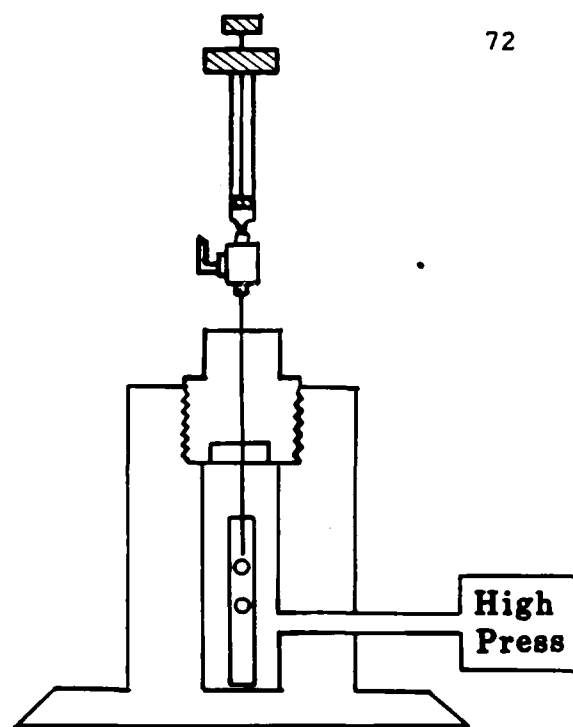
viscosity of the gel retards the drops's moving, and the smoothness of the gel prevents the drops from vaporization. This technique has been adapted from a technique developed by Apfel for producing neutron detectors based on superheated drops in a gel [23].

The next step (referred to Fig. 4.1(c)) is to get a cluster of the gel containing one superheated drop into the host water by squeezing a rubber bulb fitted to the glass tube. This cluster of gel sinks and sits on the top surface of the transducer. The gel gradually dissolves in water, then the drop floats up and is trapped by the acoustic field (referred to Fig. 4.1(d)). The amount of the gel going into water with the drop is no more than 0.1 g, which is no more than 0.05% of the amount of host water. It takes about 20 minutes for the gel to dissolve before the drop is released.

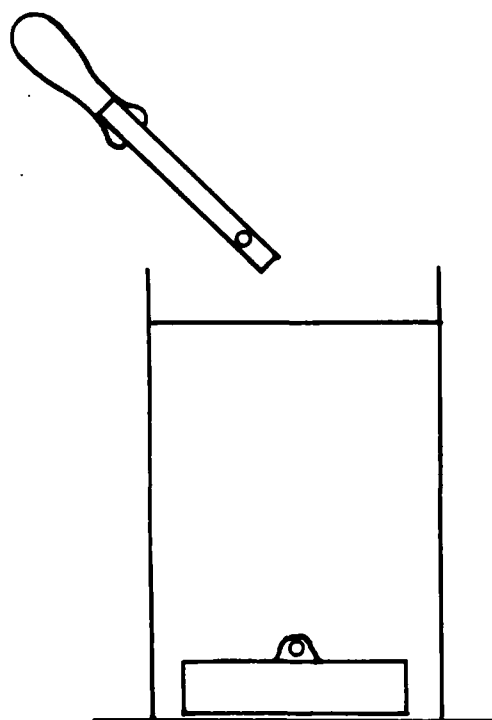
All the apparatus, such as the syringe, needle, and glass tube, used to transport the liquid are cleaned very carefully before being used, usually flushed by acetone followed by methanol then air dried. We always use the liquid directly from the bottle and conduct measurements immediately to reduce the possibility of contamination.



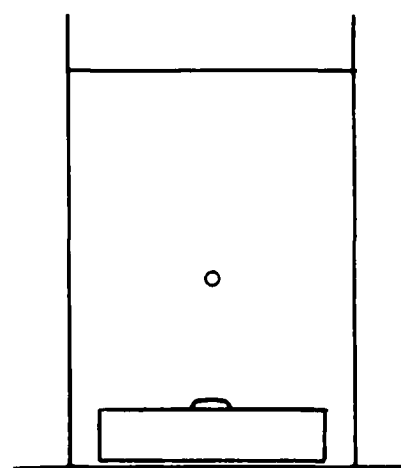
(a)



(b)



(c)



(d)

Figure 4.1: Procedure for introducing superheated liquid drops into the host water in the levitation cell.

#### 4.3 Procedure for the Size Measurements

By observing the drop through the telescope and by adjusting the levitation voltage, we can align the drop to be measured at the same position as that of the hexane drop. We then load the film holder and shoot a picture of the drop's shadow. After the frequency-phase measurement (section 4.4), we null the modulated carrier signal, adjust the levitation voltage to move the drop back to the original position, and then shoot another picture of the shadow. Then we release the drop, put one reference gauge into the cell and through the position where the drop was levitated, and take a picture of the shadow of the gauge. Two other reference gauges are used following the same procedure. It is essential for accurate size measurement to position the reference gauge through the levitation position. Very good stability of the levitated drop is required for taking good pictures. Therefore, we fine-tune the levitation frequency before exposures of the drop. These negatives are then processed for measuring the size of the drop, as mentioned in section 3.4.

#### 4.4 Procedure for the Phase-Frequency Measurement

After taking a picture of the levitated drop, we slide the film holder away from the light beam and adjust the stop and iris diaphragm, as mentioned in section 3.2. The light going through the slit is only two bright spots immediately outside the shadow of the drop. We turn on the carrier and modulation signal, drive the drop into shape oscillation, then perform the frequency-phase measurement.

#### 4.4.1 Tuning of the Carrier Frequency

To get appreciable amplitude of this shape oscillation, the carrier frequency should match a resonance frequency of the levitation system so that enough power can be fed into the transducer to generate strong standing waves therefore to give a strong radiation force on the drop; the modulation frequency should match the quadrupole resonance frequency of the drop to enhance the motion. The drop's quadrupole resonance frequency can be estimated from the apparent size of the drop and a priori interfacial tension. The carrier frequency can be tuned by monitoring the response of the drop in the following way:

We display two signals on a Tektronix T922 oscilloscope (referred to Fig. 3.1), one is the square of the modulation signal ( $v_m^2$ ) as reference, which represents the driving force (explained later in this subsection), the other one is the signal ( $v_p$ ) coming from the photomultiplier, which represents the drop's response. By varying the modulation frequency around the estimated quadrupole resonance frequency of the drop while sweeping the carrier frequency (around 510 KHz), and observing the two traces of signals ( $v_m^2$  and  $v_p$ ) on the oscilloscope, we can get a signal  $v_p$  that appears synchronous with the reference  $v_m^2$ . We fix the carrier frequency at the value where the synchronous signal appears to be strongest for a certain modulation frequency. The signal  $v_p$  includes noise in addition to this synchronous component. A low-pass filter (Krohn-Hite Model 3202 filter) helps us visualize this

synchronous component when the output of the photomultiplier is too noisy (see Fig. 3.1).

We confirm by the following observations that (the synchronous component of) the signal  $v_p$  corresponds to the drop's oscillation in its quadrupole mode. 1) The signal has the same frequency as that of  $v_m^2$ . 2) The amplitude of the signal goes up or down in phase with either the carrier or the modulation voltage. 3) The phase and amplitude of the signal vary with modulation frequency as in a regular resonance (referred to Fig. 2.1(c)). 4) By blocking the upper or lower half part of the light beam with a piece of card board, we observe that the amplitude of the signal reduces to about half, and the phase of the signal shows no change.

The frequency of the forced oscillation of a drop is the same as that of the exciting force (assuming the drop is a linear system), but it is twice the modulation frequency. This factor of 2 comes from the fact that acoustic radiation pressure is a time averaged, second-order effect. A schematic diagram, Fig. 4.2, illustrates this frequency relation. Therefore, the signal  $v_m^2$  with an amplitude 1V in rms with respect to its mean is fed into the reference channel of the lock-in amplifier (see section 3.3 and Fig. 3.1); it is also displayed on the Tektronix T922 oscilloscope to help in tuning the carrier and modulation frequencies (see Fig. 3.1). The square of the signal  $v_m$  is obtained by feeding  $v_m$  through a circuit with an MC 1495L linear, four-quadrant multiplier.

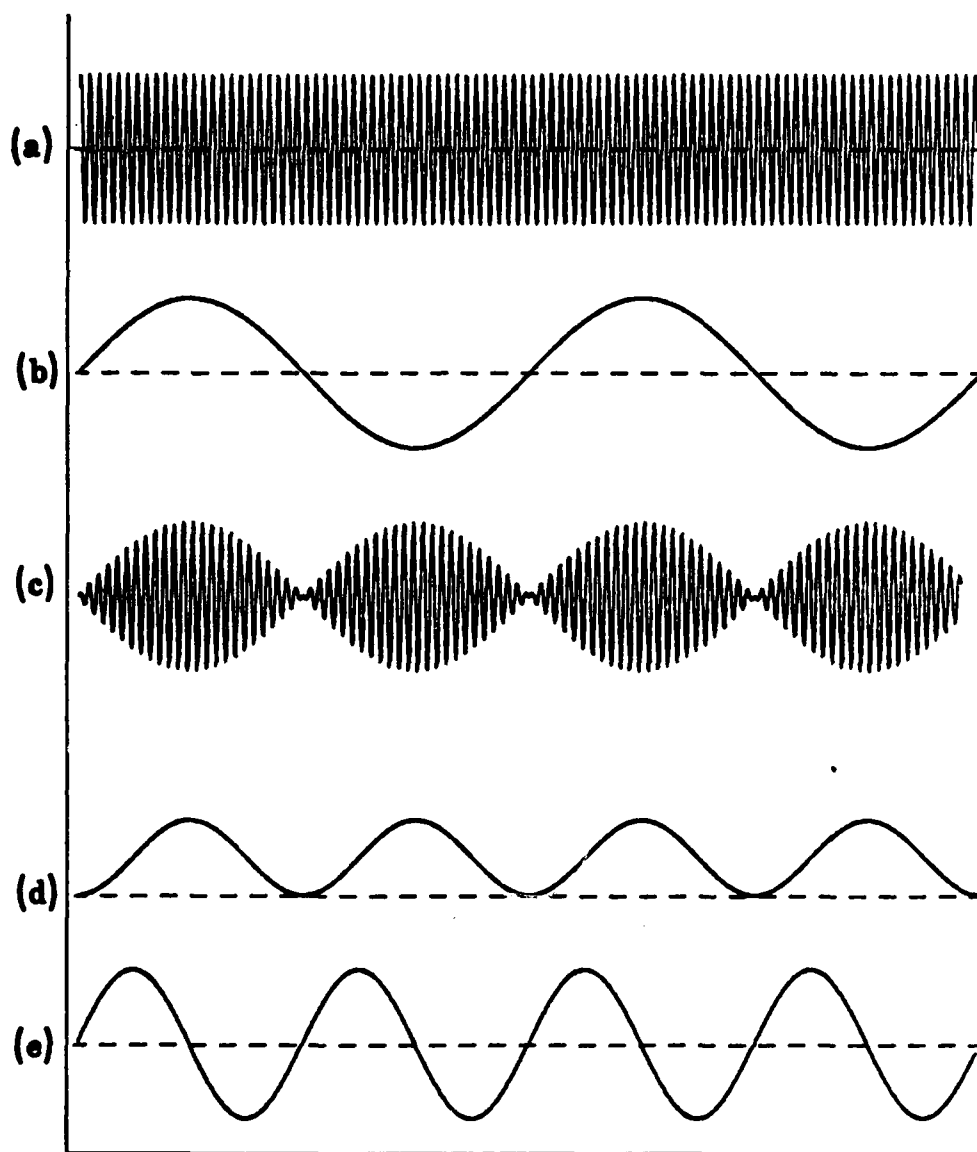


Figure 4.2: Schematic drawing showing the time variations of (a) the carrier signal ( $\sim 500$  kHz), (b) the modulation signal ( $\sim 50$  Hz), (c) the modulated input ( $v_x \times v_y$ ) responsible for the drop's shape oscillation, (d) acoustic radiation pressure, and (e) the displacement of the drop with a phase assumed to be  $90^\circ$ .

#### 4.4.2 Phase-Frequency Measurement

After tuning the carrier frequency to get an appreciable amplitude of the drop's oscillation, we feed the output of the photomultiplier into the signal channel of the lock-in amplifier, apply the  $v_m^2$  signal to the reference channel, and set the phase control  $\Lambda$  at  $\xi + 90^\circ$ , where  $\xi$  is one of several selected phase angles. The dc output of the lock-in amplifier is displayed on the storage oscilloscope as the ordinate, whereas the control voltage output of the modulation signal (a voltage proportional to its frequency) is the abscissa. Then we sweep the modulation frequency about the quadrupole resonance frequency of the drop, and obtain the  $f(\xi)$  as the frequency where the dc output of the lock-in amplifier crosses zero (see section 3.3). We sweep the modulation signal very slowly, especially when the trace is close to the zero-crossing point. Also we sweep the frequency in both directions to make sure that the sweeping rate is slow enough that sweeping up or down makes negligible difference in measured  $f(\xi)$ .

We repeat the process for several different phase angles:  $55^\circ$ ,  $67.5^\circ$ ,  $90^\circ$ ,  $112.5^\circ$ , and  $125^\circ$ , which are centered at  $90^\circ$  and chosen arbitrarily. The  $f(90^\circ)$  is measured at least three times, because it is the most significant in calculating interfacial tension. A drop of either superheated or non-superheated liquid can be acoustically levitated for more than two hours. But a levitated drop tends to be unstable in position as time goes on, possibly because that small variations in temperature or in the level of the host water de-tune the levitation system a little, or because small particles or bubbles are

introduced into the water in some way. Usually, we complete the frequency-phase measurement in 30 minutes.

#### 4.5 Procedure for the Compressadensity Measurement

The measurement of compressadensity may be either incorporated in the interfacial tension measurement or as a separate measurement. We first levitate a drop of liquid A, adjust the input voltage close to the minimum trapping voltage. We record the input voltage and mark the drop's center position by using the filar telescope. Then we release drop A and levitate a drop of liquid B. We vary the input voltage to bring drop B to the same position as was drop A, recording this input voltage. One of the two liquids A and B is considered the "reference" with known density and compressibility. By applying Eqs. (60) and (61), we can calculate the compressadensity of the other "unknown" liquid. The host liquid is water for all tests. The diameters of the drops, which need not be the same size [5], are much smaller than the acoustic wavelength.



## Chapter 5

### RESULTS AND DISCUSSION

In this chapter we present the results of the quadrupole oscillation experiments described in chapter 4. In section 5.1 we list some relevant physical properties of two common liquids (non-superheated) for which we performed experiments in order to test the accuracy of our measurements for interfacial tension. An approximate method for reducing data used in a previous work is reviewed in section 5.2. Some observations and problems associated with experiments involving gel are discussed in section 5.3. A method for inferring interfacial tension from data employing a least-squares principle is presented in section 5.4. Section 5.5 deals with the results and discussion for non-superheated liquids. In section 5.6 we present the results for superheated liquids. The last section is devoted to the results of the compressadensity measurements for three superheated liquids.

#### 5.1 Non-superheated Sample Liquids

A number of quadrupole oscillation experiments were performed for two common liquids in order to test the accuracy of our technique for measuring interfacial tension and to establish the method for data reduction. N-hexane and n-pentane were chosen; the interfacial tensions between water and each of them are known to within  $\pm 0.4\%$  (see Table 1),

and they are saturated hydrocarbon compounds similar to the superheated liquids studied in this work.

The liquid samples were from Aldrich Chemical Company, Inc.: n-hexane with 99+% purity, catalog #13938-6; n-pentane with 99+% purity, catalog #15495-4. Some relevant properties of these two liquids and water are listed in Table 1. In this table, the densities of n-hexane and n-pentane were measured using the Mettler/Parr density meter, and the measured values agree with literature values (e.g. [25]) very well. The viscosity was taken from literatures [25], as was the density of water [26]. The interfacial tension was taken from the literature [27] [28] and is compared with our measurements. In this article, wherever hexane and pentane are mentioned, they are abbreviations for n-hexane and n-pentane.

TABLE 1

Some physical properties of two sample liquids and the host.

Liquid	Temperature	Density	Viscosity $\times 10^2$	Interfacial Tension with water
	deg C	g/ml	poise	dyne/cm
n-hexane ( $\text{CH}_3(\text{CH}_2)_4\text{CH}_3$ )	20	0.6594	0.326	$51.1 \pm 0.2$
	25	0.6548	0.294	
n-pentane ( $\text{CH}_3(\text{CH}_2)_3\text{CH}_3$ )	20	0.6262	0.240	49.0
	25	0.6213	0.230	
water ( $\text{H}_2\text{O}$ )	20	0.9982	1.002	
	25	0.9971	0.955	

Note: for water-hexane interface,  $d\sigma/dt = -0.026$  dyne/cm  $^\circ\text{C}$ , where  $\sigma$  denotes interfacial tension and  $t$  denotes temperature [24].

## 5.2 Approximation by Newton's Iteration

### 5.2.1 Approximation Method

Our experiments for measuring interfacial tension may be described briefly as follows: We drive a levitated drop into forced oscillation at frequencies around its quadrupole resonance and measure the frequencies associated with several phase angles; we then compute the interfacial tension based on the resonance properties or, more specifically, the phase-frequency measurements. This phase-frequency relation incorporated with interfacial tension may be expressed by the following equation, according to the model derived by Marston (see Eq. (7)),

$$T = (\alpha\omega^{3/2} + \gamma\omega)/(\omega^{*2} - \alpha\omega^{3/2} - \omega^2), \quad (62)$$

where  $\omega^*$  is the inviscid resonance frequency and is related directly to the interfacial tension to be measured as in Eq. (16),  $T = \tan\xi$ ,  $\xi$  is the phase angle of the drop's displacement with respect to its driving force,  $\omega$  is the frequency of the forced oscillation,  $\alpha$  and  $\gamma$  are functions of the drop's size and of the properties (density and viscosity) of the host as well as the drop liquid (see Eqs. (8), (9), and (10)). The phase-frequency relation given by the simplified model derived in chapter 2 can also be expressed in the same form as Eq. (62), though  $\alpha$  and  $\gamma$  will then represent different functions of the size and the properties from that given by Eqs. (8) and (9) (see Eq. (58)).

In the work done by Marston and Apfel [11] Eq. (62) was approximated in the following way and then employed with data for deducing interfacial tension. First, Eq (62) may be rewritten as a function of  $\omega$ ,

$$f(\omega) = T\omega^2 + \alpha(1+T)\omega^{3/2} + \gamma\omega - T\omega^{*2} = 0. \quad (63)$$

By applying Newton's method of iteration, and using  $\omega^*$  as an initial approximation,  $\omega$  can be expressed as a function of  $T$  [24] [10],

$$\omega \approx \omega^* - \frac{f(\omega^*)}{f'(\omega^*)} \quad (64)$$

$$\approx (\omega^* - \frac{1}{2}\alpha\omega^{*\frac{1}{2}} + 3/8\alpha^2) - 1/T (\frac{1}{2}\alpha\omega^{*\frac{1}{2}} - 3/4\alpha^2 + \frac{1}{2}\gamma) .$$

Therefore,

$$\omega(90^\circ) \approx \omega^* - \frac{1}{2}\alpha\omega^{*\frac{1}{2}} + (3/8)\alpha^2 , \quad (65)$$

and

$$\omega(\xi) \approx \omega(90^\circ) - 1/T [\frac{1}{2}\alpha\omega^{*\frac{1}{2}} - (3/4)\alpha^2 + \frac{1}{2}\gamma] . \quad (66)$$

If we define  $s$  as

$$s = [\omega(\xi) - \omega(90^\circ)] (-T) , \quad (67)$$

then from Eq. (66), we have

$$s \approx \frac{1}{2}\alpha\omega^{*\frac{1}{2}} - (3/4)\alpha^2 + \frac{1}{2}\gamma . \quad (68)$$

The damping constant  $s$  can be obtained experimentally by substituting the data of phase-frequency measurements into Eq. (67), and  $s_e$  is used to denote it in this article. For an interface composed of two liquids with known density, viscosity, and interfacial tension,  $\alpha$  (from Eq. (8)),  $\gamma$  (from Eq. (9)), and  $\omega^*$  (from Eq. (16)) can be calculated, and a theoretical prediction of the damping constant, denoted by  $s_{th}$ , can be obtained via Eq. (68). From Eqs. (65) and (68) we have

$$\begin{aligned} \omega^* &\approx \omega(90^\circ) + \frac{1}{2}\alpha\omega^{*\frac{1}{2}} - (3/8)\alpha^2 , \\ &= \omega(90^\circ) + s + (3/8)\alpha^2 - \frac{1}{2}\gamma . \end{aligned} \quad (69)$$

Furthermore, by neglecting the last two terms of Eq. (69), we have

$$\omega^* \approx \omega(90^\circ) + s . \quad (70)$$

Eq. (70) was used to infer interfacial tensions from measurements in the work done by Marston and Apfel [11]. In this way,  $\alpha$  and  $\gamma$  were not involved in the calculation for interfacial tension.

By using artificial data (that is, a phase-frequency relation given by Eq. (62) and known radius as well as properties of liquids), we can show that Eq. (69) is a very good approximation for calculating interfacial tension, and Eq. (70) gives higher  $\omega^*$  than Eq. (69) does by about 0.7% which introduces about +1.5% error in the interfacial tension. For our measurements with hexane or pentane drops in water (those marked with \* in Table 5), the theoretical values given by Eqs. (8) and (9) are probably good approximations for  $\alpha$  and  $\gamma$ , judging from the fact that the measured damping constant  $s_e$  is very close to the theoretical value  $s_{th}$ . Therefore, we estimate that the error in deduced interfacial tension introduced by using the approximate model as in Eq. (70) is about 1.5% too high.

### 5.2.2 Examples

As an example of this procedure of calculation, we list the data for one hexane drop in Table 2. To deduce the interfacial tension from these data, we first apply Eq. (70) and have

$$\omega^* = (113.69 + 4.80)2\pi = 744.50 ,$$

then from Eq. (16),

$$\sigma_1 = \omega^{*2} R^3 \Gamma / 24 \approx 51.5 \text{ dyne/cm} ,$$

where  $\sigma_1$  is used to represent interfacial tension obtained by using Eq. (70). With the literature values listed in Table 1, the theory by

Marston gives  $s_{th} = 27.64$  (Eq. (63)),  $\alpha_{th} = 1.76$  (Eq. (8)), and  $\gamma_{th} = 13.97$

(Eq. (9)). The experimentally determined damping constant  $s_e$  (30.14) is close to the theoretical prediction  $s_{th}$  (27.64). If we use Eq. (69) with

the data in Table 2 and the above  $\alpha_{th}$  and  $\gamma_{th}$ , we get the corrected interfacial tension, denoted by  $\sigma_2$ , as 50.6 dyne/cm. This set of data is also shown in Fig. 5.1. In this figure, triangle circular symbols represents the data points, and the dashed line represents the theoretical prediction based on Marston's theory (Eqs. (62), (8), (9), and (16)) with physical properties of hexane and water given in Table 1 as well as the known radius of the drop. The data points follow the slope of the theoretical line closely, which indicates agreement between  $s_e$  and  $s_{th}$ . The measured frequencies associated with  $90^\circ$  and other phase angles are less than the theoretical prediction, which indicates that the measured interfacial tension is less than the literature value used for the theoretical prediction. The meaning of the solid line will be discussed in section 5.4.2. This is a typical example of our measurements; more data and discussion are presented in section 5.5 (see Table 5).

TABLE 2

Data for one quadrupole oscillation experiment.

Host : water Droplet: n-hexane		R=0.0825cm t=22°C	
Phase( $\xi$ ) Deg.	Frequency( $f(\xi)$ ) Hz		
90.0 90.0 90.0	113.64 113.70 113.72 <hr/> ave:113.69		
		calculation for $s_e$	
		T=tan( $\xi$ )	[ $f(\xi)-f(90^\circ)$ ]( $-T$ )
55.0	110.08	1.42815	5.15
55.0	110.24	1.42815	4.92
67.5	111.66	2.41421	4.89
112.5	115.58	-2.41421	4.57
125.0	116.80	-1.42815	4.45
			<hr/> ave:4.80
			$s_e=(4.80)2\pi=30.14$



Host: water, Droplet: hexane, Drop radius: 0.0825 cm

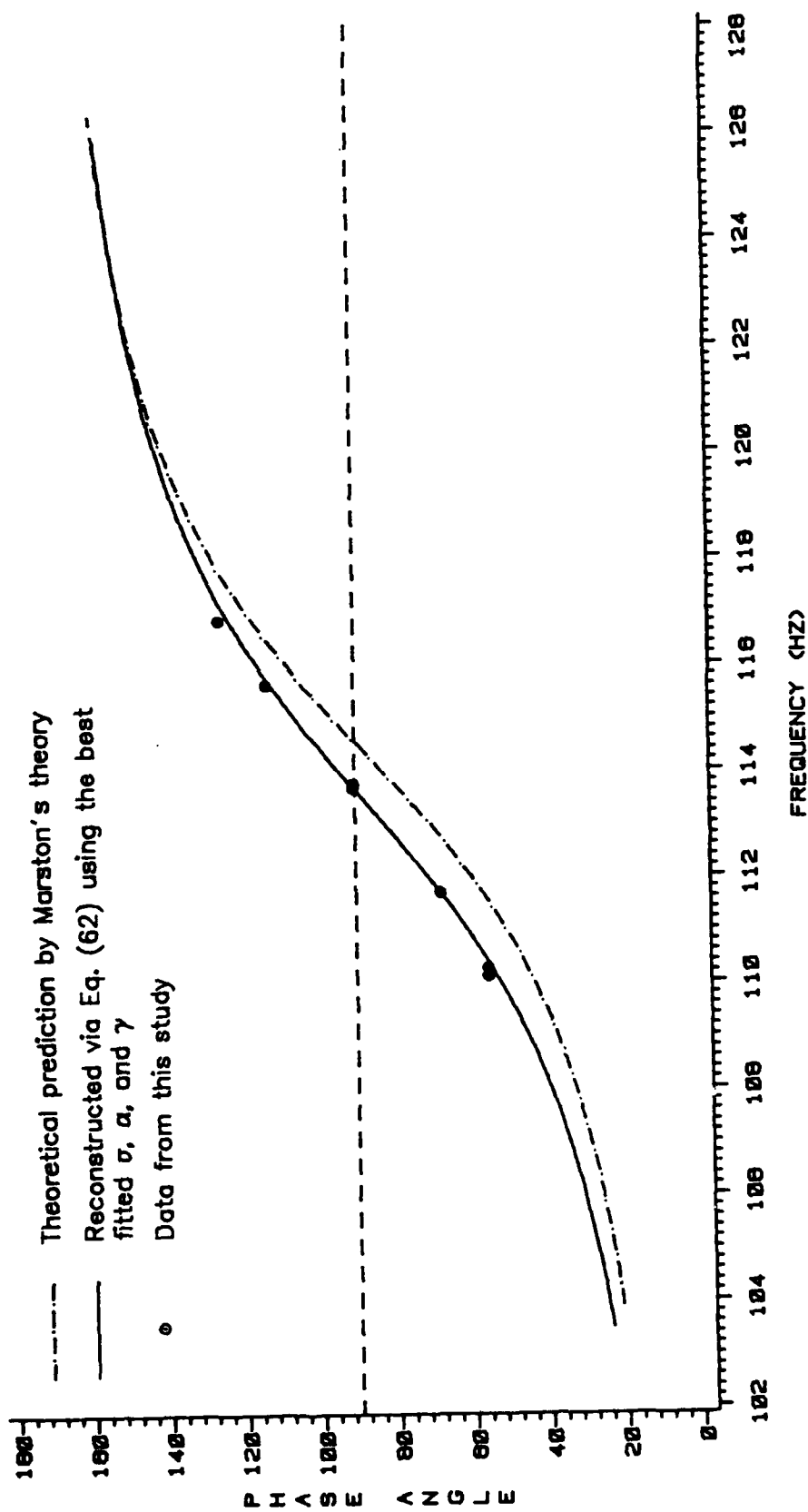


Figure 5.1: Phase vs. frequency for one experiment which involved no gel in the preparation of the drop.

### 5.3 Gel Effect

As described in section 4.2, our superheated drops was first formed in gel and then transported into the water host. It is a convenient method for introducing superheated drops into host water; other possible alternative methods would require pressurizing the whole levitation cell--up to 10 atm for propane drops or lower pressure with some cooling mechanism; technically, it is much more complicated and difficult. However, because of the contact of the test drop with the gel in the process of transport and the dissolution of gel in the host water, one must ask whether the drop's surface is contaminated and whether the interfacial tension is changed. We have done several tests to explore this issue.

First, we measured the surface tension of water against air, then put some gel (about 0.2% by volume) into the water and measured the surface tension again after the gel was dissolved in the water. A Fisher Surface Tensiometer, Model 20 (from Fisher Scientific Company), employing the ring detachment method, was used in the measurements. There was no detectable difference in the measured surface tension ( $72.1 \pm 0.1\%$  dyne/cm) due to the introduction of gel. Secondly, we performed several quadrupole oscillation experiments for hexane and pentane (those marked with \*\* in Table 5); the host water had gel dissolved in it (about 0.1 % in volume); the test drop was injected into water directly from a syringe. The measured interfacial tension agrees well with other data which were taken with clean host water, and the measured damping constant agrees well with the theoretical prediction (see Table 5).

AD-A136 996

INTERFACIAL TENSION BETWEEN WATER AND SELECTED  
SUPERHEATED LIQUIDS BY QUA. (U) YALE UNIV NEW HAVEN CT  
DEPT OF MECHANICAL ENGINEERING C J HSU DEC 83 TM-4

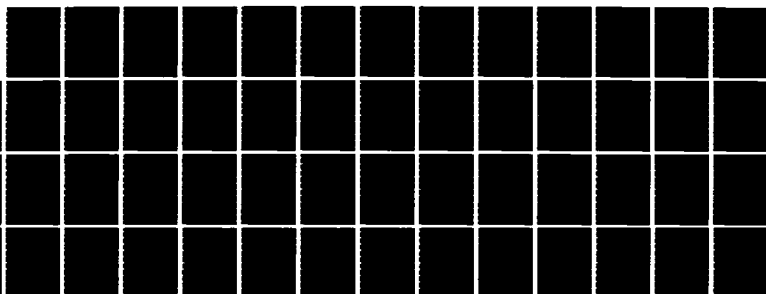
2/2

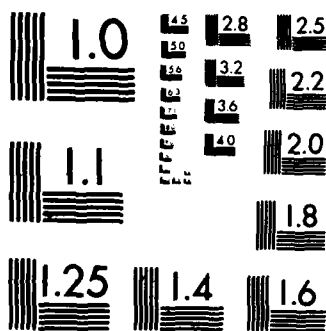
UNCLASSIFIED

N00014-76-C-0527

F/G 7/4

NL





MICROCOPY RESOLUTION TEST CHART  
NATIONAL BUREAU OF STANDARDS-1963-A

Therefore, it seems that the gel is not surface active in water-hexane and water-pentane interfaces: that is, there is no tendency for the gel to pack into or to migrate away from the interface and to change the interfacial tension by any detectable amount [29].

On the other hand, for the experiments of hexane and pentane which had the test drop first formed in gel (following the same procedure as in Fig. 4.1 but without pressurization), the oscillation of the drop exhibited much greater damping; the measured frequencies at selected phase angles showed significant difference with the theoretical prediction: the frequencies associated with  $90^\circ$  phase,  $\omega(90^\circ)$ , were lower than theoretical prediction by about 5%, and the values of  $s_e$  were higher than the theoretical value  $s_{th}$  by a factor about 2. The results of these experiments are marked with \*\*\* in Table 5. One example is shown in Fig. 5.2; the circles denote data points, and the dashed line represents theoretical prediction as mentioned in the end of section 5.2. The solid line will be discussed in the next section. These observations suggest that there might be some residue of gel on the drop's surface while the measurements were taken, though it could not be seen from the pictures of the drops. These observations also raise several questions about how to analyze the measurements which have gel involved: First of all, is Eq. (62) still a good model for the motion? If it is, then what is an appropriate way to obtain interfacial tension from the measurements of resonance properties? The values of  $\alpha$  and  $\gamma$  need to be estimated in order to employ Eq. (69) or to assess the validity of Eq. (70). The fact that the values of  $\omega(90^\circ)$  were lower and

the values of  $s_e$  were higher than theoretical values indicates that  $\alpha$  might be greater than and  $\gamma$  might be different from the theoretical values given by Eqs. (8) and (9) (see Eq. (62)). Therefore, we need a new scheme to analyze data. We have developed a method employing least-squares principle to estimate  $\alpha$ ,  $\gamma$ , and interfacial tension. Details are discussed in sections 5.4 and 5.5 and the Appendix A and B.

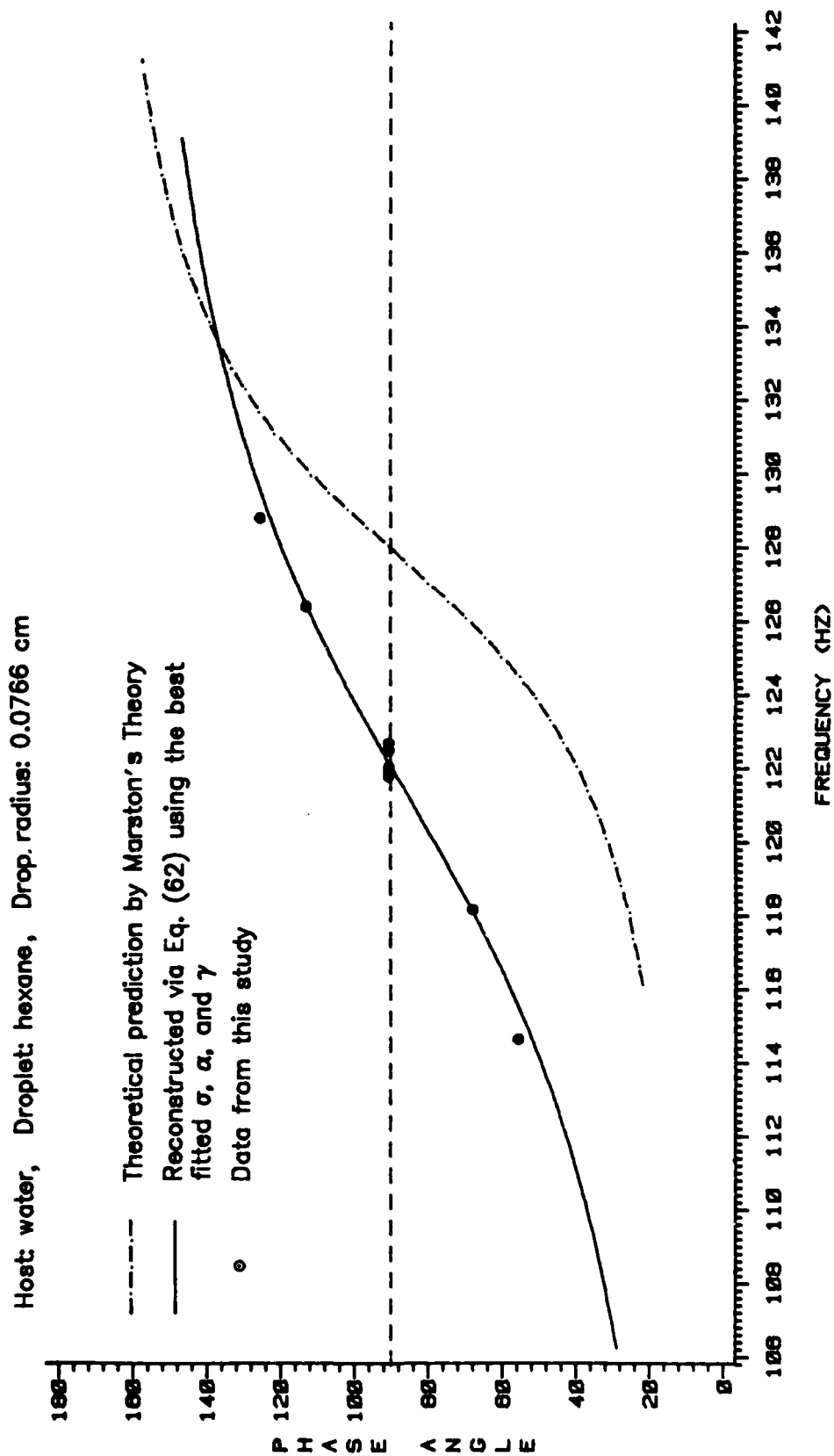


Figure 5.2: Phase vs. frequency for one experiment in which gel was used in the preparation of the drop.

## 5.4 Data Reduction by the Method of Least-squares

### 5.4.1 Model and Procedure

Several methods have been considered for computing interfacial tension from data of a drop's quadrupole resonance properties (see Appendix A); the one we chose is presented here. The basic idea is that we assume Eq. (62) is an appropriate model for the motion but leave  $\alpha$ ,  $\gamma$ , and  $\omega^*$  all as unknown and then fit this model to data. We evaluate the model by evaluating how well the fitting is and compute the best fitted  $\omega^*$ ,  $\alpha$ , and  $\gamma$  in the least-squares sense [31].

The procedure is described as follows: We partition the data of one drop into two parts and consider them separately. First we consider only the measurements associated with  $90^\circ$  phase angle. For  $\xi = 90^\circ$ , we have (from Eq. (62))

$$\omega^{*2} - \omega(90^\circ)^2 - \alpha\omega(90^\circ)^{3/2} = 0 ,$$

or in another form,

$$\alpha[\omega(90^\circ)]^{3/2} = \omega^{*2} - [\omega(90^\circ)]^2 . \quad (71)$$

By assuming an  $\omega^*$  or, equivalently, by assuming a  $\sigma$  (see Eq. (16)) and plugging the measured  $\omega(90^\circ)$  into the above equation, we obtain several equations for one variable-- $\alpha$ . We can find an "optimum"  $\alpha$  which fits these equations the best in the least-squares sense.

The next step is to consider the measurements where  $\xi \neq 90^\circ$ . From Eq. (62), we have

$$\gamma\omega = T(\omega^{*2} - \omega^2) - \alpha(1+T)\omega^{3/2} . \quad (72)$$



By assuming the pair  $(\sigma, \alpha)$  obtained in the first step as known (fixed) values and several measured  $\omega$  at different or the same phase angles, we obtain several equations for one variable-- $\gamma$ , whose optimum value is then determined by least-squares method. Therefore, for each assumed  $\sigma$ , we find associated  $\alpha$  and  $\gamma$ . An "optimum"  $\sigma$  or  $\omega^*$  is chosen based on the overall performance of the fitting. The estimate for  $\alpha$  and  $\gamma$  are obtained along with it. A general linear model (GLM) in a computer system for data analysis named SAS (stands for Statistical Analysis System) supported by Yale Computer Center was used for the least-squares regression.

#### 5.4.2 Examples

As an example, this fitting process for the data listed in Table 2 with assumed  $\sigma=50.5$  dyne/cm is shown in Appendix B. The result of the fitting for this set of data is shown in Table 3 and Fig. 5.3 (Fig. 5.3 shows only the fitting for  $\gamma$ ). The GLM printout (Appendix B) contains some information other than the estimated parameters ( $\alpha$  and  $\gamma$ ). The information includes several statistical quantities that were used together to assess the fitting: the square of the correlation function (sometimes called the coefficient of determination) ( $R^2$ ), the coefficient of variation (C.V.), and the significance probability ( $PR>|T|$ ).

The square of the correlation coefficient, denoted  $R^2$  in Table 3 and  $R$  in Fig. 5.3, measures how much variation in the dependent variable

can be accounted for by the model. The value of the right hand part of Eq. (71) or (72) obtained by employing experimental data is called the observed value. The value calculated by using the fitted parameters ( $\alpha$  or  $\gamma$ ) and data to the left hand part of Eq. (71) or (72) is called the fitted or predicted value of the dependent variables. The difference between the observed and fitted value is called the residual or error. The parameter  $R^2$  is defined as the sum of squares of the predicted values divided by the sum of squares of the observed values.  $R^2$  ranges from 0 to 1; the larger the value of  $R^2$ , the better the model's fit (see Appendix B and [30]).

In Fig. 5.3 and Table 3 the symbol "P" represents significance probability. The significance probability is the probability that the observed data would occur if a certain Null Hypothesis were true; here, the Null Hypothesis is that the parameter to be estimated ( $\alpha$  or  $\gamma$ ) is zero [32] [30]. The significance probability ranges from 0 to 1; a small value of P indicates that the Null Hypothesis is unlikely to be true or, in other words, the model is significant.

The symbol CV in Table 3 and the symbol c in Fig. 5.3 denote the coefficient of variation (C.V.) which is used to describe the amount of variation in the dependent variable (the right hand side of Eq. (71) or (72)). It is equal to the standard deviation of the dependent variable (after adjusting for the mean) divided by the mean of the dependent variable times 100. The values of C.V. shown in Fig. 5.3 is normalized so can fit into the scale between 0 and 1. Some general observations of the fitting are discussed below.

It can be seen in Table 3 that for  $\sigma$  around its "optimum" value, the fitting for  $\alpha$  is generally much better than the fitting for  $\gamma$ , which should be expected because the measurements for  $\omega(90^\circ)$  are generally much better than the measurements for other phase angles in terms of repeatability. It also shows that for different assumed values of  $\sigma$  the higher the  $\sigma$  is, the better the fitting for  $\alpha$  is ; on the other hand, the higher the  $\sigma$  is, the poorer the fitting for  $\gamma$  is, and the fitting for  $\gamma$  degenerates first gradually then dramatically (that is, the  $R^2$  decreases, while the C.V. and P increases sharply) as  $\sigma$  reaches certain value (Fig. 5.3 shows an example).

Considering the fact that the measurements of  $\omega(90^\circ)$  are the best measurements we have, and observing the fitting for both  $\alpha$  and  $\gamma$ , we choose the  $\sigma$  beyond which the fitting for  $\gamma$  degenerates very quickly as the optimum value. For most experiments, at the value of "optimum"  $\sigma$ , the fitting for  $\gamma$  has a  $R^2$  about 0.9. The value of C.V. and P for different test liquids could be very different, because they are dependent on the mean of the dependent variable which is a function of interfacial tension and other parameters. However, the variation of C.V. and P with assumed  $\sigma$  for individual experiment is clear. The significance probability of the fitting for  $\gamma$  associated with the optimum  $\sigma$  is usually no greater than 0.01, which is the significance level usually referred to as "highly significant" in statistics.

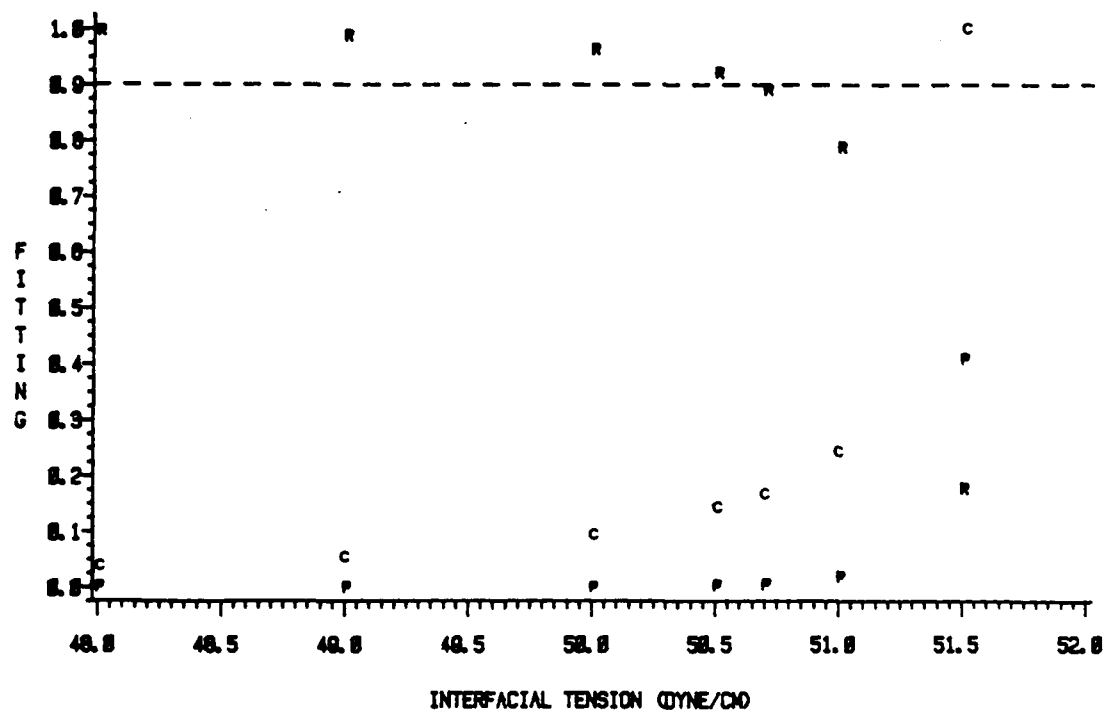
The optimum  $\sigma$  we chose for the above example (data listed in Table 2) is 50.5, and the associated  $\alpha$  and  $\gamma$  are 1.9 and 13.6 (see Table 3, Fig. 5.3, and Table 5). Employing the above  $\alpha$ ,  $\gamma$ , and  $\sigma$  obtained from least-squares fitting, we can reconstruct the phase-frequency relation by the aid of Eq. (62). The result is shown as the solid line in Fig. 5.1. The same procedure was applied to another set of data which is shown in Fig. 5.2. The results of the fitting for this set of data are summarized in Table 4 and Fig. 5.4. The solid line shown in Fig. 5.2 was reconstructed based on these "best fitted" parameters.

From the results of the fitting for the two examples mentioned above, we may assess the validity of the model of Eq. (62), especially for describing the oscillation of the drop which is formed in gel. Judged from the values of  $R^2(\gamma)$ ,  $P(\gamma)$ , and  $C.V.(\gamma)$  listed in Tables 3 and 4, it appeared that the model fitted the data well, even if the test drop was formed in gel initially. We found that this was generally true for our experiments for hexane and pentane. The summary and discussion of our results for hexane and pentane are presented in the next section.

TABLE 3

Fitting for one water-hexane experiment (droplet radius 0.825 mm)

$\sigma$	$R^2(\alpha)$	$P(\alpha)$	$CV(\alpha)$	$\alpha$	$R^2(\gamma)$	$P(\gamma)$	$CV(\gamma)$	$\gamma$
48.0	0.9979	0.0010	5.60	0.35	0.994	0.0001	8.88	51.55
49.0	0.9997	0.0002	2.19	0.92	0.987	0.0001	12.96	34.48
50.0	0.9999	0.0001	1.38	1.48	0.962	0.0005	21.94	23.41
50.5	0.9999	0.0001	1.16	1.76	0.919	0.0025	32.84	16.47
50.7	0.9999	0.0001	1.10	1.88	0.889	0.0048	39.15	13.56
51.0	0.9999	0.0001	1.01	2.05	0.786	0.0185	57.59	9.34
51.5	0.9999	0.0001	0.90	2.33	0.176	0.4080	230.15	2.31



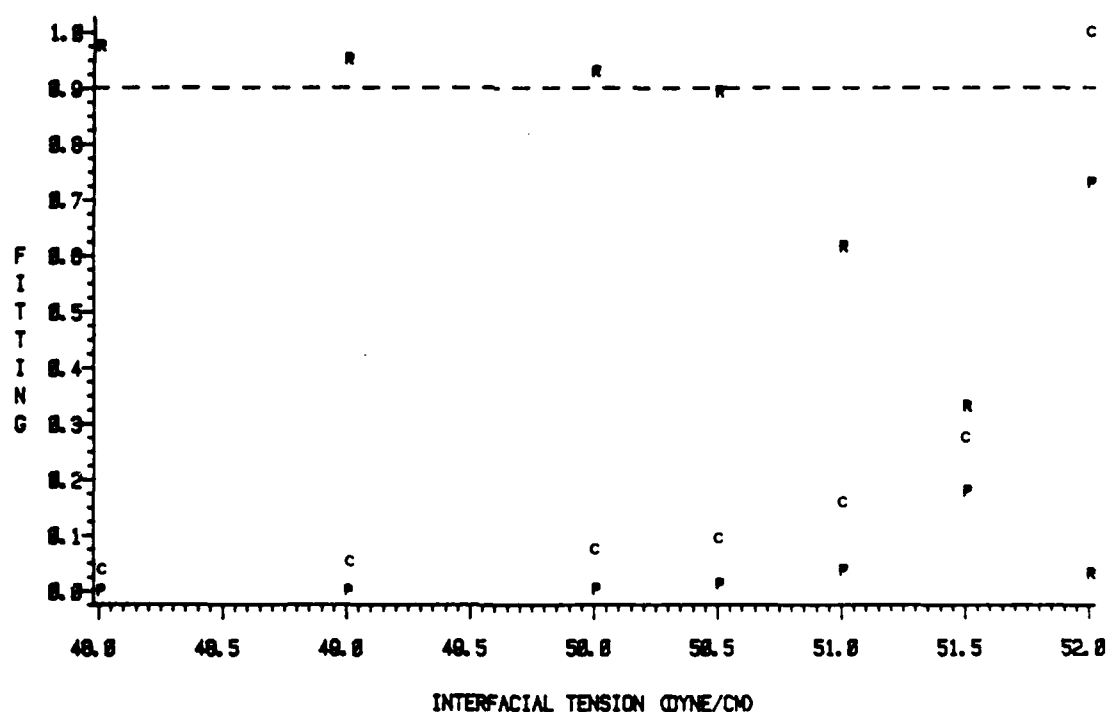
R Square of the correction coefficient  
 C The coefficient of variance (normalized)  
 P The significance probability

Figure 5.3: Some statistics for the least-squares fitting for  $\gamma$ :  
 Example for host, water; drop, hexane; drop radius, 0.0825  
 cm (referred to figure 5.1 and Table 3).

TABLE 4

Fitting for one water-hexane experiment (droplet radius 0.766 mm)

$\sigma$	$R^2(\alpha)$	$P(\alpha)$	$CV(\alpha)$	$\alpha$	$R^2(\gamma)$	$P(\gamma)$	$CV(\gamma)$	$\gamma$
48.0	0.9960	0.0001	6.96	2.68	0.973	0.0001	21.33	63.74
49.0	0.9970	0.0001	5.72	3.31	0.949	0.0004	29.40	48.46
50.0	0.9980	0.0001	4.88	3.94	0.928	0.0030	41.80	33.18
50.5	0.9983	0.0001	4.55	4.26	0.892	0.0122	52.90	21.30
51.0	0.9985	0.0001	4.27	4.58	0.614	0.0370	88.58	13.57
51.5	0.9987	0.0001	4.02	4.89	0.329	0.1785	148.64	10.11
52.0	0.9990	0.0001	3.80	5.21	0.030	0.7280	541.43	2.41



- R Square of the correction coefficient  
 C The coefficient of variance (normalized)  
 P The significance probability

Figure 5.4: Some statistics for the least-squares fitting for  $\gamma$ :  
 Example for host, water; drop, hexane; drop radius, 0.0766  
 cm (referred to figure 5.2 and Table 4).

## 5.5 Measurements for Non-superheated Liquids

### 5.5.1 Interfacial Tension

A summary of our interfacial tension measurements for water-hexane and water-pentane interfaces is presented in Table 5. Parameters with subscript "th" are theoretical values;  $s_{th}$  is calculated using Eq. (68) (assuming the interfacial tension is known and the value is taken from Table 1),  $\alpha_{th}$  is calculated by using Eq. (8), and  $\gamma_{th}$  is calculated by using Eq. (9). Subscript "f" denotes parameters obtained using the least-squares method.  $s_e$  is the experimental damping constant calculated from data and Eq. (67).  $\sigma_1$  is the approximate interfacial tension calculated via Eq. (70).  $\sigma_2$  is the corrected interfacial tension calculated using Eq. (69) with  $\alpha_{th}$  and  $\gamma_{th}$ .

For experiments which had the drops formed in water (even the water had some gel dissolved in it), it appeared that the experimental damping constant  $s_e$  agreed with the theoretical value  $s_{th}$  well, also do the fitted  $\alpha_f$  and  $\gamma_f$  with  $\alpha_{th}$  and  $\gamma_{th}$ . For these measurements of drops which were first formed in gel, the  $s_e$  were much greater than  $s_{th}$ ; the fitted  $\alpha_f$  is several times greater than  $\alpha_{th}$  while  $\gamma_f$  is close to  $\gamma_{th}$ . This effect is expected because the potential (bulk) flow (both inside and outside the drop) and the bulk viscosity are not changed much due to the presence of gel; on the other hand, the flow in the boundary layer is affected very significantly due to some residue of gel on the drop's surface enhancing the damping of the drop's motion.

For interfacial tension, the  $\sigma_f$  corresponded closely to the corrected interfacial tension  $\sigma_2$ . The data in Table 5 also demonstrate that, within the uncertainty of our measurement, the measured interfacial tension of the drops which were first formed in gel was not different from the measured value of the drops which were injected directly into host water. Considering the similarity in chemical structure between the superheated and non-superheated sample liquids used in our experiments, though without direct justification, we presume that the interfacial tension between water and the superheated liquids was not significantly changed by the gel involved in the transport process.

The average measured interfacial tension ( $\sigma_f$ ) was 50.7 dyne/cm for water-hexane interface and 48.6 dyne/cm for water-pentane interface, which were about 0.8% lower than the literature values. The total uncertainty of our interfacial tension measurement is estimated at  $\pm 0.75\%$ . This total uncertainty is computed as the square root of the sum of the square of each following error:

1.  $\pm 0.1\%$  uncertainty in the frequency measurement, which corresponds to  $\pm 0.2\%$  uncertainty in the measured interfacial tension.
2.  $\pm 0.2\%$  uncertainty in the droplet size measurement, which corresponds to  $\pm 0.6\%$  uncertainty in the measured interfacial tension.
3.  $\pm 0.1\%$  uncertainty in the density measurement, which corresponds to  $\pm 0.1\%$  uncertainty in the measured interfacial tension.



4.  $\pm 0.4\%$  uncertainty in the determination of the optimum  $\sigma_f$  based on the least-squares method.

### 5.5.2 Damping and Viscosity

In our experiments of the quadrupole oscillation of a drop in water, the damping of the motion is due to the viscous dissipation. Theoretically, we should be able to deduce information on the viscosity of either the drop or the host from the measured damping constant. Table 6 illustrates the variation of the theoretical damping constant corresponding to several arbitrarily assumed values of viscosity. For very significant (up to 30%) change in inner or outer viscosity, the corresponding variation of the  $s_{th}$  appears comparable with the typical fluctuation of the ratio  $s_e/s_{th}$  (about 15%) (see Table 5). Therefore, with the precision of our experiment, it is not practical to get any significant information about the viscosity of either the inner or the outer fluid from the measurements. The viscosity of 0.5% glycerol in water solution is 1% higher than the viscosity of pure water [26]. For experiments marked with \*\* in Table 5, the host water had no more than 0.1% gel dissolved in it. From the above example, the change of viscosity of host water due to this amount of gel is too small to show up in the measured damping constant, as it is the case we observed in Table 5.

For experiments denoted \*\*\* in Table 5, if we assume that near the interface the viscosity was changed locally, then we can estimate (by

Eq. (8)) what would be the average viscosity associated with the interface boundary to give the value  $\alpha_f$ . An example is shown in Table 7, the value of 0.03 poise is equivalent to the viscosity of a 35% glycerol in water solution [26]. The above calculation suggests the existence of gel residue on the interface for the experiments denoted \*\*\* in Table 5, as we discussed in section 5.4.

TABLE 5

Measurements for non-superheated liquids.

radius mm	f(90°) Hz	$s_e$ ra/sec	$\sigma_1$ dyne/cm	$\sigma_2$ dyne/cm	$\sigma_f$	$\alpha_f$	$\gamma_f$	$s_{th}$	$\alpha_{th}$	$\gamma_{th}$	remark
water-hexane interface											
0.749	130.63	38.3	51.3	50.4	50.5	2.3	16.4	32.8	1.8	17.0	*
0.766	122.14	64.5	51.4		50.5	4.3	21.3	31.5	1.8	16.2	***
0.787	121.63	33.8	51.3	50.5	50.5	2.0	15.8	30.0	1.8	15.4	*
0.825	113.69	30.1	51.5	50.6	50.7	1.9	13.6	27.6	1.8	14.0	*
0.895	100.23	28.1	51.3	50.5	50.7	2.0	10.1	23.9	1.5	11.9	**
0.905	94.01	57.5	51.5		51.1	4.7	16.5	23.4	1.5	11.6	***
0.985	87.20	22.4	51.4	50.6	50.5	1.5	11.8	20.1	1.4	9.8	**
1.061	77.47	23.4	51.4	50.7	50.7	1.8	8.3	17.6	1.3	8.5	*
water-pentane interface											
0.801	118.08	30.5	49.4	48.5	48.5	1.7	16.5	28.1	1.6	16.5	*
0.905	95.50	44.51	49.6	48.8	49.0	3.4	14.7	22.6	1.4	12.9	***
0.710	141.18	38.9	49.5	48.5	48.5	2.0	20.9	35.0	1.8	20.9	**
0.770	118.51	74.0	49.3	48.4	48.7	5.3	25.0	30.2	1.6	17.8	***
0.791	120.66	29.3	49.5	48.5	48.5	1.6	17.5	28.8	1.6	16.9	*
0.944	92.83	20.7	49.5	48.6	48.5	1.2	12.5	20.9	1.3	11.8	**
1.047	79.51	17.7	49.5	48.7	48.7	1.2	9.4	17.4	1.2	9.6	*

- Note: 1) The remark \* denotes that the drop was injected directly into water from a dispenser and there was no gel dissolved in the water.
- 2) The remark \*\* denotes that the drop was injected directly into water from a dispenser and there was gel dissolved in the water.
- 3) The remark \*\*\* denotes that the drop was formed first in gel then transported into water with the gel.
- 4) The  $\alpha_f$  and  $\alpha_{th}$  have a dimension of (radian/second)<sup>1/2</sup>. The  $\gamma_f$  and  $\gamma_{th}$  have a dimension of (radian/second).

TABLE 6

Variation of damping with viscosity (I).

R=0.0825 cm		$\rho_o=0.9978$ g/ml	
$\sigma=51.0$ dyne/cm		$\rho_i=0.6576$ g/ml	
$\mu_o=0.009548$ poise			
$\mu_i$ poise	$\alpha_{th}$ (rad/sec) <sup>1/2</sup>	$\gamma_{th}$ rad/sec	$s_{th}$ rad/sec
0.00313	1.67	13.97	27.64
0.002	1.43	15.52	25.66
0.004	1.82	13.20	28.84
$\mu_i=0.00313$ poise			
$\mu_i$	$\alpha_{th}$	$\rho_{th}$	$s_{th}$
0.009548	1.67	13.97	27.64
0.007	1.59	9.54	24.49
0.012	1.78	18.53	30.59

TABLE 7

Variation of damping with viscosity (II).

R=0.0766 cm		$\rho_o=0.9978$ g/ml $\sigma=51.0$ dyne/cm		
$\rho_i=0.6576$ g/ml				
$\mu_i$ poise	$\mu_o$ poise	$\alpha_{th}$ (rad/sec) $^{\frac{1}{2}}$	$\gamma_{th}$ rad/sec	$s_{th}$ rad/sec
0.00313	0.009548	1.80	16.21	31.59
0.01	0.01	2.60	14.12	39.43
0.02	0.02	3.68	28.25	56.93

## 5.6 Measurements for Superheated Liquids

### 5.6.1 Test Liquid

In this section we report measurements for butane, isobutane, and propane. Some physical properties of these three compounds are listed in Table 8. The experiments were all conducted at the condition of room temperature and atmospheric pressure, and the compounds were all in liquid state; therefore, they were superheated at a degree from 20°C to over 60°C. The boiling point at a pressure of 760 mmHg and the vapor pressure at 20°C are taken from literature [25]. The density in Table 8 was based on the density at 21°C and equilibrium pressure [25] and then corrected by using the isothermal compressibility which is extrapolated from the available data at the equilibrium state. The surface tension against its vapor listed in Table 8 is taken from a line which extrapolates the data at the equilibrium state and connects the point of zero surface tension at the critical temperature (which should be good far from the critical temperature) (for example, Fig. 5.5). The viscosity listed in Table 8 was extrapolated from the data at the equilibrium state. For these values in Table 8, the uncertainty is estimated to be  $\pm 0.2\%$  for the density,  $\pm 1\%$  for the surface tension and  $\pm 3\%$  for the viscosity.

TABLE 8

Some physical properties of three superheated liquids.

Liquid	Structure	Boiling Pt. at 760mmH	Vapor Press. at 20°C	Degree of Superheat	Density at 21°C	Surf. Tens. at 21°C	Visc. 21°C
		°C	bar	°C	g/ml	dyne/cm	cp
Butane	-c-c-c-c-	-0.50	2.07	22	0.577	12.6	0.17
Iso- butane	$  \begin{array}{c}  -c- \\    \\  -c-c-c-  \end{array}  $	-11.73	2.98	33	0.556	10.6	0.18
Propane	-c-c-c-	-42.07	8.40	63	0.502	8.0	0.093

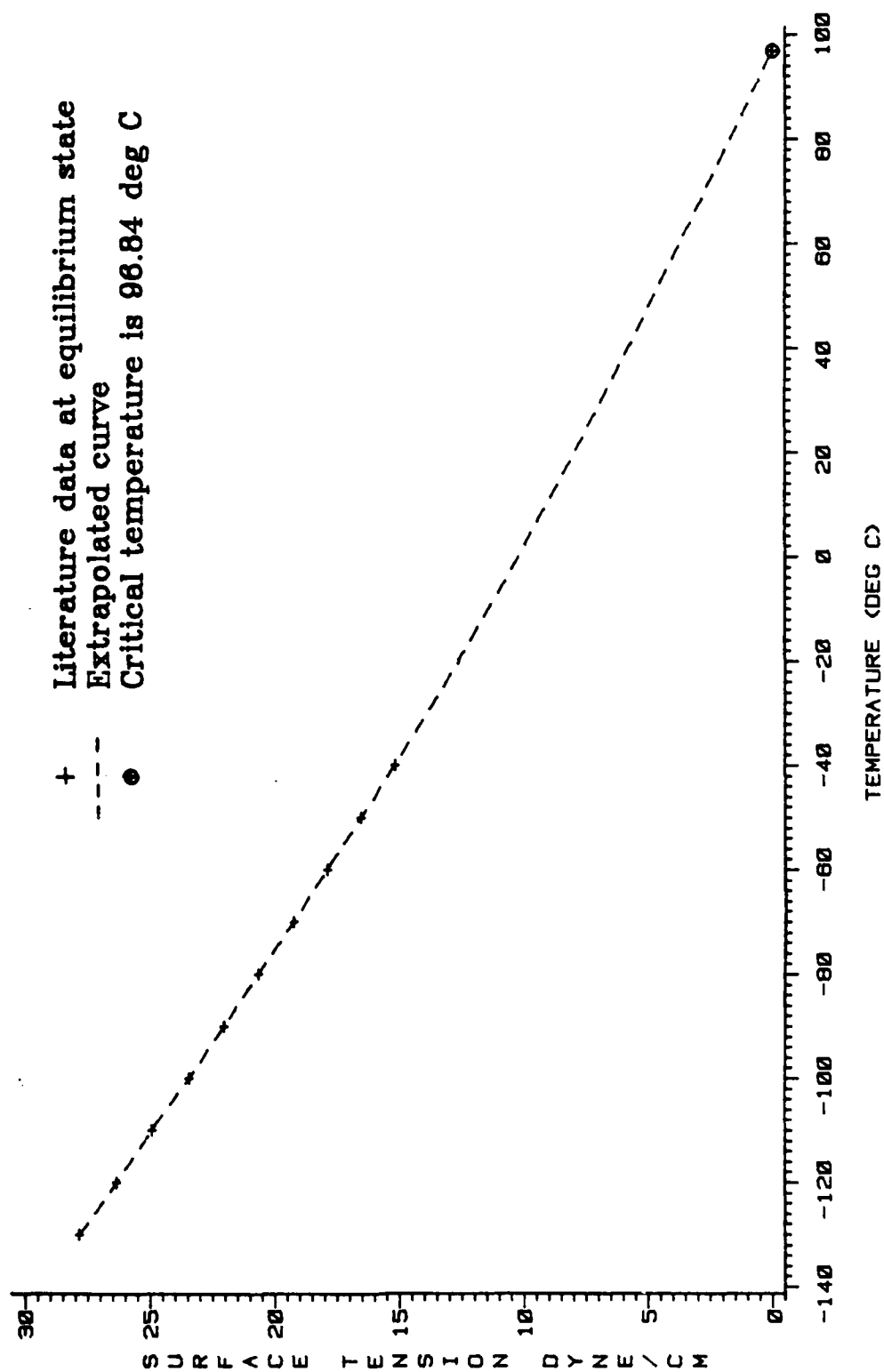


Figure 5.5: Surface tension of propane at various temperatures; curve extrapolated from literature data taken at equilibrium state.

### 5.6.2 Measurements for Butane and Isobutane

Test drops of butane and isobutane were formed in gel under pressure and then transported into water. The index of refraction of butane (1.3326) is so close to that of water (1.3333) [26] that the butane drops could barely be seen by eyes while levitated in water, and its shadow looked like a ring with very thin band. Therefore, very stable levitation and fine adjustment of the stopper (see Fig. 3.1) were required to take measurements; the signals from photomultiplier for butane drops were noisier than the signals for drops of other liquids.

The results of quadrupole oscillation experiments for butane and isobutane are listed in Table 9. As mentioned in the previous section, for the interfacial tension deduced from data,  $\sigma_1$ , denotes a first approximation calculated using Eq. (70), and  $\sigma_f$  is obtained using least-squares fittings. As shown in Table 9,  $\sigma_f$  is lower than  $\sigma_1$  by an average of 1.6%. One can also see that  $s_e$  is two to three times  $s_{th}$ ,  $\gamma_f$  is close to  $\gamma_{th}$  (within a factor of two), and  $\alpha_f$  is much greater than  $\alpha_{th}$  (by a factor about four); this behavior similarly exhibited in our data for hexane and pentane drops which were formed in gel.

From our measurements, the average interfacial tension for water-butane interface is 53.1 dyne/cm, and that for water-isobutane interface is 54.3 dyne/cm. Similar to the discussion in Section 5.5, we estimate that the uncertainty for our measurements of the water-isobutane interfacial tension is  $\pm 0.8\%$  with  $\pm 0.2\%$  uncertainty in the estimated density; the uncertainty of our measurement for the



water-butane interfacial tension is  $\pm 0.9\%$  with greater ( $\pm 0.2\%$ ) uncertainty in the frequency measurement due to the noisiness of the output signal from the photomultiplier.

TABLE 9

Measurements for butane and isobutane.

radius (mm)	$f(90^\circ)$ (Hz)	$s_e$	$\sigma_1$	$\sigma_f$	$\alpha_f$	$\gamma_f$	$s_{th}$	$\alpha_{th}$	$\gamma_{th}$
water-butane interface									
0.693	147.73	94.4	54.0	53.2	6.0	32.4	36.3	1.6	25.0
0.761	127.92	84.8	54.0	53.3	5.9	29.3	30.6	1.5	20.8
0.765	125.20	93.6	53.8	53.1	6.6	37.9	30.3	1.5	20.5
0.878	102.59	71.3	53.7	52.8	5.3	25.8	23.6	1.3	15.6
water-isobutane interface									
0.720	141.75	94.9	55.3	54.3	6.1	37.0	34.8	1.6	23.5
0.794	123.11	74.7	54.9	54.2	5.2	24.9	29.1	1.5	19.3
0.862	110.02	61.5	55.3	54.5	4.4	21.9	25.1	1.3	16.4

### 5.6.3 Measurements for Propane

Propane has the highest degree of superheating among our test liquids. Some special phenomena were observed in the measurements for propane: the frequency associated with a given phase angle increased with time, while the size of the drop decreased with time, as can be seen in Figs. 5.6, 5.7, 5.9, 5.10, 5.12, and 5.13. The propane drops dissolved significantly after being levitated in water for a couple of hours. This fact makes it impractical to apply the least-squares method, as described in section 5.4, to the data of propane with water, because the size and frequencies were drifting with time and the measurements were not taken at the same instant.

Our approach for analyzing the data is first to get averaged variation of each measurement (e.g., the frequency associated with certain phase or the size of the drop) with respect to time by fitting a line to the data plotted as a function of time, as shown in Figs. 5.6, 5.7, 5.9, 5.10, 5.12, and 5.13. Then we can arbitrarily choose an instant, read the size and frequencies from the fitted lines, and calculate the  $\sigma_1$  associated with this particular instant (using Eq. (70)). The parameters  $\alpha$  and  $\chi$  can be estimated by employing Eqs. (71) and (72) with the  $\sigma_1$ ,  $R$ ,  $\omega(90^\circ)$ , and  $\omega(\xi)$  at a certain instant.

It was found that the interfacial tension between water and propane obtained in this way was also time dependent; it decreased with time, as shown in Figs. 5.8, 5.11, and 5.14. This decrease of interfacial tension with time is presumably due to the dissolution of propane in

water; the concentration of propane in water near the interface increased with time, reducing the differential attraction force between molecules across the interface.

The assumption that the concentration of propane in the water near the interface increased with time is supported by the following argument: If the diffusivity,  $\kappa$ , of propane into water (molecules/unit time/unit area) is constant, then the rate of change of the drop's radius should be inversely proportional to the cube of the radius, that is,  $dR/dt \sim -\kappa/R^3$ . But, as shown in Figs 5.7, 5.10, and 5.13, the slope of the data line is very different from cubic; the rate of decrease of the radius was much less than a cubic relation would predict. Therefore, we presume that the  $\kappa$  was not a constant but decreased with time, as would occur if the concentration of propane in water near the interface increased.

Assuming that the true interfacial tension is 1.6% lower than  $\sigma_1$ , as observed in previous data, then the interfacial tension between water and propane was about 58 dyne/cm when a propane drop has contacted with water for about 10 minutes and continuously decreased to about 54.5 dyne/cm when the propane drop had remained in water for two hours. We estimate the uncertainty of this measurement to be  $\pm 1\%$  which is of the same order as that of measurements for butane.

Host: water, Droplet: propane.

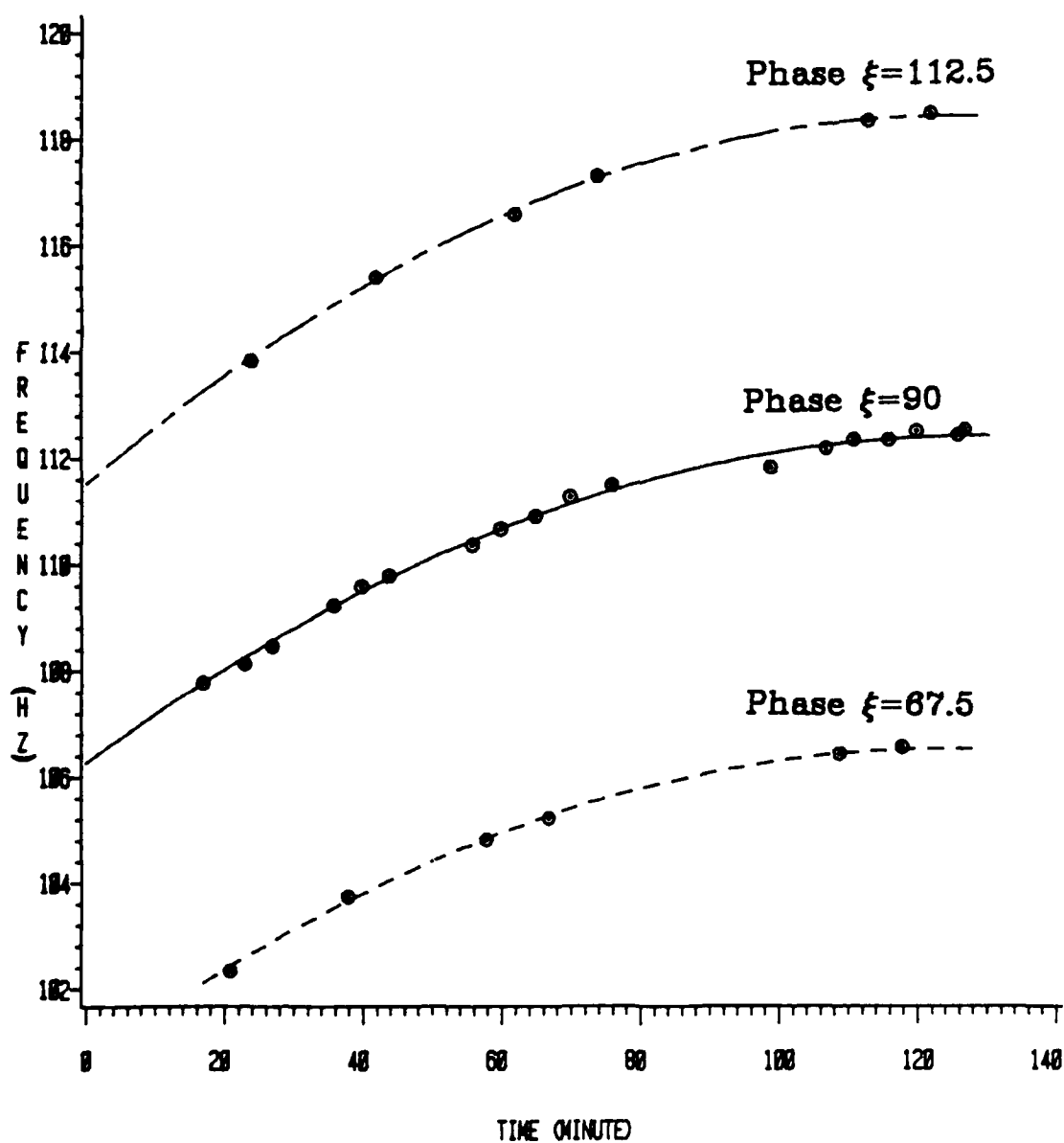


Figure 5.6: Variation of frequency with time for three selected phase angles, experiment #0409.

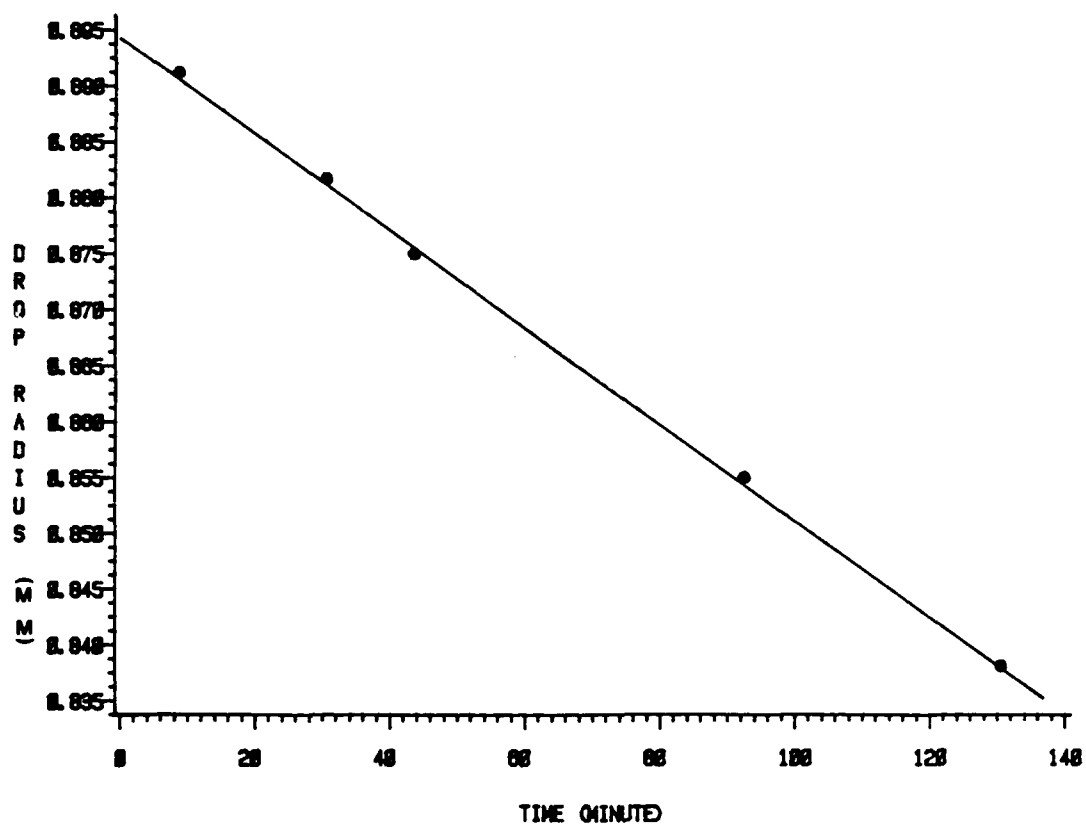


Fig. 5.7: Variation of drop radius with time for experiment #0409.

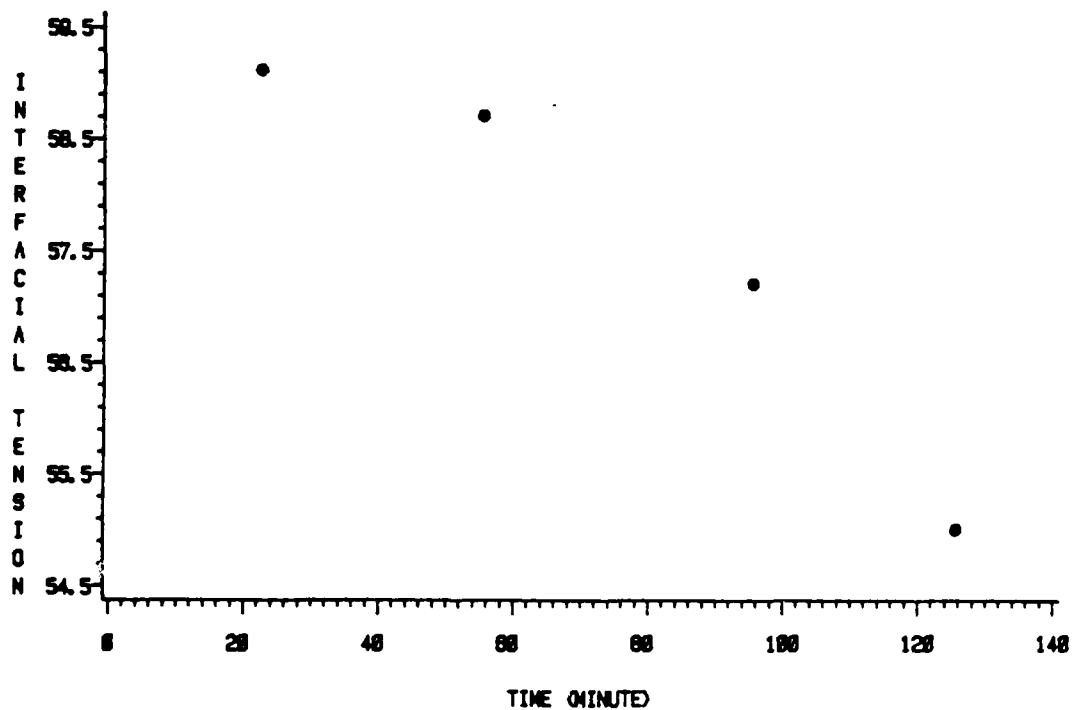


Fig. 5.8: Variation of the interfacial tension between water and propane with time for experiment #0409.

Host: water, Droplet: propane.

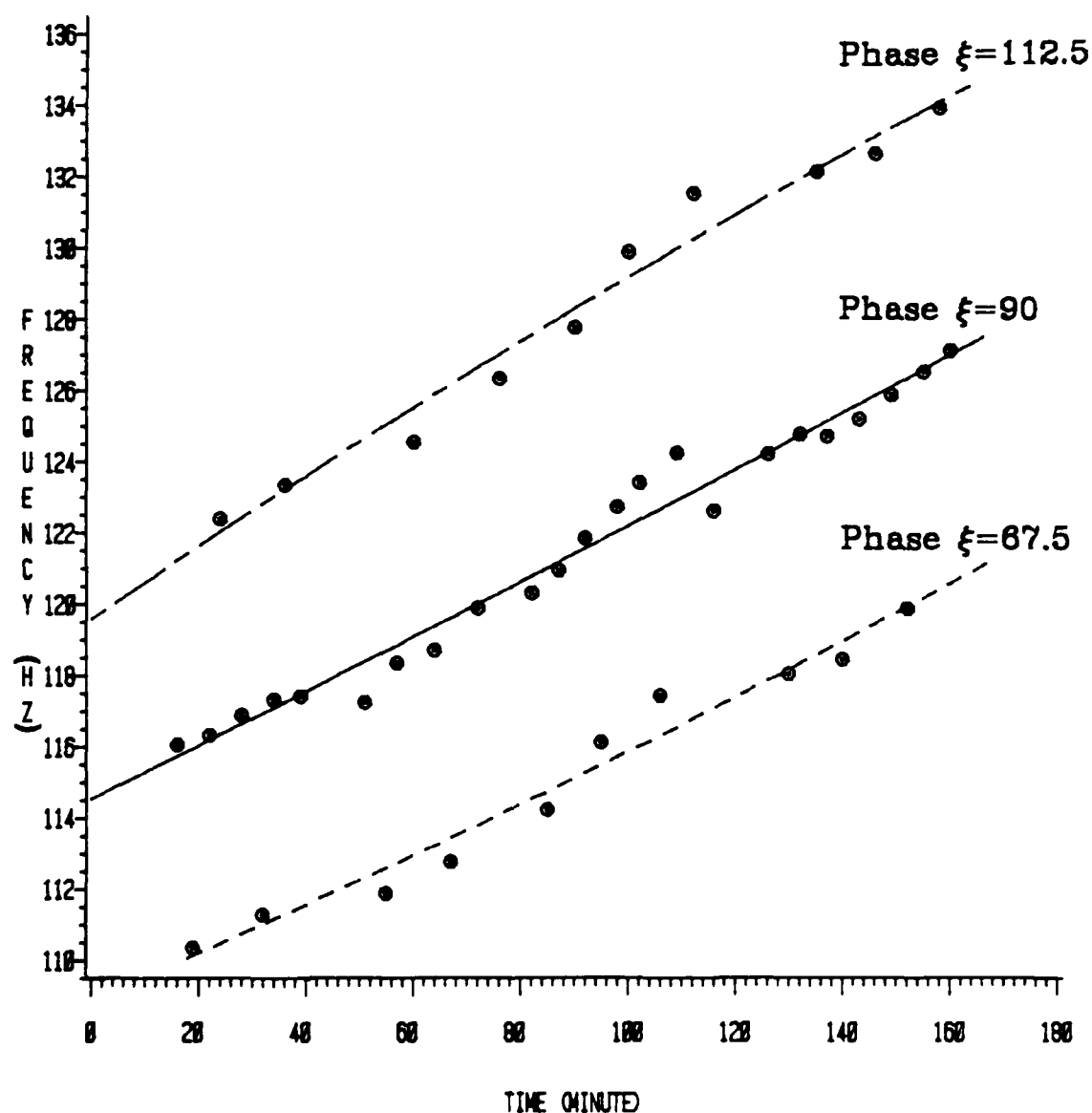


Figure 5.9: Variation of frequency with time for three selected phase angles, experiment #0411.

Host: water, Droplet: propane

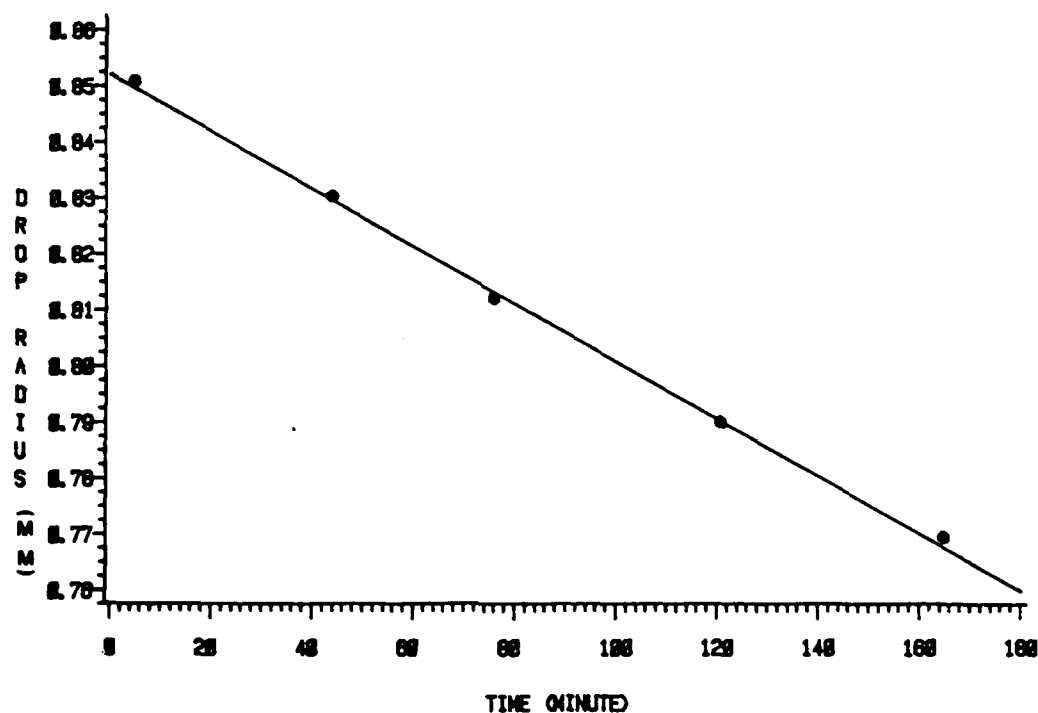


Fig. 5.10: Variation of drop radius with time for experiment #0411.

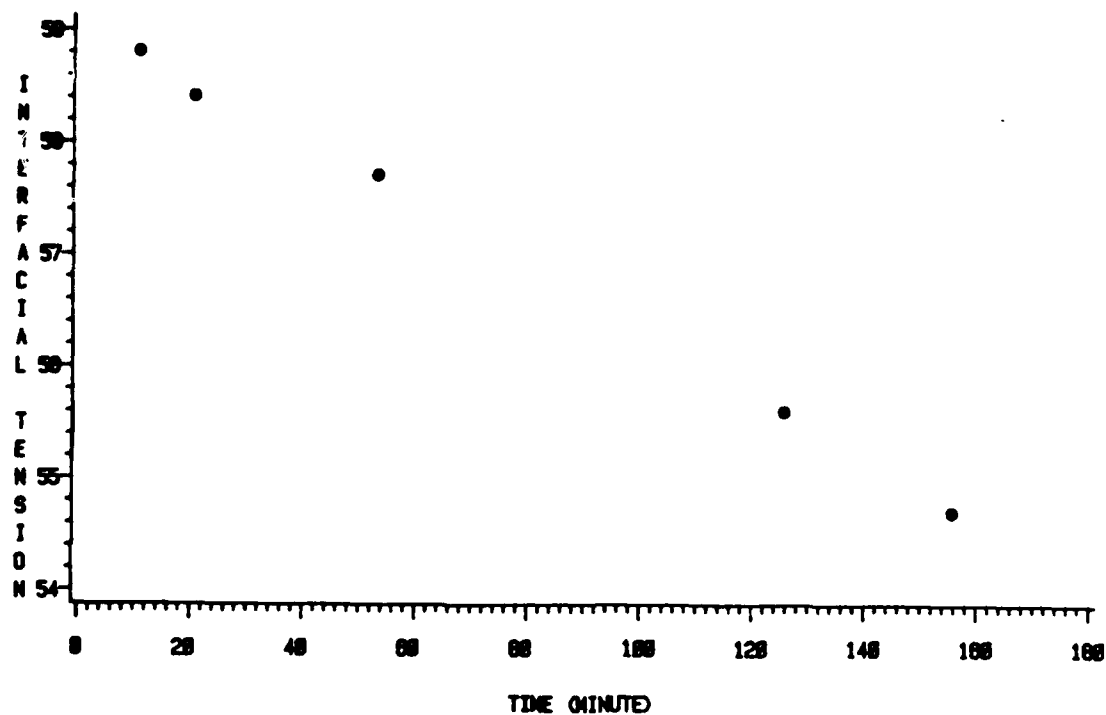


Fig. 5.11: Variation of the interfacial tension between water and propane with time for experiment #0411.



Host: water,    Droplet: propane.

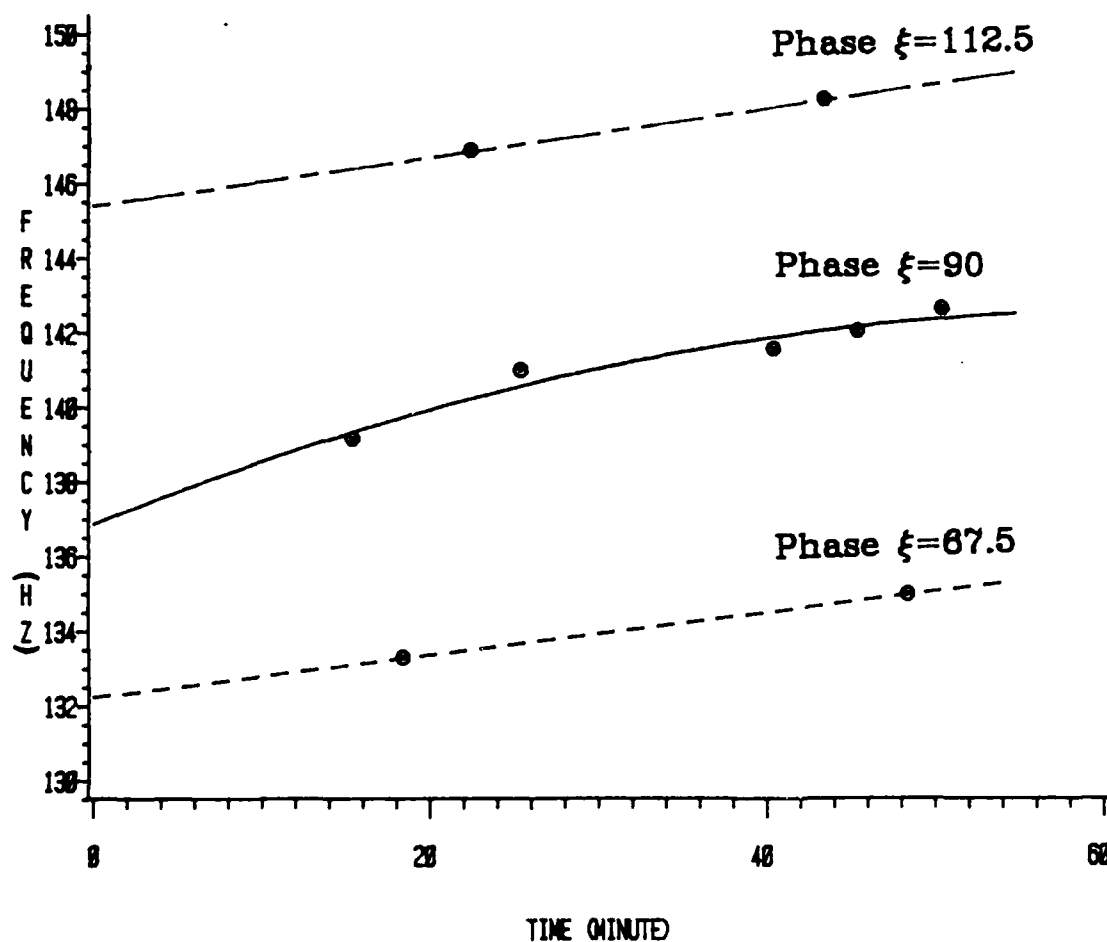


Figure 5.12: Variation of frequency with time for three selected phase angles, experiment #0408.

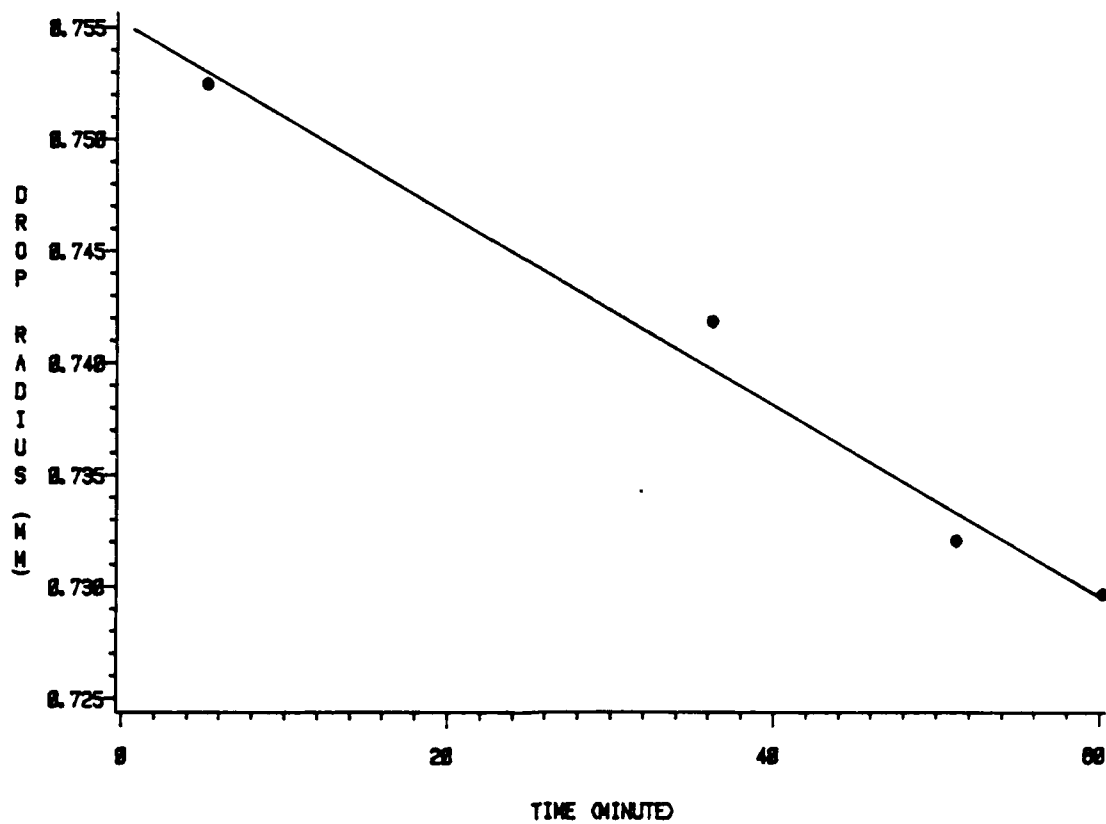


Fig. 5.13: Variation of drop radius with time for experiment #0408.

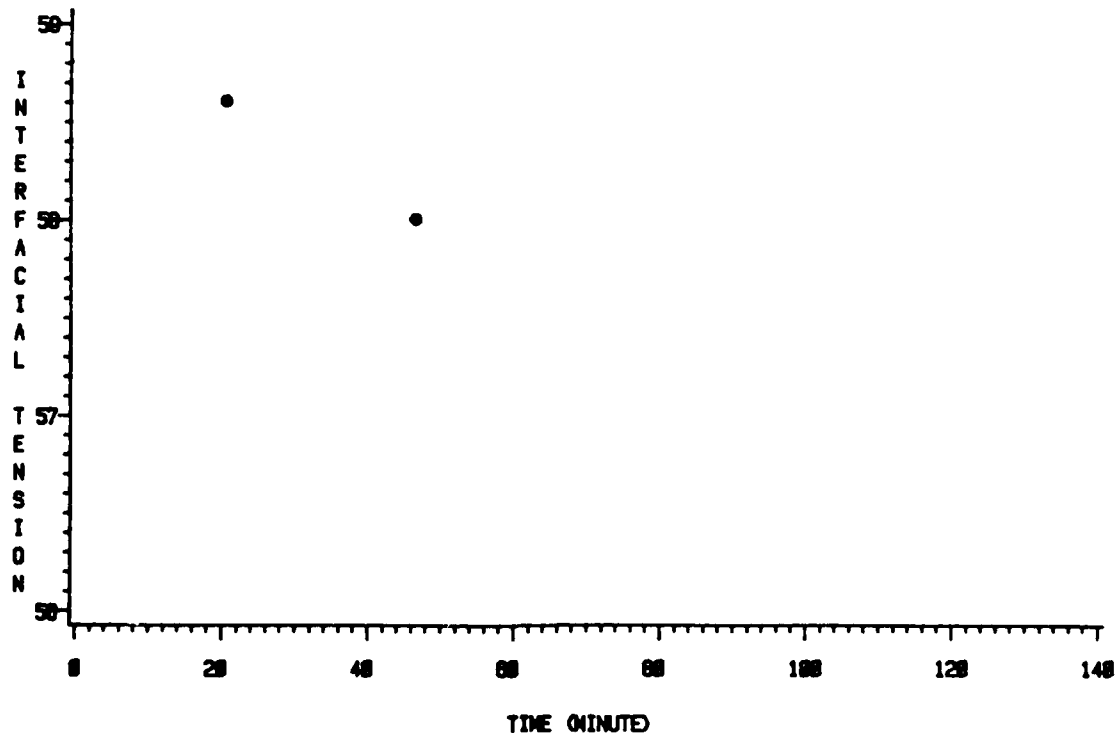


Fig. 5.14: Variation of the interfacial tension between water and propane with time for experiment #0408.

#### 5.6.4 Comparison with Fowkes Theory

The results of our measurements for interfacial tension are summarized in Fig 5.15. In this figure, the square symbols represent data from the literature; the circles represent data from this work; the curve represents the calculated value given by Fowkes' equation (referred to Eq. (1)). Those literature data of several hydrocarbons with water denoted by squares in Fig. 5.15 (except that of pentane) were used by Fowkes to calculate the part of the surface tension of water due to dispersion force, which he obtained was  $21.8 \pm 0.7$  dyne/cm (referred to section 1.6 and [13]). The surface tension of the superheated liquids are taken from Table 8. The interfacial tension between water and propane shown in this figure is 58 dyne/cm which corresponds to the measurements taken at an "early stage" in the period of measurement (refer to section 5.6.3). Fig. 5.15 demonstrates that for the three superheated liquids, the agreement between our data and Fowkes' theory is fair, similar to that between the data of pentane with water and Fowkes' prediction; the trend of increasing interfacial tension with decreasing surface tension in this region of lower surface tension is clearly shown in both data and Fowkes' theory.

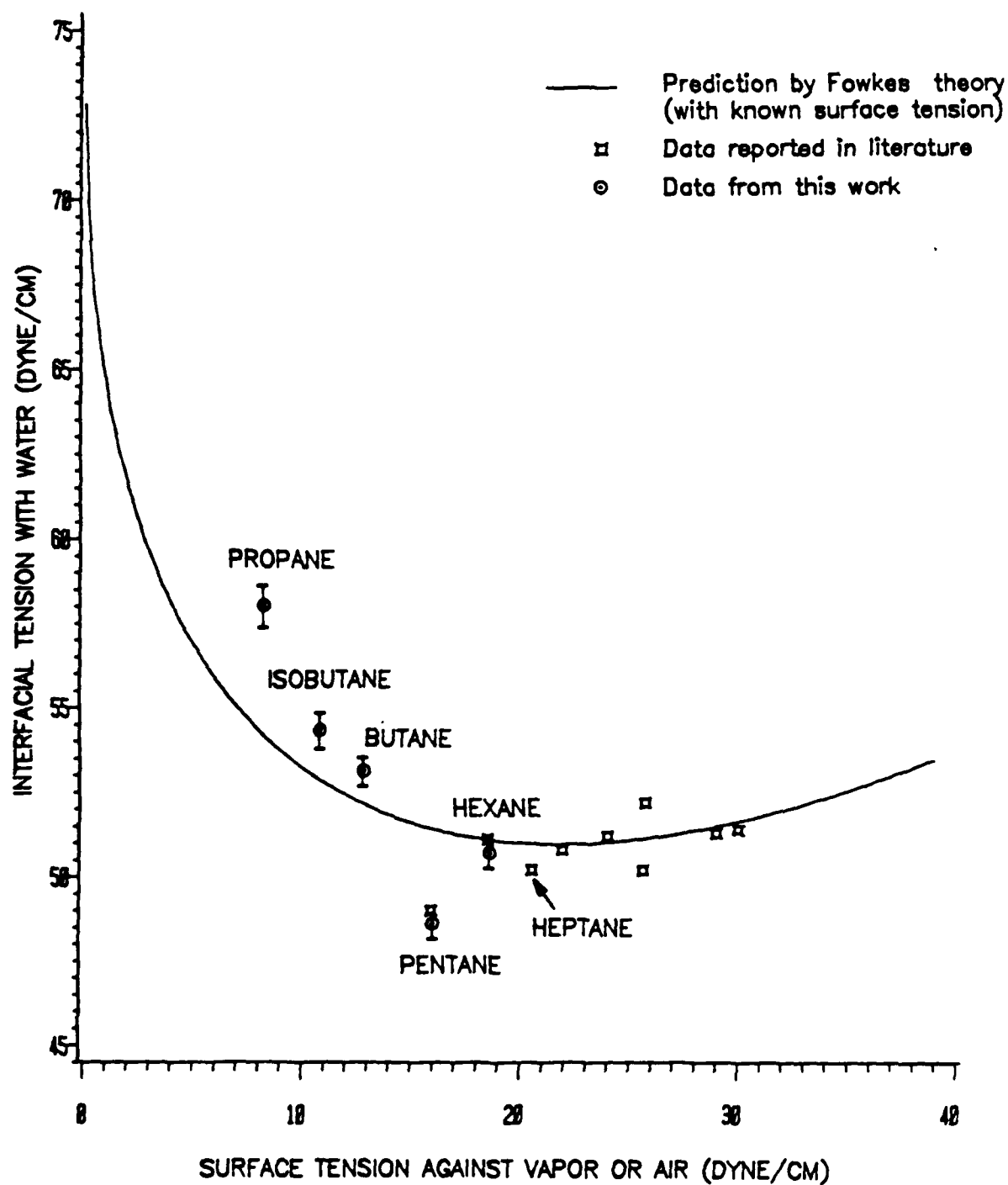


Figure 5.15: Comparison between data and Fowkes theory.

## 5.7 Measurements for Compressadensity

Applying the established acoustic levitation technique, we measured the compressadensity, which is a bulk property, of the three superheated liquids. The procedure is outlined in section 4.5, and the calculation is based on Eqs. (60) and (61).

### 5.7.1 Control Experiment

As a test of the accuracy of the levitation technique for measuring adiabatic compressibility ( $\beta$ ) (assuming the density is known), control experiments were performed in which one of the two liquids, n-heptane and n-pentane, was considered an unknown, and the other liquid a reference. The sound speed ( $C$ ) in the "unknown" liquid was measured by a direct method (see section 3.5). Making use of the relation  $C^2 = 1/\rho\beta$ , we can compare the results obtained from levitation technique with that obtained from the direct method. The results are summarized in Table 10. The densities of n-heptane and n-pentane in Table 10 were measured using the Mettler/Parr density meter. The density of water is taken from the literature (e.g. [26]). The sound speeds in the three liquids were measured using Nusonics sonic solution monitor (see section 3.5).

Our data show that the precision of our measurements for compressibility is about 1%, and for sound speed is about 0.5%. The overall uncertainty of this measurement is composed of the following errors [5]:

1.  $\pm 0.2\%$  uncertainty in the voltage measurement, which is attributable to the precision of the digital ac voltmeter and the deviation of the actual experimental condition from the assumption that the pressure of the incident waves for both the unknown and reference drops is proportional to the input voltage to the transducer.
2.  $\pm 0.002\text{cm}$  uncertainty in droplet position monitoring, which corresponds to  $\pm 0.2\%$  uncertainty in voltage measurement.
3.  $\pm 0.1\%$  uncertainty in density measurement.
4.  $\pm 0.1\%$  uncertainty in sound speed measurement for host and reference liquid.

The compressibility and sound speed measured using the levitation technique agreed well with that obtained using traditional technique, with the difference within the uncertainty of our levitation measurements.

#### 5.7.2 Compressadensity of Superheated Liquids

The same procedure was applied to butane, isobutane, and propane liquid, which were superheated, to measure their adiabatic compressibility and sound speed. Two references, n-heptane and n-pentane, were used in all measurements. The densities of the superheated liquids are taken from Table 8. The results are listed in Table 10. We estimate the total uncertainty to be about 1% for sound speed and 2% for compressibility. The results shown in Table 10 demonstrate that the results for the two

different references are consistent with each other, the difference being within the uncertainty of this measurement. Since the compressibility and sound speed are bulk properties of liquids, we judged that the data should not be affected by the presence of little amount of residue of gel on the interface. There are no other data available for the results of the superheated liquids listed in Table 10 to compare with. However, the trend that the liquid of higher degree superheating behaves closer to being in gaseous state (greater compressibility and lower sound speed) is clear.

TABLE 10

Results of levitation technique for compressadensity measurement.

(assuming density is known)

TEMP. °C	LIQUIDS (REFERENCE)	DENSITY( $\rho$ ) g/ml	SOUND SPEED(C) m/s		COMPRESSIBILITY( $\beta$ ) $\times 10^9$ m <sup>2</sup> /N	
			TRADITIONAL TECHNIQUE	LEVITATION TECHNIQUE $C^2 = 1/\rho\beta$	TRADITIONAL TECHNIQUE $\beta = 1/\rho C^2$	LEVITATION TECHNIQUE
22	Heptane (Pentane)	0.6819	1142	1146	1.125	1.117
22	Pentane (Heptane)	0.6242	1019	1015	1.543	1.556
21	Butane (Heptane)	0.577		883		2.22
21	Butane (Pentane)	0.577		888		2.20
22	Isobutane (Heptane)	0.556		803		2.79
22	Isobutane (Pentane)	0.556		807		2.76
21	Propane (Heptane)	0.502		695		4.12
21	Propane (Pentane)	0.502		700		4.06



## Chapter 6

### SUMMARY AND CONCLUSIONS

In this work, we have studied a technique for measuring the interfacial tension between two liquids and applied it to the interfaces between water and each of three superheated liquids. The method of measurement is based on the resonance properties of a drop which is levitated in another liquid (the host) and also driven into quadrupole shape oscillation by an acoustic force. The shape oscillation technique described here has the special advantage that the host liquid provides a very smooth and clean container for the levitated drop, thereby greatly improving its time of survival in the superheated state.

We have developed a simplified model to describe the motion of a drop oscillating in a quadrupole mode in a host liquid. In this model, the flow field is partitioned into several parts: the potential (bulk) flow in the outer (host) and inner (drop) fluid as well as the boundary layer in the outer and inner fluid contiguous to the interface; they are superimposed in an ad hoc manner to describe the whole flow. The phase-frequency relation deduced from this simplified model agrees well with that given by previous theories (e.g. Marston's) which were derived in an exact approach. This simplified model reveals the physical nature of the problem more explicitly. Though the derivation of this simplified model was specified to the quadrupole mode, the procedure should be applicable to oscillations of higher modes.

The apparatus of this experiment is similar to that of some previous work, with some modifications. The accuracy of the size measurement has been improved and it contributes significantly to the precision of our measurements for interfacial tension. Our results for the interfaces between water and each of two common liquids were lower than the literature values by about 0.8%. The uncertainty of the measurements was estimated to be  $\pm 0.75\%$ . Though the damping of the drop's oscillation is due to viscous dissipation, it appeared that, within the precision of our experiment, it is impractical to get any significant information about the viscosity of either the drop or the host liquid from the measurements.

We developed a process for introducing a liquid drop into water by the aid of a gel which is immiscible with the drop but soluble in water. It is a convenient way to handle superheated liquids. However, test drops that underwent this process exhibited much greater damping in their shape oscillation and this fact raised questions as to whether we could infer the interfacial tension from measurements by using the approximation method used in a previous work. We therefore developed a method based on the least-squares principle for estimating interfacial tension and damping parameters. The results of this least-squares method for two common liquids demonstrate that the interfacial tension and the viscous dissipation in the bulk flow were not affected by detectable amounts due to the presence of the gel, while the viscous dissipation in the boundary layer increased very significantly.

Measurements of interfacial tension were reported for the interfaces between water and butane, isobutane, as well as propane. These three compounds were in the superheated liquid state under our experimental condition (room temperature and atmospheric pressure). The uncertainty of the measurements was estimated to be  $\pm 1\%$ . The size of propane drops decreased gradually over a two hour period in water; the interfacial tension decreased with time due to the increase of propane concentration in water near the interface. Our results show fair agreement with the prediction given by Fowkes' theory.

We have reported the sound speed and compressibility of those three superheated liquids which were measured using an established acoustic levitation technique. The uncertainty is estimated at  $\pm 1\%$  for the sound speed measurement and at  $\pm 2\%$  for the compressibility measurement. Our results show that the sound speed decreases and the compressibility increases as the degree of superheat increases, as one should expect.

This work, as one among others, demonstrates that the acoustic levitation technique is a useful tool for studying either surface properties (e.g. interfacial tension) or bulk properties (e.g. sound speed and compressibility) of fluids with a special advantage in dealing with metastable liquids. This work reports data which were previously unavailable for the interfacial tension and compressibility of three superheated liquids and may have applications in various fields (referred to page 1, 5, and 11). Though we judged that the measured interfacial tensions were not affected by the presence of gel, any

uncertainty on this point can only be removed by conducting experiments without using gel or other material in the preparatory steps prior to the actual interfacial tension measurements.

Some future work relating to this technique is desirable. The approach of the simplified analytical model may be extended to some special situations in which the exact approach may have difficulty due to the geometry, such as when the equilibrium shape of the drop is non-spherical. It is also possible to superimpose terms such as interfacial viscosity and interfacial elasticity into this simplified model for describing some situations such as when there is a surface-active film or membrane between the two fluids; with this modification in the analytical model and by performing measurements as described in this manuscript, we should have a sensitive method of characterizing the surface layer.

## APPENDIX A

## Methods for Data Reduction

The model that we used to describe the motion of an oscillating drop in a liquid host is expressed in Eq. (62),

$$\tan \xi = (\alpha \omega^{3/2} + \gamma \omega) / (\omega^2 - \alpha \omega^{3/2} - \omega^2) , \quad (62)$$

where  $\xi$  and  $\omega$  are measured in our experiments (see section 5.2.1). By measuring three frequencies ( $\omega$ ) associated with three different phase angles ( $\xi$ ), and by substituting them into the above equation, we get a system of three linear equations and, theoretically, we can solve the three unknowns:  $\alpha$ ,  $\gamma$ , and  $\omega^2$  (or  $\sigma$ ) by direct methods such as Cramer's rule or Gauss elimination. However, it appears that the system of equations mentioned above is "ill-conditioned", and the direct methods are of very little use for inferring interfacial tension from the phase-frequency measurements with the precision we can achieve in our measurements. An example is shown below in two steps:

(i). Making use of Eq. (16), we may rewrite Eq.(62) in the following form:

$$[(T \cdot 24) / (R^3 \Gamma)] \sigma - (\omega) \gamma - [(1+T) \omega^{3/2}] \alpha = T \omega^2 . \quad (73)$$

Assuming  $R=0.0825$  cm,  $\alpha=1.88$ ,  $\gamma=13.56$ ,  $\sigma=50.7$  (dyne/cm) (see Table 5),

$\rho_o=0.9978$ ,  $\rho_i=0.6576$  (see Table 1), and employing Eq. (62), we may get a set of "artificial data", such as:

$f(H_z)$	$\xi(\text{deg.})$
111.729	68.257
114.081	95.180
117.609	128.363

Substituting this set of artificial data into Eq. (73), we get a system of linear equations  $[A] [X] = [B]$ , where

$$[X] = [\sigma \quad \gamma \quad \alpha]^T$$

$$[A] = \begin{bmatrix} 27005.89 & -702.02 & -65238.53 \\ -118809.38 & -716.79 & 192502.12 \\ -13606.97 & -738.95 & 5290.33 \end{bmatrix} \quad (74)$$

and

$$[B] = \begin{bmatrix} 1235708.00 \\ -5667649.00 \\ -689871.87 \end{bmatrix}$$

Employing Cramer's rule, we solve the unknown matrix,

$$[X] = [50.71 \quad 13.50 \quad 1.91]^T,$$

which is very close to the original assumed values.

(ii) If we make a small change in the artificial data, say, one of the frequency from 117.609 to 117.800, then it produces "small" changes in the coefficients:

$$[A] = \begin{bmatrix} 27005.89 & -702.01 & -65238.53 \\ -118809.37 & -716.79 & 192502.12 \\ -13606.97 & -740.15 & 5303.22 \end{bmatrix}$$

$$[B] = \begin{bmatrix} 1235708.00 \\ -5667649.00 \\ -692114.56 \end{bmatrix}$$

But the corresponding changes of the solution are very "large".

$$[X] = [60.67 \quad -126.41 \quad 7.54]^T.$$

The performance of direct methods can be predicted by a theory in numerical analysis (e.g. [33]) which provides an estimate of the relative error:

$$\frac{1}{\|A\| \|A^{-1}\|} \frac{\|AX_c - B\|}{\|B\|} \leq \frac{\|X_c - X_t\|}{\|X_t\|} \leq \|A\| \|A^{-1}\| \frac{\|AX_c - B\|}{\|B\|}$$

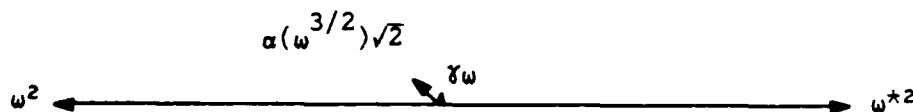
where  $\|\cdot\|$  denotes a matrix norm, subscript c denotes the computed value, subscript t denotes the true value, and all variables are matrix. The term  $\|A\| \cdot \|A^{-1}\|$  is usually called the condition number and its size is a measure of how good a solution we can expect direct methods to generate. The condition number satisfies the inequality  $\|A\| \cdot \|A^{-1}\| \geq 1$ . Following a specific definition of the matrix norm[33], we can calculate the condition number for the above example (referred to Eq. (74)), such as:

$$\|A\|_1 \cdot \|A^{-1}\|_1 = 1.6 \times 10^4 \gg 1$$

$$\|A\|_\infty \cdot \|A^{-1}\|_\infty = 3.6 \times 10^4 \gg 1$$

The above calculation indicates that, with the precision we can achieve in our measurements, if we use direct methods to solve [X], the relative error could be unacceptably large.

The problem can also be demonstrated by the following observations. First, the typical magnitudes of the terms in Eq. (62) are very different, as shown in the following vector diagram which is drawn approximately to scale for the above example with  $f = 114.081 \text{ Hz}$  and  $\xi = 95.180$  degree,



where  $\omega^{*2} = 546062$ ,  $\omega^2 = 513791$ ,  $\gamma\omega = 9720$ , and  $\alpha(\omega^{3/2})\sqrt{2} = 51023$ .

Secondly, the dependence on  $\omega$  of the two damping terms ( $\gamma\omega$  and  $\alpha\omega^{3/2}$ ) is rather close, and the variation in frequency is rather small for the range of phase angles covered in our measurements.

The idea of our approach to analyze the data is formed by the following reasoning. To avoid the difficulty in direct methods and to use all the data we have for one experiment (usually more than three phase-frequency measurements), we employ a least-squares principle to fit the model in Eq. (62) to our data. To give greater emphasis relatively to the terms  $\gamma\omega$  and  $\alpha(\omega^{3/2})$ , we assume that  $\omega^*$  is known by guessing a value for the interfacial tension. Then the terms  $\omega^{*2}$  and  $\omega^2$  almost cancel out each other. In the remaining two unknowns,  $\gamma$  and  $\alpha$ , only  $\alpha$  affects the value of  $f(90^\circ)$  (see Eq. (71)); also, our measurements for  $f(90^\circ)$  are usually much better than  $f(\xi)$ , where  $\xi \neq 90^\circ$ , in terms of repeatability. Therefore, we first employ the least-squares method and only the data of  $f(90^\circ)$  to get the best fitted  $\alpha$ . We then use the assumed  $\omega^*$ , fitted  $\alpha$ , and the data of  $f(\xi \neq 90^\circ)$  to obtain the best fitted  $\gamma$ . The assumed  $\omega^*$  which is the closest to the "true" value should lead to the best fitting (referred to section 5.4). Details of the procedure are described in section 5.4 and Appendix B.



## APPENDIX B

## An Example for the Least-squares Fitting

This appendix provides an example for the process of least-squares fitting that we employed to analyze our data. The first part of the attached printout is the data set used in this example (see Table 2). The remaining part of this printout is the GLM printout (see section 5.4). Relevant terms are marked with numbers and are explained as follows:

- (1). the data used in this example (see Table 2)
- (2). the assumed interfacial tension.
- (3). the coefficient of  $\alpha$  in the left hand part of Eq. (71).
- (4). the right hand part of Eq. (71).
- (5). the sum of squares for the dependent variable in (4).
- (6). the sum of squares for the predicted dependent variable in (10).
- (7).  $R^2$ , the ratio produced by dividing (6) by (5).
- (8). the difference between (4) and (10).
- (9). the sum of squares of (8).
- (10). the value obtained by employing the estimated parameter (15) into Eq. (71).
- (11). (9) divided by the DF (degree of freedom).
- (12). the square root of (11).
- (13). the mean value of (4).
- (14). (12) divided by (13), then times 100, (the coefficient of variation).
- (15). the estimated parameter based on minimizing (9).
- (16). the value for testing the null hypothesis that the parameter equals zero, which equals

$$\frac{(13)-0.0}{(12)/\sqrt{n}}$$

where  $n$  is the number of observations ( $n=3$  in this example) [32].

(17). This value answers the questions, "If the parameter is really equal to zero, what is the probability of getting a larger value of (16)?" Based on the assumption that the dependent variable has a normal distribution with mean zero and estimated standard deviation obtained from  $n$  observations (the term (12)), the value of (17) is then the probability to get a greater value of (16) or, equivalently, a greater value of (13) [30] [32].

(1)  
 \*\*\*\*\*Substitute the data in Table 2 into Eq. (71),  
 assume the interfacial tension to be 50.5 dyne/cm, and  
 invoke SAS GLM program to fit alfa: (2)

# STATISTICAL ANALYSIS SYSTEM

OBS	ALFA (3)	INER (4)
1	190.795	340.816
2	190.946	335.434
3	190.996	333.641

# STATISTICAL ANALYSIS SYSTEM

## GENERAL LINEAR MODELS PROCEDURE

DEPENDENT VARIABLE: INER

SOURCE	DF	SUM OF SQUARES	MEAN SQUARE	F VALUE
MODEL	1	(6) 339956.84381956	339956.84381956	22129.25
ERROR	2	(9) 30.72466672	(11) 15.36233336	PR > F
UNCORRECTED TOTAL	3	(5) 339987.56848628		0.0001

R-SQUARE	(14) C.V.	(12) STD DEV	INER MEAN	(13)
0.999910 (7)	1.1643	3.91948126	336.63020000	

SOURCE	DF	TYPE I SS	F VALUE	PR > F
ALFA	1	339956.84381956	22129.25	0.0001

# STATISTICAL ANALYSIS SYSTEM

## GENERAL LINEAR MODELS PROCEDURE

DEPENDENT VARIABLE: INER

SOURCE	DF	TYPE IV SS	F VALUE	PR > F
ALFA	1	339956.84381956	22129.25	0.0001

PARAMETER	(15) ESTIMATE	T FOR H0: PARAMETER=0 (16)	PR >  T  (17)	STD ERROR OF ESTIMATE
ALFA	1.76326420	148.76	0.0001	0.01185316

OBSERVATION	(4) OBSERVED VALUE	(10) PREDICTED VALUE	(8) RESIDUAL
1	340.81640000	336.42146348	4.39493652
2	335.43360000	336.68806903	-1.25446903
3	333.64060000	336.77676122	-3.13616122

# S T A T I S T I C A L   A N A L Y S I S   S Y S T E M

## GENERAL LINEAR MODELS PROCEDURE

DEPENDENT VARIABLE: INER

SUM OF RESIDUALS	0.00430626
SUM OF SQUARED RESIDUALS	30.72466672
SUM OF SQUARED RESIDUALS - ERROR SS	-0.00000000
FIRST ORDER AUTOCORRELATION	-0.05139501
DURBIN-WATSON D	1.15400921

\*\*\*\*\* The end of SAS GLM output.

## REFERENCES

1. Jasper, J.J.  
Measurement of Surface and Interfacial Tension  
in Treatise on Analytical Chemistry, ed. Kolthoff I.M. and Elving  
P.J.  
John Wiley & Sons, New York, part 1, vol. 7, chap. 82, 1967.
2. Adamson, A.W.  
Physical Chemistry of Surfaces, 4th ed  
John Wiley & Sons, New York, 1982.
3. Skripov, V.P.  
Metastable Liquids  
John Wiley & Sons, New York, 1974.
4. Apfel, R.E.  
Vapor Nucleation at a Liquid-Liquid Interface  
J. Chem. Phys., 54, p. 62, 1971.
5. Apfel, R.E.  
Technique for measuring the adiabatic compressibility, density, and  
sound speed of submicroliter liquid samples  
J. Acoust. Soc. Am., 59(2), pp. 339-343, 1976.
6. Baidakov, V.G., Kaverin, A.M., and Skripov V.P.  
Measurement of Ultrasonic Speed in Stable and Metastable Liquid  
Methane  
J. Chem. Thermodynamics, vol. 14, pp. 1003-1010, 1982.
7. Rayleigh, J.W.S.  
Theory of Sound  
Dover, New York, sect. 364, 1945.
8. Lamb, H.  
Hydrodynamics  
Dover, New York, sect. 275, 355, 1945.
9. Miller, C.A., and Scriven, L.E.  
The Oscillations of a Fluid Droplet Immersed in Another Fluid  
J. Fluid Mech., vol. 32, part 3, pp. 417-435, 1968.
10. Marston, P.L.  
Shape Oscillation and Static Deformation of Drops and Bubbles  
Driven by Modulated Radiation Stresses--Theory  
J. Acoust. Soc. Am., 67(1), pp. 15-26, 1980.

11. Marston, P.L., and Apfel, R.E.  
Quadrupole Resonance of Drops Driven by Modulated Acoustic Radiation Pressure--Experimental Properties  
J. Acoust. Soc. Am., 67(1), pp. 27-37, 1980.
12. Trinh, E., Zwern, A., and Wang, T.G.  
An Experimental Study of Small-amplitude Drop Oscillations in Immiscible Liquid System  
J. Fluid Mech., vol. 115, pp. 453-474, 1982.
13. Fowkes, F.M.  
Attractive Forces at Interfaces  
Ind. Eng. Chem., vol. 56(12), pp. 40-52, 1964.
14. Bikerman, J.J.  
On a Theory of Interfacial Tension  
J. Adhesion, vol. 3, pp. 19-22, 1971.
15. French, A.P.  
Vibration and Waves  
W.W. Norton & Company Inc., New York, 1971.
16. Lock, R.C.  
The velocity Distribution in the Laminar Boundary Layer between Parallel Streams  
Quart. Journ. Mech. and Applied Math., Vol. IV, Pt. 1, 1951.
17. Batchelor, G.K.  
An Introduction to Fluid Dynamics  
Cambridge University Press, London, 1967.
18. Chu, B.T., and Apfel, R.E.  
Acoustic Radiation Pressure Produced by a Beam of Sound  
Review and Tutorial [10], J. Acoust. Soc. Am., Vol. 72, No. 6., 1982.
19. Marston P.L., Goosby S.G., Langley D.S., and LoPorto-Arione S.E.  
Resonances, Radiation Pressure, and Optical Scattering Phenomena of Drops and Bubbles  
Proceeding of the Second International Colloquium on Drops and Bubbles  
Monterey, California, November 19-21, 1981, ed. LeCroissette D.H., JPL Publication 82-7.
20. Yosioka, K., and Kawasima, Y.  
Acoustic Radiation Pressure on a Compressible Sphere  
Acustica, Vol. 5, 1955.
21. Herrey, E.M.J.  
Experimental Studies on Acoustic Radiation Pressure  
J. Acoust. Soc. Am., 27(5), 1955.

22. Baxter, K., Apfel, R.E., and Marston, P.L.  
Versatile Resonance-Tracking Circuit for Acoustic Levitation Experiments  
Rev. Sci. Instrum. 49(2), 1978.
23. Apfel, R.E.  
Detector and Dosimeter for Neutrons and Other Radiation  
U.S. pat. 4, 143, 274.
24. Uspensky, J.V.  
Theory of Equations  
McGraw-Hill, New York, pp. 174-177, 1948.
25. Vargaftik, N.B.  
Tables on the Thermophysical properties of Liquids and Gases, 2nd ed.  
Hemisphere Publishing Corp., Washington, D.C. 1975.
26. Weast, R.C., and Astle, M.J.  
CRC Handbook of Chemistry and Physics, 59th ed.  
CRC press, Inc., Florida, 1978-1979.
27. Harkins, W.D., Clark, G.L., and Roberts, L.E.  
in International Critical Tables, ed. E.W. Washburn  
McGraw-Hill, New York, vol. 4, pp. 436-437, 1928.
28. Girifalco, L.A., and Good, R.J.  
A Theory for the Estimation of Surface and Interfacial Energies  
J. Phys. Chem., vol. 61, pp. 904-909, 1957.
29. Shaw D.J.  
Introduction to Colloid and Surface Chemistry, 2nd ed.  
Butterworth, Boston, 1970.
30. Helwig, J.T.  
SAS Introductory Guide  
SAS Institute Inc. North Carolina
31. Daniel, C.T., and Wood, F.S.  
Fitting Equations to Data  
John Wiley & Sons, Inc., New York, 1971.
32. Davies, O.L.  
Statistical Methods in Research and Production  
Imperial Chemical Industries Ltd., London, 1957.
33. Johnson, L.W., and Riess, R.D.  
Numerical Analysis  
Addison-Wesley Publishing Company, Massachusetts, 1977.

February 1983

REPORTS DISTRIBUTION LIST FOR ONR PHYSICS DIVISION OFFICE  
UNCLASSIFIED CONTRACTS

Director Defense Advanced Research Projects Agency Attn: Technical Library 1400 Wilson Blvd. Arlington, Virginia 22209	3 copies
Office of Naval Research Physics Division Office (Code 412) 800 North Quincy Street Arlington, Virginia 22217	3 copies
Office of Naval Research Director, Technology (Code 200) 800 North Quincy Street Arlington, Virginia 22217	1 copy
Naval Research Laboratory Department of the Navy Attn: Technical Library Washington, DC 20375	3 copies
Office of the Director of Defense Research and Engineering Information Office Library Branch The Pentagon Washington, DC 20301	3 copies
U.S. Army Research Office Box 1211 Research Triangle Park North Carolina 27709	2 copies
Defense Technical Information Center Cameron Station Alexandria, Virginia 22314	12 copies
Director, National Bureau of Standards Attn: Technical Library Washington, DC 20234	1 copy
Commanding Officer Office of Naval Research Western Detachment Office 1030 East Green Street Pasadena, California 91101	3 copies
Commanding Officer Office of Naval Research Eastern/Central Detachment Office 495 Summer Street Boston, Massachusetts 02210	3 copies



Director U.S. Army Engineering Research and Development Laboratories Attn: Technical Documents Center Fort Belvoir, Virginia 22060	1 copy
ODDR&E Advisory Group on Electron Devices 201 Varick Street New York, New York 10014	3 copies
Air Force Office of Scientific Research Department of the Air Force Bolling AFB, DC 22209	1 copy
Air Force Weapons Laboratory Technical Library Kirtland Air Force Base Albuquerque, New Mexico 87117	1 copy
Air Force Avionics Laboratory Air Force Systems Command Technical Library Wright-Patterson Air Force Base Dayton, Ohio 45433	1 copy
Lawrence Livermore Laboratory Attn: Dr. W. F. Krupke University of California P.O. Box 808 Livermore, California 94550	1 copy
Harry Diamond Laboratories Technical Library 2800 Powder Mill Road Adelphi, Maryland 20783	1 copy
Naval Air Development Center Attn: Technical Library Johnsville Warminster, Pennsylvania 18974	1 copy
Naval Weapons Center Technical Library (Code 753) China Lake, California 93555	1 copy
Naval Training Equipment Center Technical Library Orlando, Florida 32813	1 copy
Naval Underwater Systems Center Technical Center New London, Connecticut 06320	1 copy

Commandant of the Marine Corps Scientific Advisor (Code RD-1) Washington, DC 20380	1 copy
Naval Ordnance Station Technical Library Indian Head, Maryland 20640	1 copy
Naval Postgraduate School Technical Library (Code 0212) Monterey, California 93940	1 copy
Naval Missile Center Technical Library (Code 5632.2) Point Mugu, California 93010	1 copy
Naval Ordnance Station Technical Library Louisville, Kentucky 40214	1 copy
Commanding Officer Naval Ocean Research & Development Activity Technical Library NSTL Station, Mississippi 39529	1 copy
Naval Explosive Ordnance Disposal Facility Technical Library Indian Head, Maryland 20640	1 copy
Naval Ocean Systems Center Technical Library San Diego, California 92152	1 copy
Naval Surface Weapons Center Technical Library Silver Spring, Maryland 20910	1 copy
Naval Ship Research and Development Center Central Library (Code L42 and L43) Bethesda, Maryland 20084	1 copy
Naval Avionics Facility Technical Library Indianapolis, Indiana 46218	1 copy

ADDITIONAL DISTRIBUTION LIST

(1 copy each)

Professor L. Crum  
Physics Department  
University of Mississippi  
Oxford, MS 38677

Professor Philip L. Marston  
Physics Department  
Washington State University  
Pullman, WA 99164

Professor Floyd Dunn  
Bioacoustics Research Lab.  
University of Illinois  
1406 W. Green Street  
Urbana, IL 61820

Professor Steven Garrett  
Physics Department  
Naval Postgraduate School  
Monterey, CA 93940

Professor Joseph Katz  
Dept. of Chemical Engineering  
The Johns Hopkins University  
Charles and 34th Streets  
Baltimore, MD 21218

Dr. Eugene Trinh  
MS 183-901  
Jet Propulsion Laboratory  
4800 Oak Grove Drive  
Pasadena, CA 91103

Dr. I. Rudnick  
Physics Department  
University of California  
Los Angeles, CA 90024 •

Dr. M. Greenspan  
Institute for Basic Standards  
National Bureau of Standards  
Washington, D.C. 20234

Dr. C.F. Quate  
Physics Department  
Stanford University  
Stanford, CA 94305

Dr. D.T. Blackstock  
Applied Research Lab.  
University of Texas  
Austin, Texas 78712

Dr. F. Fisher  
Marine Physical Lab.  
UCSD, Scripps Oceanog. Institute  
San Diego, CA 92152

Dr. D. Turnbull  
Div. of Engineering & Applied  
Physics  
Pierce Hall  
Harvard University  
Cambridge, MA 02138

END

FILMED

2-84

DTIC